

C.3

LAMS-2883

CIC-14 REPORT COLLECTION
**REPRODUCTION
COPY**

**LOS ALAMOS SCIENTIFIC LABORATORY
OF THE UNIVERSITY OF CALIFORNIA ○ LOS ALAMOS NEW MEXICO**

STUDY OF FISSION NEUTRON SPECTRA WITH
HIGH-ENERGY ACTIVATION DETECTORS

LOS ALAMOS NATIONAL LABORATORY

3 9338 00371 2246

LEGAL NOTICE

This report was prepared as an account of Government sponsored work. Neither the United States, nor the Commission, nor any person acting on behalf of the Commission:

A. Makes any warranty or representation, expressed or implied, with respect to the accuracy, completeness, or usefulness of the information contained in this report, or that the use of any information, apparatus, method, or process disclosed in this report may not infringe privately owned rights; or

B. Assumes any liabilities with respect to the use of, or for damages resulting from the use of any information, apparatus, method, or process disclosed in this report.

As used in the above, "person acting on behalf of the Commission" includes any employee or contractor of the Commission, or employee of such contractor, to the extent that such employee or contractor of the Commission, or employee of such contractor prepares, disseminates, or provides access to, any information pursuant to his employment or contract with the Commission, or his employment with such contractor.

Printed in USA. Price \$ 2.75. Available from the

Office of Technical Services
U. S. Department of Commerce
Washington 25, D. C.

UNIVERSITY OF CALIFORNIA

LOS ALAMOS SCIENTIFIC LABORATORY
 (CONTRACT W-7405-ENG-36)
 P. O. Box 1663
 LOS ALAMOS, NEW MEXICO

IN REPLY
 REFER TO:

April 2, 1965

To: Copyholders of LAMS-2883
 From: Report Library
 Subject: Errata to LAMS-2883

PLEASE INSERT THIS PAGE INSIDE LAMS-2883

The experimental results which compare fission spectra and corresponding unreflected critical assembly spectra (Section 3.5, Table 3-8) fail to reflect the detector diameter correction in the fission spectra results (p. 54) and are in error. Corrected ratios of spectral indices (Table 3-8), shown below, do not support the interpretation given in the abstract and Sections 3.5, 4.6, and 4.7. The Godiva spectrum reveals a small degradation of the U^{235} fission spectrum, while in the Jezebel assemblies, no significant departure is apparent. Errors in Table 3-8 are of the order of 2%.

Table 3-8: Ratio of Spectral Indices Between Thermal-Neutron-Induced Fission Spectra and Corresponding Fast, Critical Assembly Spectra*

<u>Detectors</u>	<u>Godiva U235</u>	<u>Jeze-23 U233</u>	<u>Jeze-49 Pu239</u>
$\frac{P(n,p)}{Al(n,p)}$	1.056	1.041	1.033
$\frac{P(n,p)}{Fe56(n,p)}$	1.058	1.036	0.998
$\frac{P(n,p)}{Al(n,\alpha)}$	1.034	1.018	1.00
$\frac{P(n,p)}{Cu63(n,2n)}$	1.031	1.040	1.004
$\frac{Al(n,p)}{Al(n,\alpha)}$	0.979	0.978	0.968

*Corrected table 9/63.



LAMS-2883
UC-34, PHYSICS
TID-4500 (19th Ed.)

LOS ALAMOS SCIENTIFIC LABORATORY
OF THE UNIVERSITY OF CALIFORNIA LOS ALAMOS NEW MEXICO

REPORT WRITTEN: March 1963

REPORT DISTRIBUTED: May 20, 1963

STUDY OF FISSION NEUTRON SPECTRA WITH
HIGH-ENERGY ACTIVATION DETECTORS

by

James A. Grundl

Contract W-7405-ENG. 36 with the U. S. Atomic Energy Commission

All LAMS reports are informal documents, usually prepared for a special purpose and primarily prepared for use within the Laboratory rather than for general distribution. This report has not been edited, reviewed, or verified for accuracy. All LAMS reports express the views of the authors as of the time they were written and do not necessarily reflect the opinions of the Los Alamos Scientific Laboratory or the final opinion of the authors on the subject.





ABSTRACT

The energy spectra of neutrons from the fission of U235, U233, and Pu239 have been studied with seven high-energy activation detectors covering the range 0.6 to 16 Mev. Interpretation is in terms of the Maxwellian spectral function $E^{1/2} \exp(-E/T)$. By means of a unique cavity arrangement within a moderator to obtain pure thermal-neutron-induced fission neutrons, the average energies of the three spectra are found to be in the ratios U235: U233: Pu239 = (1): (1.016±0.003): (1.039±0.003).

Differences between the normalized spectra are most pronounced at high energies as exemplified by the relative Pu239:U235 flux ratios 1.17±0.013 for $6 < E < 11$ Mev, and 1.35±0.03 for $E > 11$ Mev.

Comparable detector responses within unreflected critical assemblies of U235, U233 and Pu239 metal are consistent with an increase of at least 2% in the average energy of the fission spectrum component of each assembly relative to the corresponding thermal-fission spectrum. This may be associated with the approximately 1.5 Mev average energy of the assembly neutrons inducing fission.

Through extensive detector calibration at the Los Alamos Van de Graaff, average detector cross section ratios or spectral indices are established for the U235 fission spectrum:

$$\frac{U235(n, f)}{U238(n, f)} = 4.14 \pm 0.23$$

$$\frac{Np237(n, f)}{Fe56(n, p)} = 1310 \pm 110$$

$$\frac{Np237(n, f)}{U238(n, f)} = 4.33 \pm 0.22$$

$$\frac{Np237(n, f)}{Al(n, \alpha)} = 1880 \pm 180$$

$$\frac{Np237(n, f)}{P(n, p)} = 33.5 \pm 3.4$$

$$\frac{Np237(n, f)}{Cu63(n, 2n)} = 12500 \pm 1400$$

$$\frac{Np237(n, f)}{Al(n, p)} = 306 \pm 25$$

Uncertainties assigned, applicable to spectral analysis, do not include absolute cross section errors. Indices involving Cu63(n,2n) show that the U235 fission spectrum yields approximately 20% fewer neutrons above 11 Mev than predicted by the Maxwellian spectral function. Though all other independent indices fall within two error intervals, they consistently suggest that the observed spectrum is shifted to higher energies.

The associated development of the activation detectors as a comprehensive tool for measuring distributed neutron spectra is described in detail.

ACKNOWLEDGEMENTS

The completion of this dissertation and any success it may enjoy rests in large part upon the sustained encouragement and support of Drs. Gordon E. Hansen and Hugh C. Paxton of the Los Alamos Critical Assemblies Group. Their patience and generous effort in criticizing both content and presentation were essential to the final result.

It is a pleasure also to recognize the opportunity provided by the Los Alamos Scientific Laboratory and the cooperation of the University of New Mexico which made possible my participation in the Advanced Study Program. In particular the author is indebted to Dr. Christopher P. Leavitt of the University of New Mexico for his interest in the research undertaken, and to Dr. Victor H. Regener as representative of the Physics Department faculty faced with the difficult problem of assessing a doctoral candidate whose main research activities were conducted off-campus.

Recognition must be included of the help furnished by the Chemistry and Metallurgy Division of the Laboratory in the preparation and analysis of source and detector disks. The services of the machinists assigned to the Critical Assemblies Group was also essential.

Individual acknowledgements for invaluable assistance are many. At the Van de Graaff, Mr. R. K. Smith made available his experimental arrangement as well as his wide experience in monoenergetic cross section measurements. Cockcroft-Walton irradiations were carried out with the cooperation of R. W. Davis. Members of the Critical Assemblies Group assisting with the extensive task of counting and data reduction were Carl Henry, Edward Damour, and Bennie Peña. Particular appreciation goes to Thelma Thomas for preparing—and changing—the many illustrations involved, and to Antonia Flores for typing from often obscure handwritten manuscripts.

TABLE OF CONTENTS

	Page
ABSTRACT	iii
ACKNOWLEDGEMENTS	v
LIST OF TABLES	ix
LIST OF ILLUSTRATIONS	xii
INTRODUCTION	1
Chapter 1: THEORY AND APPLICATION OF HIGH-ENERGY ACTIVATION DETECTORS	6
1.1 Activation Detectors—Advantages and Limi- tations	6
1.2 The Activation Equation	8
1.3 Relative Response and Terminology	10
1.4 Spectral Indices and Related Calibration Considerations	13
1.5 Spectral Sensitivity	16
1.6 Selection and Specification of Detectors	17
1.7 Experimental Application	24
Chapter 2: PRODUCTION OF PURE FISSION SPECTRUM NEUTRONS	30
2.1 Conventional Fission Converters	30
2.2 Cavity Fission Spectrum	31
2.3 Cavity Arrangement and Source-Detector Assembly	35
2.4 Flux Profiles and Detector Backgrounds	41
Chapter 3: FISSION SPECTRA COMPARISON MEASUREMENTS	48
3.1 Experimental Procedure and Processing of Counting Data	48
3.2 Relative Flux Correction and Response Ratios	53
3.3 Reliability and Final Experimental Values	59
3.4 Background Measurements	64
3.5 Comparison with Fast, Metal, Critical- Assemblies	68
Chapter 4: INTERPRETATION OF COMPARISON MEASUREMENTS	72
4.1 The Maxwellian Density Function	72

TABLE OF CONTENTS (continued)

	Page
4.2 Computed Spectral Indices and Variation with Average Energy	73
4.3 Graphical Display of Fission Spectrum Average Energy Shift	77
4.4 Average Energy Shift Based On All Independent Detector Combinations	81
4.5 Final Specification of Spectral Shifts and Comparison with Other Measurements	86
4.6 Fission Spectrum Changes in the Fast, Critical Assemblies	89
4.7 Theoretical Considerations and Experimental Correlation	91
 Chapter 5: SUPPLEMENTARY STUDIES—DETECTOR CALIBRATION AND SHAPE OF U235 FISSION SPECTRUM	 97
5.1 Van de Graaff Calibration	98
5.2 U235(n, f) Detector Response in the U235 Fission Spectrum	105
5.3 Spectral Indices and Comparison with Maxwellian Fission Spectrum Function	111
5.4 Adjustment of the Maxwellian Spectrum	120
 Appendix 1: VERSATILE, HIGH-STABILITY PROPORTIONAL COUNTER FOR ACTIVATION MEASUREMENTS	 126
A1.1 General Principles and Development	126
A1.2 Counter Design and Performance Specification	130
 Appendix 2: COAXIAL DISK GEOMETRY	 136
 Appendix 3: COMPUTATION OF CAVITY RETURN SPECTRA	 143
A3.1 Monte-Carlo Method	143
A3.2 DSN Multigroup Transport Method	144
 REFERENCES	 154

LIST OF TABLES

Table	Page
1-1 Neutron-Energy Activation Detectors	19
1-2 Counting Conditions and Physical Properties of Detector Disks	20
1-3 Detector Activity Transmission Factors	29
2-1 Fission Spectrum Perturbation by a 1.3cm Diameter Sphere of Iron	39
2-2 Source Disk Specifications	40
2-3 Fission-Neutron Return Background for 10cm Cavity In a D ₂ O Reflector	46
3-1 Typical Counter Responses for 20min. Irradiation at $\sim 3 \times 10^9$ Neut/cm ² sec	52
3-2 Experimental Results — Fission Detectors	57
3-3 Experimental Results — High Energy Detectors	58
3-4 Final Response Ratios and Ratios of Spectral Indices	62
3-5 Source-Reactor Background Measurements	63
3-6 Response Ratios for 7" Diameter Cavity	67
3-7 Response Ratios with Brass Scatterer	68
3-8 Ratio of Spectral Indices Between Thermal-Neutron- Induced Fission Spectra and Corresponding Fast, Critical Assembly Spectra	70
4-1 Computed Average U235 Fission Spectrum Cross Sections	74
4-2 Ratio of Np(n,f)/B Spectral Indices	79
4-3 Ratios of All Independent Spectral Indices Com- paring Pu239 and U233 Fission Spectra to U235	82

LIST OF TABLES (continued)

Table	Page
4-4 Fission Spectrum Average Energy Shift Predicted by each Independent Detector Combination	83
4-5 Six-Group Display of Spectral Comparison	89
4-6 Average Energy Ratio Between the Spectra of Fast Critical Assemblies and Corresponding Thermal-Fission Spectra	90
5-1 Cross Section Determinations and Calibration Ratios	101
5-2 Fission Detector Response Ratios in Improved Arrangement	108
5-3 Fission Detector Spectral Indices for the U235 Fission Neutron Spectrum	110
5-4 Observed Spectral Indices for the U235 Fission Neutron Spectrum	112
5-5 Experimental Average Detector Cross Sections for the Fission Spectrum of U235	114
5-6 Observed U235 Fission Spectrum Compared with Maxwellian and Watt Spectral Functions	116
5-7 Average Experimental Departures from Maxwellian Fission Spectrum Function	120
5-8 Six-Group Specification For Fission Spectrum Adjustment	122
5-9 Six-Group Adjusted U235 Fission Neutron Spectrum	123
5-10 Average Absolute Departures of Observed Spectral Indices Involving a Single Detector	125
A3-1 Total Neutron Return for Cavity Fission Spectrum (Monte-Carlo)	146

LIST OF TABLES (continued)

Table		Page
A3-2	Normalized Flux Spectrum for Neutrons Returning to Cavity (Monte-Carlo)	147
A3-3	Flux Spectrum of Cavity Return Neutrons (Multi-group Transport Approx.)	150

LIST OF ILLUSTRATIONS

Figure	Page
I-1 Experimental Neutron Flux Spectrum	2
1-1 Fundamental Detector Cross Sections	21
1-2 Detector Response Functions for the Fission Spectrum	25
2-1 Sixteen-group Representation of Cavity Return Background	33
2-2 Hydro Source Reactor and Cavity Fission Spectrum System	36
2-3 Source-Detector Assembly	38
2-4 Effective Flux Distribution Between Coaxial U235 Source Disks	43
2-5 Flux Profiles Over Detector Region	45
3-1 Detector Counting Schedule	51
3-2 Primary Detector Arrangements and Corresponding Flux Profiles	55
4-1 Variation of Average Cross Section with Average Fission Spectrum Energy	75
4-2 Display of Fission Spectrum Comparison	78
4-3 Average Fission Neutron Energy As a Function of \bar{v}	95
5-1 Van de Graaff Arrangement for Detector Calibration	99
5-2 Energy Distribution Incident On Detectors	103

LIST OF ILLUSTRATIONS (continued)

Figure		Page
A1-1	Proportional Counter Chamber	131
A1-2	High-Stability Proportional Counter	132
A2-1	Coaxial Disk Geometry	137
A2-2	Effective Flux for Detector Disks Between Coaxial Source Disks	140
A2-3	Average Distance Between Coaxial Source and Detector Disks	142
A3-1	Angular Divisions for Monte-Carlo Cavity Calcul- ation	145
A3-2	Return Flux at Center of Spherical Cavity in D_2O by Monte-Carlo Method	148
A3-3	Return Flux at Cavity Center for Various Reflectors	151

INTRODUCTION

Less than two months after the discovery of nuclear fission in 1939, neutrons were found to accompany the new nuclear process (39Hal, Halban, Joliot, Kowarski); a short time later, the average number of such neutrons per fission was observed to be about 3.5 (39Ha2). This energetic and disruptive nuclear process, capable of reproducing itself, was thus quickly assured of lasting interest. One aspect of nuclear fission, the energy spectrum of the emitted neutrons, has received continuing attention. Several independent methods—cloud chamber, nuclear plates, proton recoil counters, time-of-flight (52Bo, 56Cr1, 52Wa)—show a Maxwellian-like flux distribution with 2 Mev average energy. Two semiempirical expressions in common use fit experimental data quite well:

$$\text{Watt: } N(E) = \text{const} \times \exp(-0.965E) \sinh(2.29E)^{1/2}, \quad \text{I-1}$$

$$\text{Maxwellian: } N(E) = \text{const} \times E^{1/2} \exp(-0.775E). \quad \text{I-2}$$

Fig. I-1 shows the best existing data fitted with the Maxwellian function.

Most early spectral measurements involved neutrons from U235 fission, and the single early published work on Pu230 by Nereson (52Ne) noted no apparent departure from the U235 spectrum. In 1956, however, Grundl and Neuer (56Gr)

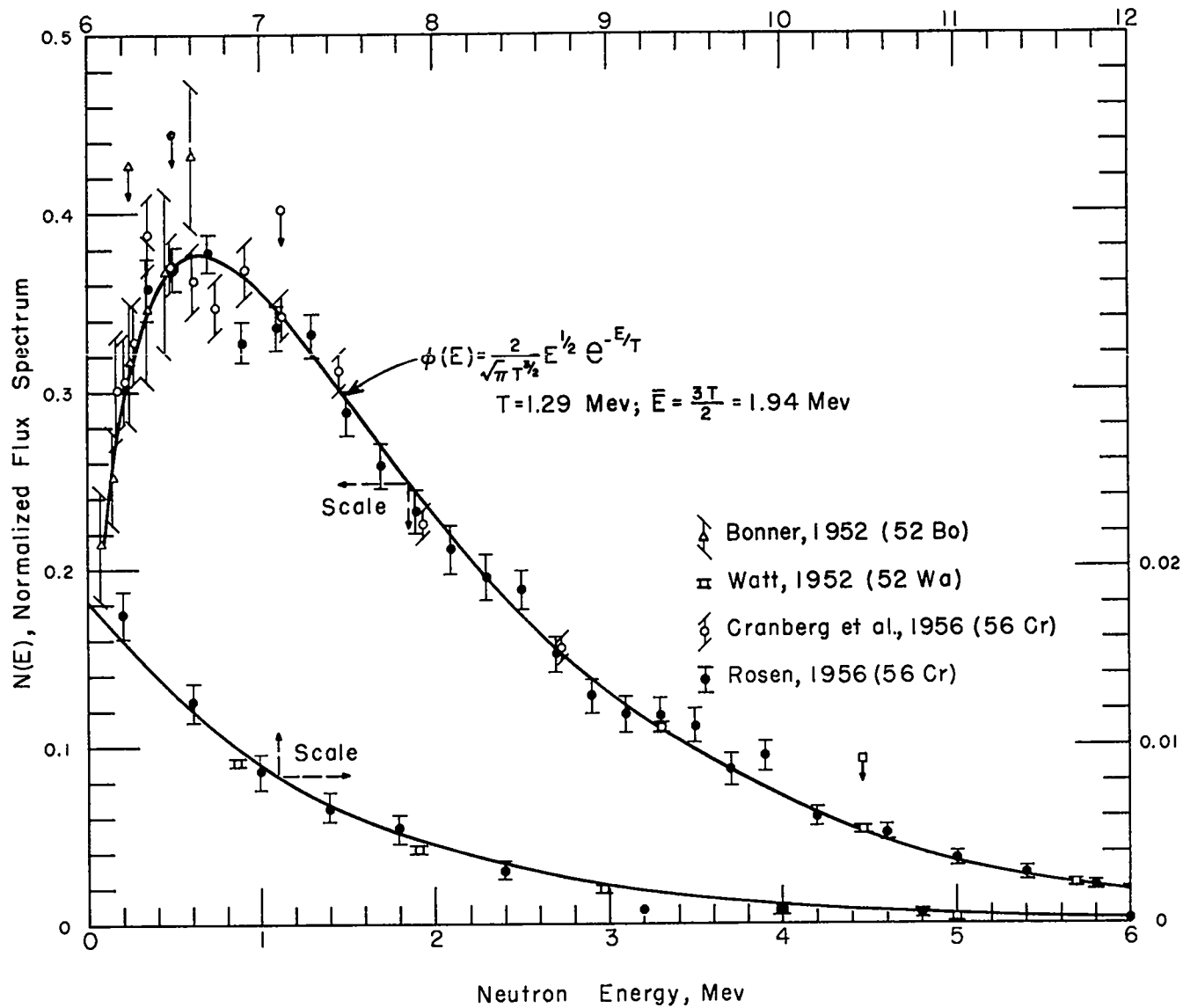


Fig. I-1: Experimental neutron flux spectrum from thermal-neutron-induced U235 fission. Methods of measurement were: Bonner, cloud chamber; Watt, proton recoil; Cranberg, time-of-flight; Rosen, nuclear emulsion. The solid line shows a best fit with the Maxwellian spectral function (normalized to unity), and arrows indicate normalization point for each set of data.

using activation detectors—one of the earliest methods verifying fission neutron emission (40Tu)—reported a Pu239 fission neutron spectrum slightly more energetic than that from U235. A re-examination of the earlier photoplate work by Nereson supported this result. More recent measurements by Bonner (61Bo1) using a differential moderation technique and Kovalev et al. (57Ko) using activation detectors also agree, but are mostly limited to the lower energy region. An introductory discussion of fission spectra can be found in a review article by Halpern (59Ha).

This report proposes to compare in some detail the thermal-neutron-induced fission neutron spectra of U235, U233, and Pu239. From the response of eight activation detectors the shift in average energy between spectra will be ascertained and the validity of the Maxwellian function (Eq. I-2) to describe the shift investigated. In addition, a comparison of each fission spectrum with the spectrum inside unreflected critical assemblies of the corresponding metal will discern spectral distortions arising from the fact that the source neutrons in this case are themselves fission spectrum rather than thermal.

Two papers (59Te, 58Ko) consider the theoretical significance of these comparisons on the basis of neutrons evaporated from fast-moving variably excited fission fragments. The observed shifts in average energy will be examined in the light of the first, by James Terrell (59Te). Finally, extensive calibration and verification of detector excitation

functions at the Los Alamos Van de Graaff make it possible to deduce information on the shape of the U235 fission spectrum itself.

Activation detector development, treated in Chapter 1, includes a general discussion of these detectors as spectral indicators leading to definitions and equations. Following, in the same chapter, is a description of the eight detectors selected and their general experimental application. Chapter 2 takes up the problem of obtaining pure fission neutrons. The final unique arrangement, a spherical cavity within a moderator, yields abundant fission neutrons, and is amenable to accurate calculations of the neutrons scattered back to the detectors. The experimental set-up presented makes use of a compact source reactor coupled to a large tank of D₂O containing a 4" diameter cavity and small source-detector assembly. The material of these first two chapters, considered to be generally applicable to reactor and shield spectra measurements, is discussed somewhat more extensively than required for the fission spectrum studies.

Chapter 3 describes the comparison of fission spectra and gives the direct experimental results including comparison with spectra of corresponding unreflected fast, critical assemblies. Interpretation of the results and correlation with theory appear in Chapter 4.

The final chapter is concerned with the U235 fission spectrum itself. Results of the Van de Graaff calibration, discussed in detail, lead to fully corrected spectral indices for the U235 fission spectrum; comparison of these observed indices with those computed from both the Maxwellian and Watt spectral functions show significant departures. A six-group energy division provides a basis for specifying a fission spectrum more consistent with the experimental detector responses.

CHAPTER 1

THEORY AND APPLICATION OF HIGH-ENERGY ACTIVATION DETECTORS

1.1 Activation Detectors—Advantages and Limitations

Neutron-induced radioactivity of the elements served as the earliest means of neutron detection. All such activation detectors are sensitive to the energy of the incident neutrons and de facto are spectral indicators. Their resolution of course is very broad, but if the distribution of neutrons be reasonably smooth they give a good idea of what the distribution is like. If, in addition, something is known of the spectral shape and a one or perhaps two parameter function may be assumed to describe the spectrum, neutron activation detectors can: (1) establish those parameters; (2) verify that the assumed spectral function is correct, and suggest changes if it is not; and (3) for comparison of similar spectra, establish parametric differences with a degree of accuracy much higher than is practicable by conventional differential methods. When detector excitation functions become more accurate it may be possible

to specify more parameters and even generalize the spectral function. Suggestions and formalisms along this line have already been published (61Mo) although it is not clear, presently, that such exotic approaches for unknown spectra will yield more information than simple histogram techniques (62Die). The latter is always preferable when detector results are being used to verify or guide multigroup neutron transport computations.

Beyond these considerations of interpretation, simplicity of measurement, low flux requirements, and usually negligible gamma sensitivity are significant advantages. Adaptable to almost any experimental condition they become indispensable for such problems as the measurement of reactor spectra.

In view of the place neutron activation detectors have as spectral analyzers, surprisingly little comprehensive effort has been directed toward their potential. With few exceptions they appear in the literature as qualitative indicators based, at best, upon inadequate excitation functions (61Mo, 58Tr, 60Gr). Lack of good excitation functions is indeed the main limitation to this method though the situation is improving; one might hope that the effort here, to make eight particular detectors a comprehensive spectral measuring tool, will focus the attention of experimenters on the reactions involved.

The discussion to follow will be restricted to

detector application based upon gross beta-gamma counting of irradiated disks of the reaction element. As will become evident, all spectrum information can be obtained from relative detector response, relative cross sections, and a relative calibration in a spectrum of known energy distribution (e.g. monoenergetic or fission)—absolute counting is not necessary nor even desirable. The latter usually introduces additional absolute errors into a spectral measurement. The viewpoint will be maintained that spectral analysis with activation detectors always involves a spectral comparison.

1.2 The Activation Equation

For a detector disk A exposed to a neutron spectrum X and the induced activity subsequently counted, the response of the counter is given by an activation equation:

$$A_X(\alpha) = [\Gamma_A(\alpha) N_A] \bar{\sigma}_{AX} (\varphi T)_{AX} F_A(\lambda_A, T), \quad 1-1$$

where,

$A_X(\alpha)$ = counter response for detector A in spectrum X under experimental conditions α . For a simple exponential decay the counting rate at the end of the irradiation is commonly used, and for a composite decay (e.g. gross fission product counting) the counting rate at some specified

time after the end of the irradiation.

$(\varphi T)_{AX}$ = total flux incident on detector A.
 $F_A(\lambda_A, T)$ = saturation factor. For a simple exponential activity after irradiation for a time T,

$$F_A(\lambda_A, T) = \lambda_A \int_{-T}^0 \varphi(t) \exp(\lambda_A t) dt / \int_{-T}^0 \varphi(t) dt,$$

which for a rectangular irradiation profile gives the familiar result $[1 - \exp(-\lambda_A T)]/T$. For a complex decay, an experimental determination of $F(T)$ for expected irradiation shapes and duration is often required.

$$\bar{\sigma}_{AX} = \int_0^{\infty} \sigma_A(E) N_X(E) dE \quad 1-2$$

is the average cross section of detector A in spectrum X or simply the response integral. The integrand $\sigma_A(E) N_X(E)$ is called the response function, where $N_X(E)$ = neutron spectrum normalized to unity, and $\sigma_A(E)$ the excitation function for detector A.

$\Gamma_A(\alpha)$ = efficiency factor. Includes all experimental influences on response not in the other factors of the activation equation. The symbol α refers to these factors which may vary and are therefore meaningful to specify.

N_A = number of detector atoms.

A host of matters are lumped into the efficiency factor: (1) counting efficiency which includes detector disk positioning and shielding, counter sensitivity, electronic discrimination, dead time, etc; (2) transmission of radiation by disk; (3) flux attenuation in detector disk; (4) nonuniform density of activation; (5) for composite decay dependence upon neutron energy; (6) environment and orientation during irradiation . . .

Clearly it is important to standardize procedures obtaining detector responses in the known and unknown spectra with as few changes as possible.

1.3 Relative Response and Terminology

Activation equations may be written for each detector in each spectrum—those to be determined plus at least one calibrating spectrum with a known distribution of neutron energies.⁽¹⁾ When experimental conditions are identical, the equations for two different detectors A and B in the same spectrum X may be combined in pairs to eliminate the absolute flux:

(1)

Monoenergetic accelerator neutrons need not be distinguished from other known spectra since the energy spreads usually encountered require integrating a response function similar to the case of a more widely distributed spectrum.

$$\frac{A_X}{B_X} = \frac{\Gamma_A N_A F_A(\lambda_A, T)}{\Gamma_B N_B F_B(\lambda_B, T)} = \frac{\bar{\sigma}_{AX}}{\bar{\sigma}_{BX}}.$$

Suitable double ratios may then be formed and average cross section ratios in the unknown spectra obtained:

$$\frac{(A/B)_X}{(A/B)_K} = \frac{(\bar{\sigma}_A / \bar{\sigma}_B)_X}{(\bar{\sigma}_A / \bar{\sigma}_B)_K}; \left(\frac{\bar{\sigma}_A}{\bar{\sigma}_B} \right)_X = \frac{(A/B)_X}{(A/B)_K} \left(\frac{\bar{\sigma}_A}{\bar{\sigma}_B} \right)_K, \quad 1-3$$

where K refers to a known spectrum and $(\bar{\sigma}_A / \bar{\sigma}_B)_K$ have been computed. This last step eliminates the efficiency factors Γ , detector atoms N, and saturation factors $F(\lambda, T)$, as well as the normalization used to compute average cross sections (the exception for composite decays has been mentioned). For direct comparison of a set of similar spectra, K refers to that spectrum to which a neutron distribution has been assigned. On this basis experimental results depend only upon maintaining a stable counting system and uniform procedures; interpretation involves, in addition, the known neutron distribution and detector excitation functions.

The definitions below follow from these considerations and assume identical irradiation profiles and other experimental conditions:

1. Response Ratio: $R_{AB} \equiv \frac{A}{B} \frac{(\varphi T)_B}{(\varphi T)_A}$, counter response ratio corrected for relative flux incident on each detector disk.

2. Calibration Factor: $G_A \equiv \frac{A}{\bar{\sigma}_A (\varphi T)_A}$. This factor,

obtained in the known spectrum, requires only relative flux values for a set of detectors, except when absolute fluxes are being measured. The ratio G_A/G_B will be called the calibration ratio.

$$\begin{aligned}
 3. \text{ Spectral Index: } S_{AB}(X) &\equiv \frac{\bar{\sigma}_{AX}}{\bar{\sigma}_{BX}} = \frac{\int_0^{\infty} \sigma_A(E) N_X(E) dE}{\int_0^{\infty} \sigma_B(E) N_X(E) dE} \\
 &= (R_{AB})_X \frac{G_B}{G_A}, \quad 1-4
 \end{aligned}$$

the average cross section ratio for detectors A and B in spectrum X. The average cross section $\bar{\sigma}_A$ in the calibration factor must be consistent with $\sigma_A(E)$ in the response function.

$$4. \text{ Ratio of Spectral Indices: } C_{XY} = \frac{(S_{AB})_X}{(S_{AB})_Y} = \frac{(R_{AB})_X}{(R_{AB})_Y}.$$

This double ratio is useful for comparing similar spectra. Calibration factors cancel out making this quantity more accurate and simple to measure than either component. Less spectral information, of course, results.

$$\begin{aligned}
 5. \text{ Response Factor: } K_A &= \frac{\text{counter response}}{\text{no. of act. atoms produced}} \\
 &= \frac{A}{N_A \bar{\sigma}_A (\varphi T)_A}.
 \end{aligned}$$

This quantity included for completeness is convenient for absolute flux determination, and is related to the usual counter efficiency ϵ for a simply decaying sample by

$$\epsilon_A = \frac{K_A}{F(\lambda_A T)}.$$

1.4 Spectral Indices and Related Calibration Considerations

The spectral index is the customary quantity given to characterize a neutron spectrum; it is a measured and computable quantity linking the experimental results to conclusions from theoretical models. For n detectors $n(n-1)/2$ indices may be formed, each preferentially comparing two energy regions of an unknown neutron distribution X . A spectrum is sought which will give a computed set of indices consistent with those found experimentally. Experimental indices are obtained through a "known" or calibrating spectrum as indicated above,

$$S_{AB}(X) = (R_{AB})_X \frac{G_B}{G_A}.$$

Symbolically, we can write computed indices as

$$S_{ABX}(\sigma_A, \sigma_B, \beta_1, \beta_2, \dots, \beta_i); \quad i \leq \text{no. of detectors},$$

where σ_A and σ_B are the excitation functions involved, and the β 's are spectral parameters, i.e. parameters of analytic spectral functions, or perhaps simply group flux values in a histogram approach.

The set of equations,

$$S_{ij}(X) = S_{ijX}(\beta_1, \beta_2, \dots), \quad i \neq j,$$

may in principle be inverted to extract the spectrum, tempting one to call upon the vast potential of a modern computer to obtain many parametered spectra in a twinkling. This may be possible if and when precision cross sections are available; presently, it seems advisable to keep the number of parameters much smaller than the number of detectors, and to use simple, reasonable spectral functions which allow the effect of cross section uncertainty upon spectral parameters to be more easily evaluated. For a spectrum describable by a one parameter analytic function (e.g. fission or evaporation spectrum) convenient plots and tables determine the parameter and the adequacy of the spectral function—see chapter 4. Extension to two parameters would seem possible.

Comparison of experimentally observed indices with those computed from a spectrum predicted by reactor calculations may verify that spectrum or guide the adjustment of input data. For such application the method outlined here is better than any independent, absolute cross section ratio determination (e.g. absolute fission counting or 4π absolute beta counting). The latter will check a combination of spectra and absolute cross section, not spectra alone.

As has been stated the matter of calibration is approached here in the manner of a comparison; poorly known

neutron distributions may be related to those better known. "Known" spectra include neutrons from particle accelerators, thermal neutrons from a reactor, and the fission spectrum. In this connection one advantage of fission spectrum calibration may be mentioned. Since the fission spectrum is one of the best known distributed spectra and is a major component of most fission-derived neutron distributions, using it as a reference greatly reduces the largest uncertainty in applying activation detectors, namely, the excitation functions. In general, a known spectrum close to the one being determined reduces the dependence upon excitation function; the closer the spectra the more accurately they may be compared.

Calibration with accelerator neutrons (i.e. simultaneous irradiation of the detector set subtending not too large an angle with the target) is not always simple: (1) neutron intensities are often marginal; (2) severe structure in many detector excitation functions give rise to difficult interpretation problems; (3) secondary interactions in the target often result in neutrons of energies other than those of the primary reaction; and (4) for fissile materials the gross (and individual) activity of fission products may be expected to depend upon neutron energy since the fission mode changes. This last is a particular worry when calibrating with 14 Mev neutrons from the D-T reaction. Calibration in the fission spectrum,

probably the best known and most easily obtained distributed neutron source, largely overcomes these difficulties.

1.5 Spectral Sensitivity

Nothing has been said here of thresholds—effective or otherwise. It is felt that interpreting any activation detector in terms of a threshold is unfruitful and often confusing. On one hand, describing a detector in terms of a threshold can lead to overestimating its ability to sample a certain energy region, while, on the other hand, the inability to define a generally meaningful threshold (since it is always spectral dependent) leads to belittling the usefulness of activation detectors as accurate spectral indicators. With some exceptions the measured excitation functions do not even remotely exhibit a true threshold shape except that the cross section is zero below some energy. The response function (Eq. 1-2) is fundamental and should be the center of interpretation; using average cross section ratios directly is not difficult, and is trivial if a computer is available.

It remains true that something is needed to indicate for a given spectrum the general energy region where a detector is sensitive. Specifying a crude Gaussian fit to the response function $\sigma(E)N(E)$ suggests itself, though the usual prominent structure and asymmetry make this difficult

(see Fig. 1-2). A simple qualitative characterization to be used here is the mid-energy E_m of the response curve, along with the energy intervals ΔE_1 and ΔE_2 , below and above E_m , which encompass 80% of the response:

$$\int_0^{E_m} \sigma(E) N(E) dE = 0.5 \int_0^{\infty} \sigma(E) N(E) dE, \quad 1-5$$

$$\int_{E_m - \Delta E_1}^{E_m} \sigma(E) N(E) dE = \int_{E_m}^{E_m + \Delta E_2} \sigma(E) N(E) dE = 0.4 \int_0^{\infty} \sigma(E) N(E) dE.$$

A detector-spectrum sensitivity appropriate to the fission neutron study is just the slope of the function,

$$\sigma_{AX}(T) = \frac{2}{\pi^{1/2} T^{3/2}} \int_0^{\infty} \sigma_A(E) E^{1/2} \exp(-E/T) dE,$$

around the relevant value of $T = 1.3$ ($\bar{E} = 2.0$ Mev).

This "figure-of-merit" will prove useful in the discussion of precision spectral comparisons.

1.6 Selection and Specification of Detectors

Turning to the selection of specific detectors one may quickly reduce the vast array of activation reactions by compromising on certain desirable characteristics: (1) measured excitation function, (2) relevant energy sensitivity, (3) half-life in the range 10 min to 10 hr for high

sensitivity and rapid data acquisition, (4) no competing activities of similar half-life or large cross section, (5) convenient physical and chemical properties, and (6) large cross section. These criteria, based on using the method of gross beta-gamma counting of irradiated disks of the detector element, are not of equal importance. For this investigation prime consideration was given to the availability and consistency of measured excitation functions.

The set of eight detectors finally chosen have sensitivities distributed over the energy range 0.6 to 15 Mev; Table 1-1 lists them, along with most of the important features of spectral indication as applied to fission spectrum studies.⁽¹⁾ Note the spectacular increase in sensitivity as one goes to higher energy detectors. Table 1-2 presents counting procedures and physical properties for the detector disks. In Appendix 1 the counters are described in detail.

The fundamental detector cross sections used in this report, and displayed in the three sections of Fig. 1-1, are a compromise between references listed in Table 1-1 and extensive calibrations carried out at the

(1)

For fast-neutron, metal, critical assembly measurements, the capture detector I^{127} is added along with four auxiliary detectors: $Th^{232}(n, f)$, $Th^{232}(n, \gamma)$, $U^{238}(n, f)$, $U^{238}(n, \gamma)$, and $Pu^{239}(n, f)$.

Table 1-1: Neutron-Energy Activation Detectors

Detector Reactions	Half-life ^b	Primary Radiations		Competing Reactions	Half-life	Activities		σ_f (mb) U235 fission spec. ^d (experimental)	Fission Spec. Response ^e (MeV)			Fission Spec. Sensitivity ^f (%/keV)	Cross Section Reference
		E_β^c (MeV)	E_γ (MeV)			E_β^c (MeV)	E_γ (MeV)		min	mid	max		
U235(n, f) ^a	(t ^{-1.17})			U238(n, f) U238(n, γ)	-- 23.5m		0.074	1296	--	--	--	0	58A1
Np237(n, f)	(t ^{-1.45})			Np(n, γ) Np(n, 2n)	2.1d 22h		1.0(54) .04(40) .045(21)	1355	0.8	1.8	4.1	1	59Sc
U238(n, f)	(t ^{-1.48})			U238(n, γ) U238(n, 2n)	23.5m 6.75d	1.2 <0.3	0.074 0.04(36) 0.2(20)	313	1.6	2.7	5.6	4	58A1
P ³¹ (n, p)Si ³¹	157.5m	1.48(100)	1.26 (<0.1)	P ³¹ (n, γ)	14.5d	1.7	--	40.4	2.2	3.7	6.0	8	58Gr, 60Cu, 60Li
Al ²⁷ (n, p)Mg ²⁷	9.47m	1.75(58) 1.59(42)	0.84 (70) 1.02 (30)	Al ²⁷ (n, γ) Al ²⁷ (n, α)	2.3m 900m	2.9	1.8(100)	4.4 ₃	4.0	5.7	8.2	16	58Hu, 60Li
Fe ⁵⁶ (n, p)Mn ⁵⁶	154m	2.81(50) 1.04(30) .65(20)	.85 (100) 1.81 (30) 2.13 (20)	Fe ⁵⁴ (n, 2n)	899m	2.6		1.03 ₅	5.4	7.3	10.5	24	58Te, 60Li, 52Fo
Al ²⁷ (n, α)Na ²⁴	900m	1.39(100)	2.75 (100) 1.37 (100)	Al ²⁷ (n, γ) Al ²⁷ (n, p)	2.3m 9.47m	2.9	1.8(100)	0.72 ₃	6.7	8.2	11.0	28	60Sc, 60Li, 52Fo
Cu ⁶³ (n, 2n)Cu ⁶²	9.7m	2.9	~1 (<10)	Cu ⁶⁵ (n, γ) Cu ⁶³ (n, γ) Cu ⁶⁵ (n, 2n) Cu ⁶³ (γ , n)	5.1m 763m 9.7	2.6 0.6 2.9	1.0(10) 1.3(~0.5)	0.109	12.2	13.6	16.3	52	52Br, 62Bo, 50Fo, 52Fo 54Be

^aFission detector decay over short intervals follows a power law determined largely by the characteristics of the counter response.

^bHalf-lives are those consistently obtained from least-squares analysis of counting data. Other values are summarized in Ref. 58St.

^cBeta-ray end-point and gamma-ray energy from 58St. Branching ratios in percent given in parenthesis.

^dMeasured average U235 fission spectrum cross section normalized to U238(n, f) value—see Chapter 5; Table 5-5.

^eEqual detector response occurs above and below the mid-response energy. The maximum and minimum energies define the region within which 90% of the response takes place—see Eqs. 1-5.

^fPercent change in detector response for average energy change of one keV in the fission spectrum—see section 4.2.

Table 1-2: Counting Conditions and Physical Properties of Detector Disks

Detector Disks (Set 1)	COUNTING ^(a)					Total Thickness ^(b)	Detector Weight(gm)	Detector Atoms $\times 10^{20}$	Set (1) ^(c)		FORM ^(d)
	Slot	Aluminum Shield (in.)	Counting Interval (min.)	Response Time (min.)	Bkg (c/m)				Set (2)		
25-3-6	S2	0.062	105-140	120	300	0.015"	0.0843	2.02	1.001	Enriched uranium (93.5% U235, 5.3% U238, 1.2% U234) metal (0.003" thk 0.38" Dia.) encased in 0.045g aluminum can.	
27-3	S4	0.050	45-100	60	40,000	0.032"	0.097	~2.5	1.000	HfO_2 encased in 0.22g nickel can.	
28-3-4	S2	0.062	45-100	60	1400	0.012"	0.110	2.78	1.033	Depleted uranium (4350:1) metal (0.003" thk., 0.38" Dia) encased in 0.044g aluminum can.	
P-10	S1	--	80-150	ICR	--	0.037"	0.070	13.6	1.007	C.P. red phosphorous powder encased in 0.046g aluminum can: Ca, Al, Na <0.1%; all other metallic impurities <0.01%.	
A1-20-10	S1	--	15-60 (n,p) 145-200 (n, α) 350-1400	ICR	--	0.021"	0.135	30.2	0.995	Pure aluminum: 0.02% Si; all other metallic impurities <0.01%.	
Fe-18-3	S1	--	70-170	ICR	--	0.017"	0.271	29.2	0.99	C. P. Iron formed by powder metallurgy: all metallic impurities <0.001%.	
Cu63-15-1	S1	0.032	10-50	ICR	--	0.278"	0.015	26.6	0.96	Enriched Cu63, Oak Ridge Lot #Du-497(a) Cu63: 99.40 ± 0.01 a/o Cu65: 0.598 ± 0.016 a/o	

^aCounting interval indicates period during which detector is counted. Counting rate at response time defines detector response; ICR (initial counting rate) is the counting rate which would be observed at the end of the irradiation.

^bAll detectors are cylindrical disks 0.450" total diameter. For the encased materials the diameter of the actual detector element is 0.380".

^cIntercalibration between nearly identical sets of detector disks from simultaneous activation in a fast spectrum.

^dSample canning is done by drawing and crimping 2 mil aluminum foil with a simple punch and die assembly.

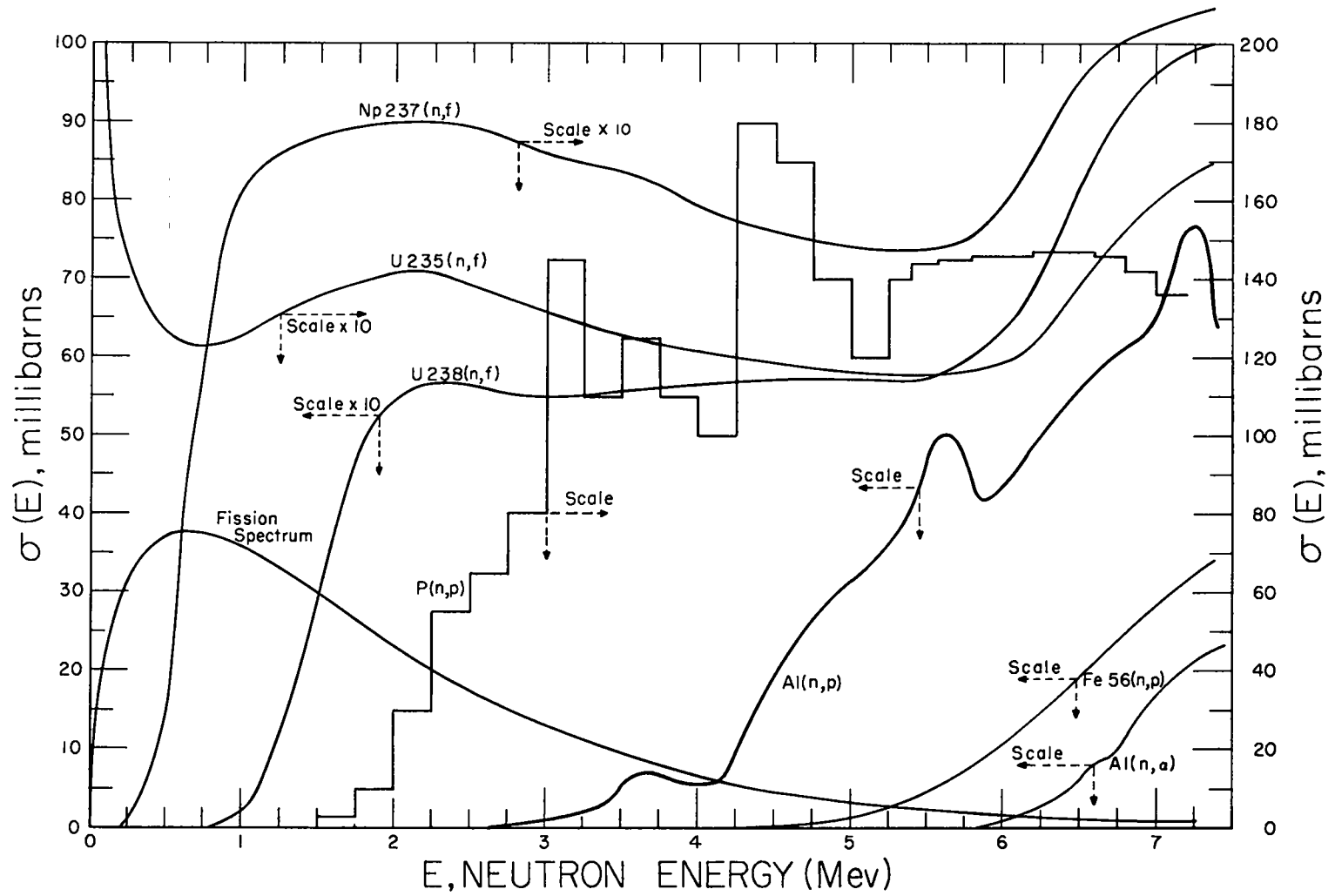


Fig. 1-1: Fundamental detector cross sections, the basis for all spectral analysis. The $P(n,p)$ cross section is plotted in histogram form because of severe structure which is not precisely known. $Cu63(n,2n)$ appears separately, along with experimental measurements, because of its importance and as an illustration of the kind of accuracy to be associated with these cross sections.

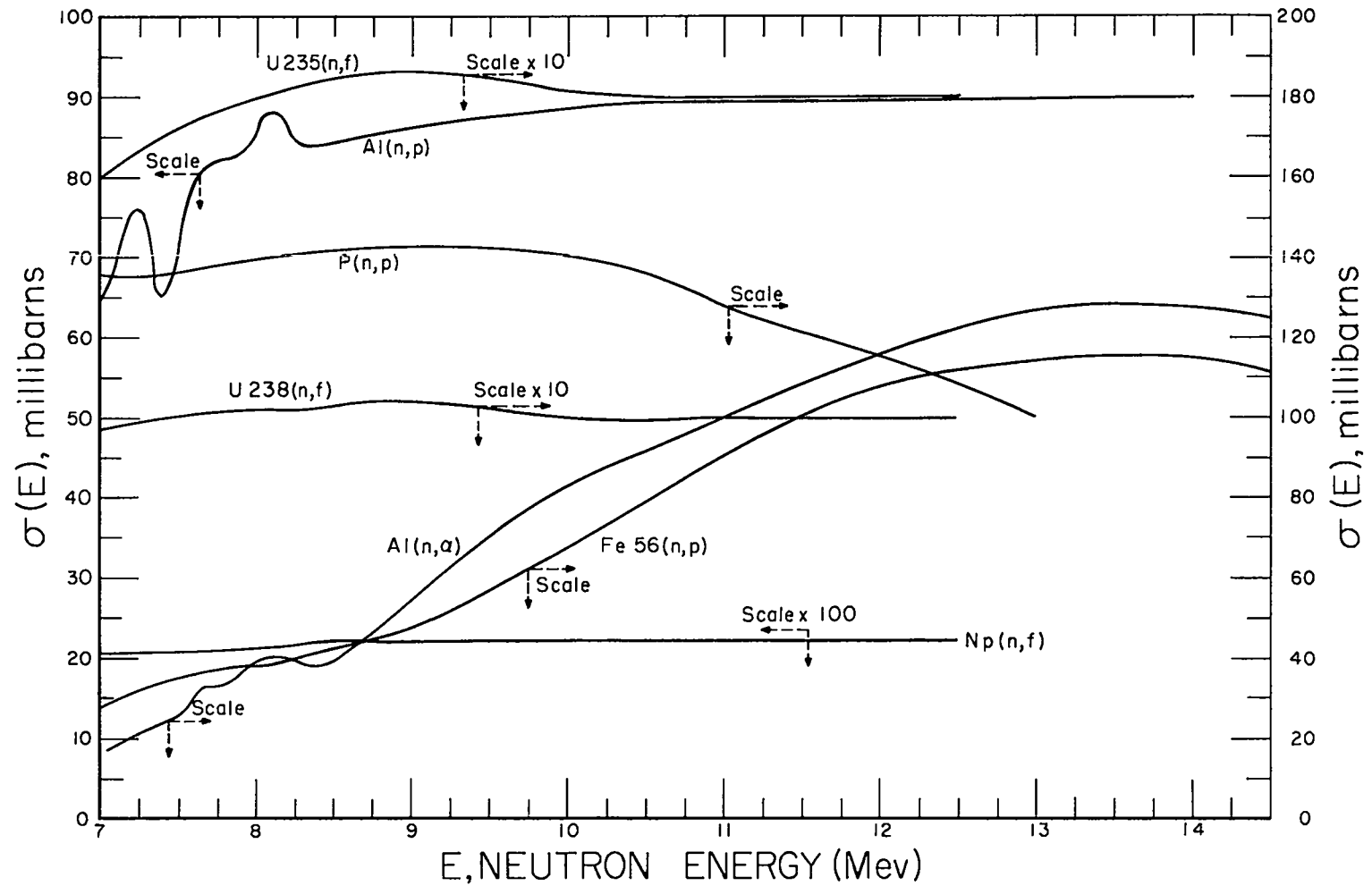


Fig. 1-1: Continued

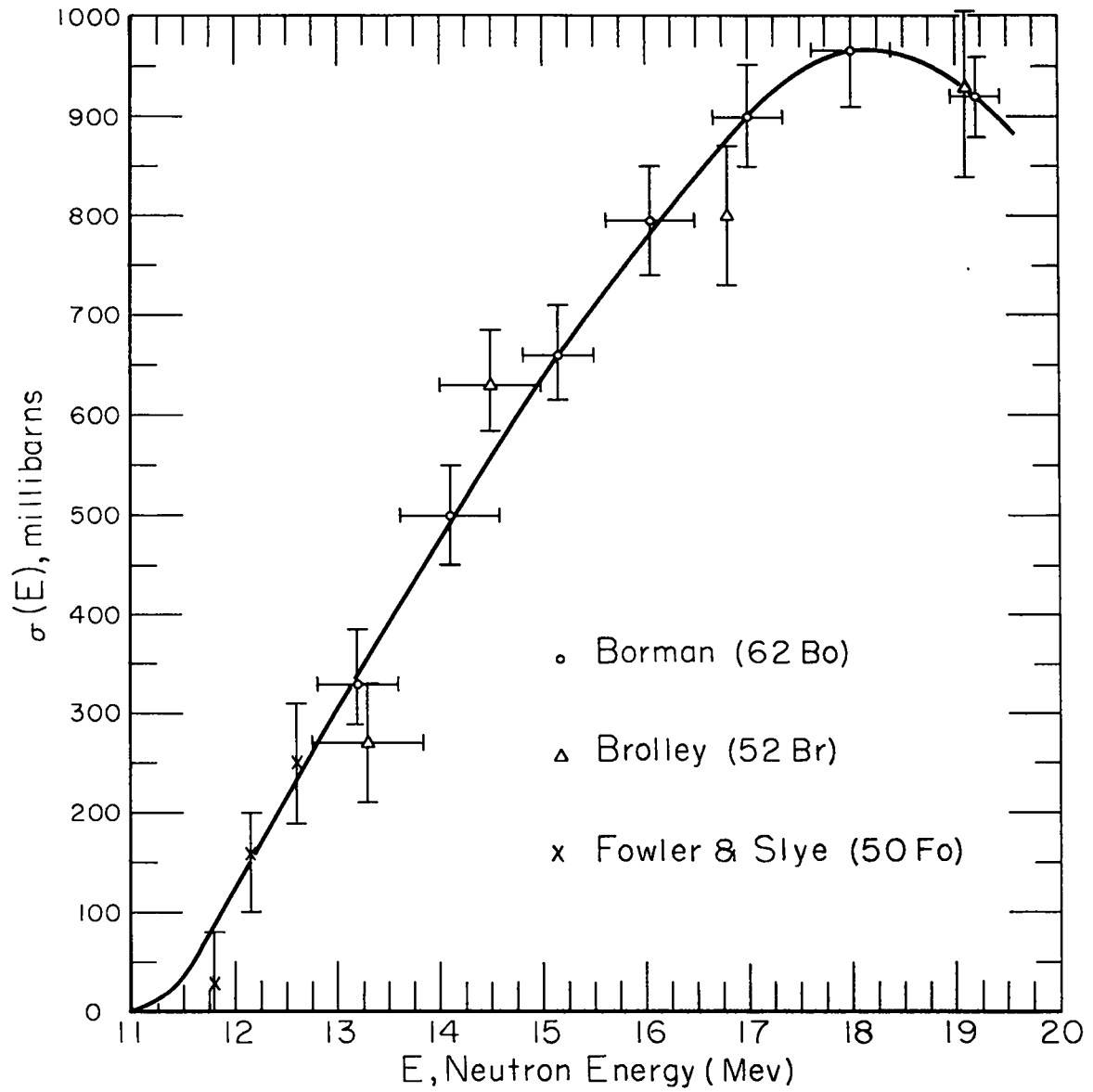


Fig. 1-1: Continued

Los Alamos Van de Graaff (see Chapter 5).

Response functions for each detector in the U235 fission spectrum, $\sigma(E)E^{1/2} \exp(-E/1.29)$, appear in Fig. 1-2 along with the mid-response energies and response ranges. The great overlap of detector response indicates that spectral sensitivity will depend markedly upon which detectors are compared. Fig. 1-2 also illustrates the importance of the initial rise of the excitation function when these detectors are applied to a spectrum decreasing rapidly with energy.

1.7 Experimental Application

A reliable counting system is one of the main factors upon which spectral analysis depends, and the necessary effort was put into designing a versatile, high-stability counting system especially for direct counting of activation detectors. The final system, a small-volume, windowed, methane-flow proportional counter provides for variable sample positioning and shielding; Appendix 1 discusses this development and specifies the final design and operating characteristics. Two identical systems are in operation along with associated automatic readouts and computer processing.

Counting data are analyzed with a least-squares code for IBM 704 computers (61Ch) which, after background and

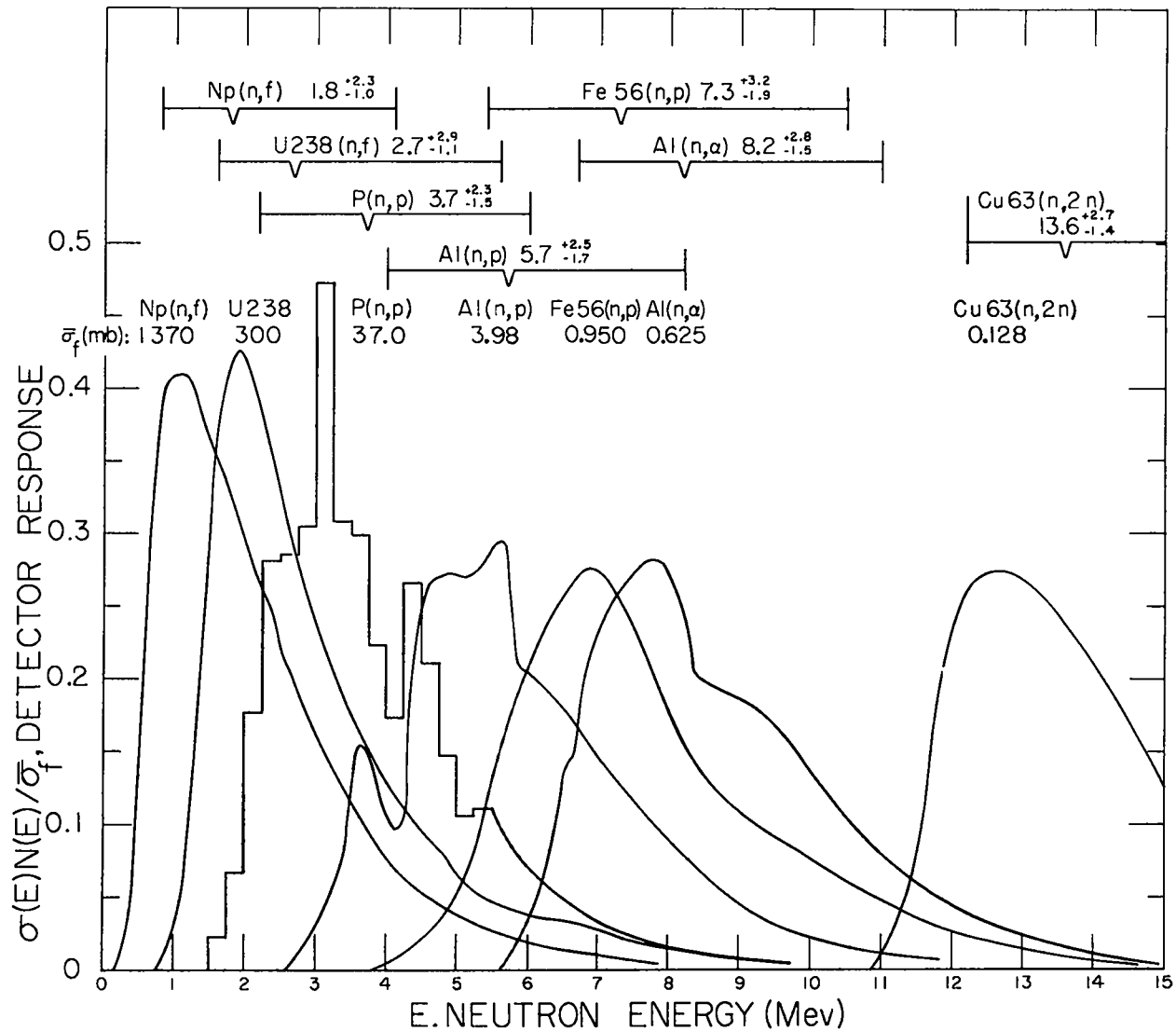


Fig. 1-2: Detector response functions for the fission spectrum normalized to unity. Identification of each curve appears above the maximum along with the average fission-spectrum cross section computed with $N(E) \sim E^2 \exp(-E/1.29)$. Brackets and labels at the top indicate detector response range with a break at the mean response energy.

counter loss correction, fits the appropriate number of exponentials to the data. A power law (for fission decay over short intervals) as well as tabulated functions (for long time fission decay) may also be applied to counting data. The code will fix any combination of abundances and decay parameters, a useful feature permitting consistent treatment of results, and convenient removal of competing activities. Print-outs from the computer record deviations of individual counts along with a final χ^2 -test on the fit. In the computer analysis, counts which did not agree with the fitted exponentials to better than three standard deviations were discarded. This seemed justified in view of the large number of counts on a single detector disk (as many as fifty) and the manifold possibility of gross deviation due to malfunction of scalers, clocks, and automatic readouts, or short term drifts. Such counts were infrequent and rarely exceeded two in a single set of counts.

Fission detector decays are straightforward: aluminum shields reduce the response to capture activities by a large factor relative to the fission product activity (> 500 for U238); and, for all spectra considered here, the n,p and n, α activities in the aluminum cans are sufficiently reduced so as to require no correction. For U238 and Np237 a fixed power law is fit to the counting data and

the counting rate at sixty minutes after shutdown obtained. This is the counter response for the U238 and Np237 fission detectors. For the U235 fission detector a similar procedure applies, except that the response time is 120 minutes after shutdown and the activity equivalent to 6% U238 impurity is subtracted to yield the final counter response. The latter comes directly from the counter response of the U238 detector.

Phosphorous (n,p), Iron56 (n,p), and Aluminum (n, α) likewise present no special problems as they are essentially free of competition over wide time ranges. A small correction for the aluminum can enclosing the phosphorous powder is conveniently obtained thru intercalibration with the aluminum detector. Counting data is first analyzed with decay constant free to check for the correct activity; then, with the decay constant fixed, the final counter response (initial counting rate) is determined.

Two competing activities, though small, must be considered in the Al(n,p) data processing: (1) Al(n, γ) contribution in the primary 15-60 minute data is ascertained from analysis of early counting data (8-15 minute), and entered as a fixed activity; (2) Al(n, α) activity is fixed according to long time counting data.

The problem of competing activities in Cu63(n,2n) is the most serious of all and only its well known excitation function plus important energy response region make it

worth the effort of extraction. A 0.032" aluminum shield easily removes almost all of the capture activity in Cu63, and the remainder is determined by applying the shield factor (0.033) to long time unshielded counts. There is no appreciable photoneutron yield below 20 Mev photon energy (48Ba) so that fission spectrum applications are not affected. The half percent Cu65 impurity, however, results in a 5 minute capture activity which for fission spectrum work contributes up to 25% of the counting rate during the relevant time interval. With no possibility of shielding this activity, an indirect measurement of its contribution is necessary and carried out by means of a physically identical enriched Cu65 disk irradiated simultaneously with the Cu63. The intense Cu65 activity is easily obtained and verified with just a few counts. A thermal irradiation of both disks gives an experimental ratio of the Cu65(n, γ) activity between disks of 0.00466 (a thirty percent discrepancy with specified Cu65 concentration in the Cu63 isotope — see Table 1-2). With this technique, aided by machine computations, the 9.7 minute (n,2n) activity is successfully isolated.

To complete the experimental specification of these detectors a word must be said about beta absorption in the detector disks; this can be important when there is significant spatial variation of neutron flux over the thickness of a detector so that a mean detector position is affected

by the transmission of the radiation that is counted. Curves of transmission vs depth were obtained experimentally by a simple self-shielding technique for each of the detectors described in Table 1-2, and the counters as described in Appendix 1. From these plots, transmission factors, or more accurately effective source strengths, were formed for five equal zones of detector thickness. With physical thicknesses normalized to unity, Table 1-3 lists the effective source strengths for each zone. Absorption by the aluminum can which enclose both the phosphorous and neptunium detectors has been included.

Table 1-3: Detector Activity Transmission Factors

<u>Thickness</u>	<u>P</u>	<u>Al(n,p)</u>	<u>Fe,Cu63</u>	<u>Al(n,α)</u>	<u>Np</u>
0 - 0.2	0.29	0.32	0.36	0.34	0.42
0.2 - 0.4	0.23	0.24	0.23	0.24	0.28
0.4 - 0.6	0.20	0.19	0.17	0.18	0.17
0.6 - 0.8	0.15	0.14	0.13	0.14	0.08
0.8 - 1.0	0.13	0.11	0.11	0.10	0.05

The final set of counter responses (i.e. counting rates of each detector activity at a specified time) after correction for relative flux at each detector may be combined in pairs to form relevant response ratios. Measurement of response ratios for the three fission spectra will be described in Chapter 3, and spectral information extracted from the experimental results in Chapters 4 and 5.

CHAPTER 2

PRODUCTION OF PURE FISSION SPECTRUM NEUTRONS

2.1 Conventional Fission Converters

The conventional converter or fission plate technique for obtaining fission spectrum neutrons is described by Hughes (^{53}Hu): slow neutrons from a thermal column are converted to fission neutrons in a plate of fissile material located close to the reactor shield. Experiments may be carried out right at the plate or a distance away. Disadvantages of this method are: (1) uncertainty as to the purity of the fission spectrum obtained due to scattering from the massive structures nearby as well as material close to the fission plate—canning substance, support materials and the fission plate itself; (2) radiation hazard which usually precludes other activities in the vicinity; and (3) large intensity reduction over that available inside the reactor. The unpleasantness connected with externally produced fast neutrons is well illustrated by preliminary fission spectrum work carried out with a fission

plate at the Los Alamos Water Boiler. Irradiating late at night to avoid interference with normal operations, complaints were still heard because activity induced in the magnet of a beta-ray spectrometer some seventy feet away from the fission source made it unusable the following day!

For experiments which do not require collimation or a large volume for the measuring device, e.g. activation measurements, a fission spectrum inside the pile will overcome the last two objections. Such a proposal has been made by Meuhlhouse of the National Bureau of Standards (^{59}Mu) suggesting the use of heavily loaded cylindrical fuel elements with a boron lined cylindrical cavity.

2.2 Cavity Fission Spectrum

A different cavity arrangement, which also overcomes the problem of background, proves successful for fission spectrum studies. If a small disk of fissionable isotope is at the center of a rather small spherical cavity inside a large thermalizing medium fed by a reactor core, only a small fraction of the fission neutrons produced will return to the disk. One may compute the fraction returning as well as its energy spectrum by straightforward multigroup transport or Monte-Carlo techniques. Such calculations indicate that if cadmium covered detectors be placed such that the average fission source to detector distance is not

greater than about one tenth the cavity diameter the background due to scattered neutrons will be almost negligible for any high-energy detector and small for low energy fission detectors. The reactor neutrons, of course, must be well thermalized as in any fission converter system.

In Appendix 3 a discussion of Monte-Carlo calculations, involving 3, 4, and 10 inch diameter cavities in 24 and 36 inch diameter reflectors of D_2O (^{59}Ca), presents normalized return spectra and total return fluxes. According to the results a 10 inch thickness of D_2O surrounding a cavity is essentially infinite.

Recently, source calculations with Carlson's DSN Multigroup Transport Code (^{58}Ca) have become routine, making it possible to verify the Monte-Carlo results and extend cavity return calculations to include other diameters as well as graphite and H_2O reflectors. These results, which are also detailed in Appendix 3, appear in Figure 2-1 as the normalized return spectrum above 0.4 ev for a 4" diameter cavity in a D_2O reflector—the primary arrangement for the fission spectrum studies. The complete distribution extends down to thermal energies as may be noted from Table A3-3. We see that less than 4% of the flux returning from a fission spectrum source is above 1 Mev, though some 40% of the return is greater than 0.1 Mev. According to Table A3-3 the total return flux above 0.4 ev

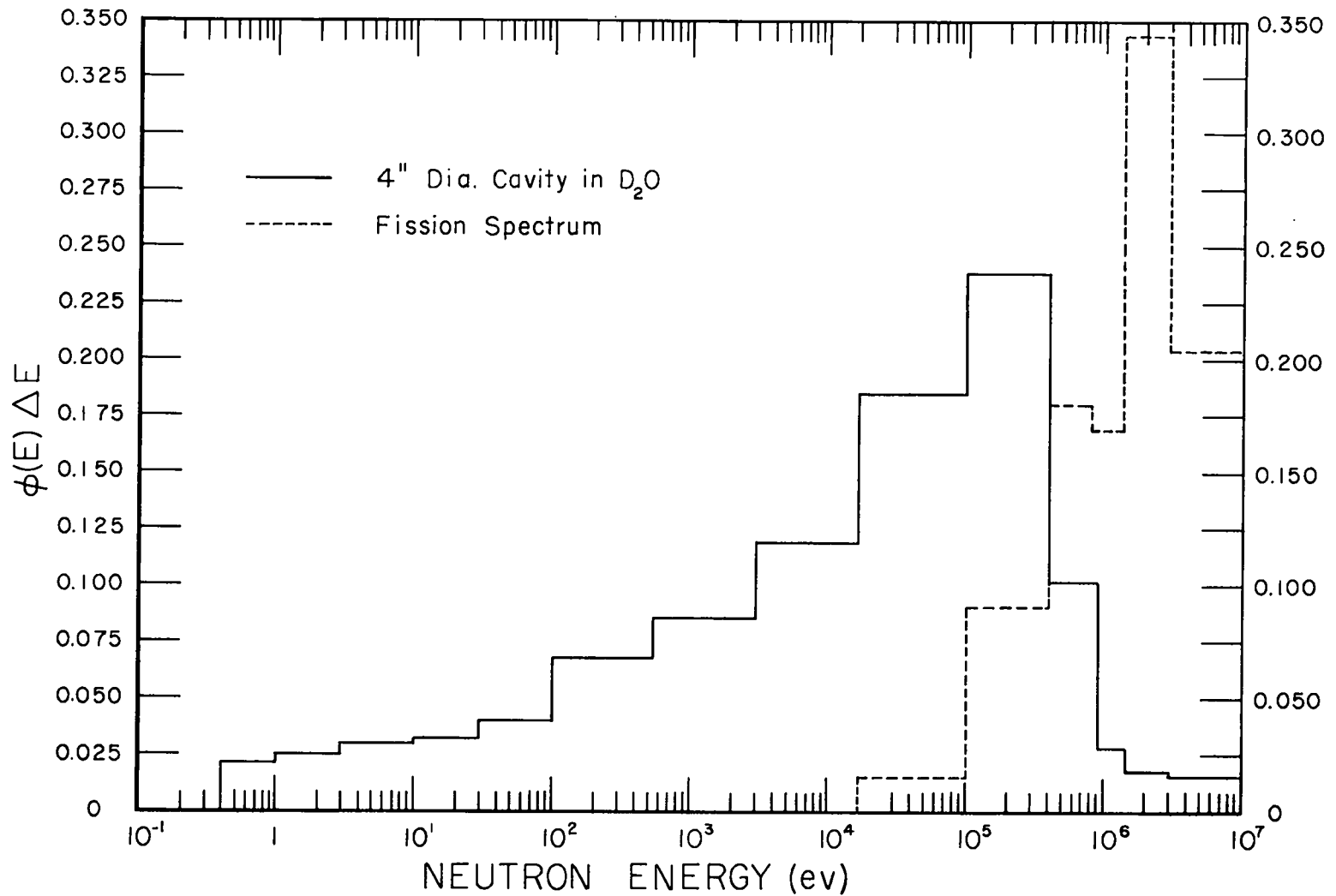


Fig. 2-1: Sixteen-group representation of spectrum of neutrons returning to the center of a spherical cavity containing a fission neutron source. The entire spectrum extends to thermal energies, but is cut off at 0.4 eV under the assumption that detectors will be cadmium covered. The spectrum is normalized to unity as is the U235 fission spectrum included for comparisons.

for a unit fission neutron source is $0.004 \text{ neut/cm}^2 \text{ sec}$ so that at the center of the 4" diameter cavity we can expect a background of less than 1% for high-energy detectors which are within 1 cm of the source.

Though the neutrons below 0.4 ev may be removed by shielding detectors with cadmium, the continuous distribution over the rest of the energy range must be considered when using a low energy detector like U235, and nonnegligible backgrounds will be common. The fraction of the activity induced in a detector by returning source neutrons is given by

$$\text{Background} \simeq [\varphi_{\text{return}}] 4\pi \bar{Z}^2 \frac{\bar{\sigma}_{\text{return}}}{\bar{\sigma}_{\text{fiss. spec.}}}, \quad 2-1$$

where \bar{Z} is the average source-detector distance, φ_{return} the total central return flux, $\bar{\sigma}_{\text{return}}$ the average detector cross section for the return spectrum, and $\bar{\sigma}_{\text{fiss. spec.}}$ the average detector cross section for the fission spectrum. When a background estimate is required therefore the return spectrum must be known, and in addition, an estimate or calculation of the average source to detector distance becomes necessary. Clearly it is advantageous to reduce \bar{Z} by using small, closely spaced source-detector assemblies. The determination of $\bar{\sigma}_{\text{return}}$, using calculated return spectra of Appendix 3, is straightforward, except in the case of detectors with resonance response which can

give rise to appreciable background from resonance activation. This problem is treated briefly, later on, for the U235 fission detector.

Details of detector geometry and backgrounds will be discussed in terms of the actual experimental arrangement described below.

2.3 Cavity Arrangement and Source-Detector Assembly

The fission spectrum system was built around the small, source-reactor Hydro (60Ch), consisting of a water-cooled cylindrical core of U235 metal (6" diameter, 5" high) surrounded on the side and bottom by a six-inch thick water reflector.

For these measurements the exposed upper surface of the core was covered with two 5/8"-thick plates of normal uranium, 1" of steel, 2" of lead, and 2" of nickel to reduce initially the energy of core neutrons by inelastic scattering. Placed on top, a 31" diameter stainless steel tank containing D₂O to a height of 37½" formed a "thermal column." A sketch of the system in Fig. 2-2 shows a 4" diameter glass-walled spherical cavity (1/32" thick glass) at the tank center and accessible from the top. Hydro operating at about 1.5 kilowatts produces a thermal flux of roughly 2.5×10^9 neut/cm² sec at the center of the cavity, and a cadmium ratio for U235 fission of about 800.

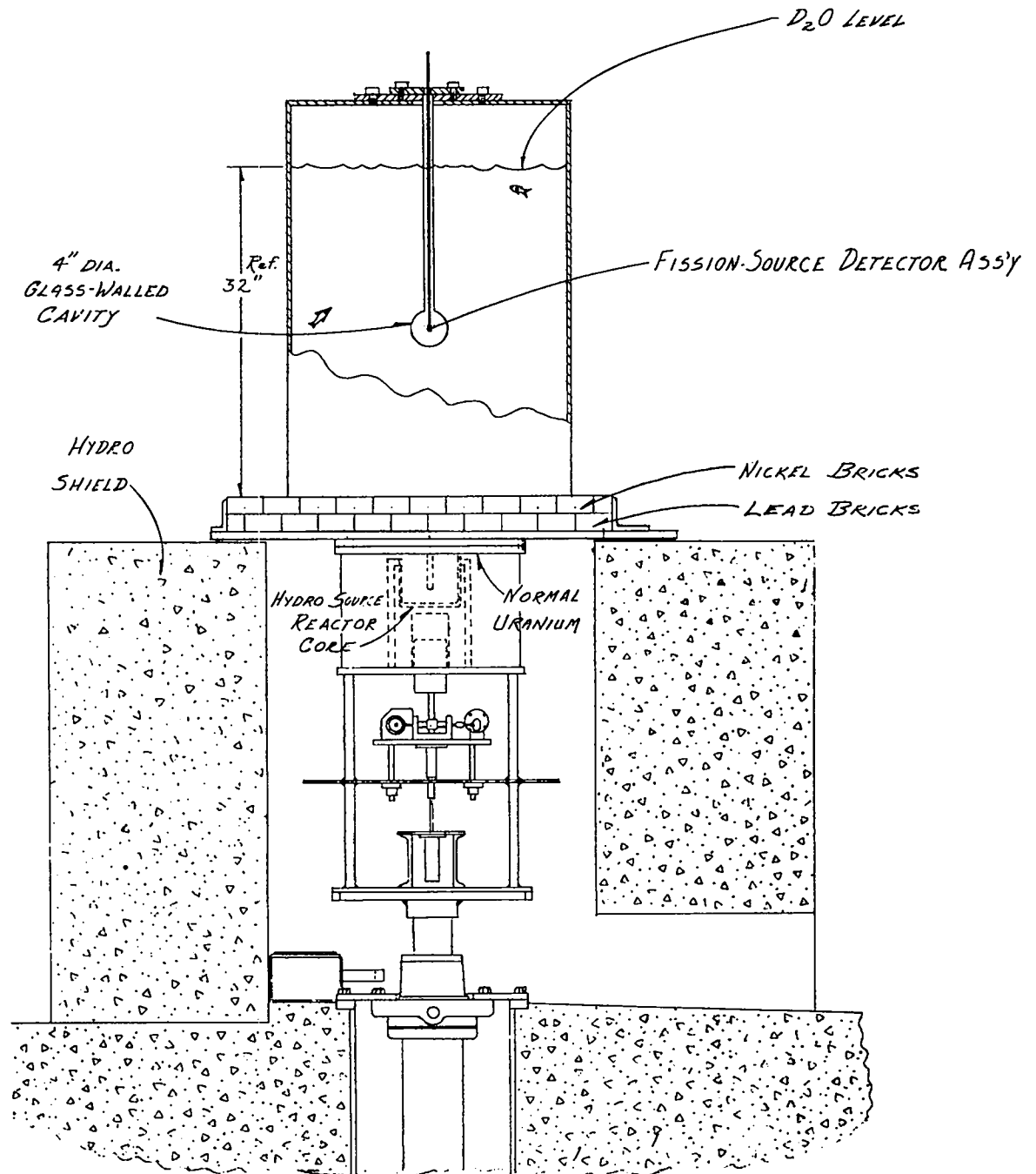





Fig. 2-2: Hydro source reactor within its shield, and cavity fission spectrum system above. Neutrons from Hydro, thermalized in the D_2O , diffuse into the cavity and are converted into fission spectrum neutrons by the two source disks in the ends of the source-detector assembly—see Fig. 2-3.

The source-detector assembly, suspended at the center of the cavity, employs coaxial disk geometry combining the advantages of simple fabrication with symmetry and versatility. Fig. 2-3 is a cross sectional view of a typical source-detector assembly. The detector disks surrounded by 0.030" thick cadmium are exposed to fission neutrons from the two source disks outside the cadmium. All three cadmium pieces, two disks and one cylinder, were well fitted and the detectors centered to eliminate activation from any residual thermal neutron leakage. The increased spacing of source disks shown in the figure reduces position sensitivity by flattening the flux distribution at the detectors. The thermal flux diffusing into the cavity is not isotropic and gives rise to unequal source strengths for the upper and lower source disks. Interchange of each source disk with its cadmium end plate makes possible a simple measurement of the epithermal background of reactor neutrons with the same intervening materials.

Perturbation of the fission neutrons by the source-detector assembly itself was initially estimated by hand, and on the basis of a 0.3" thick solid cadmium cylinder with a transport cross section of $3.6b$, and an inelastic cross section of $1.5b$ corresponds to 7% elastic and 3% inelastic scattering. The elastic scattering does not

MATERIAL IDENTIFICATION	
ALUMINUM	
CADMIUM	
FISSION SOURCE	

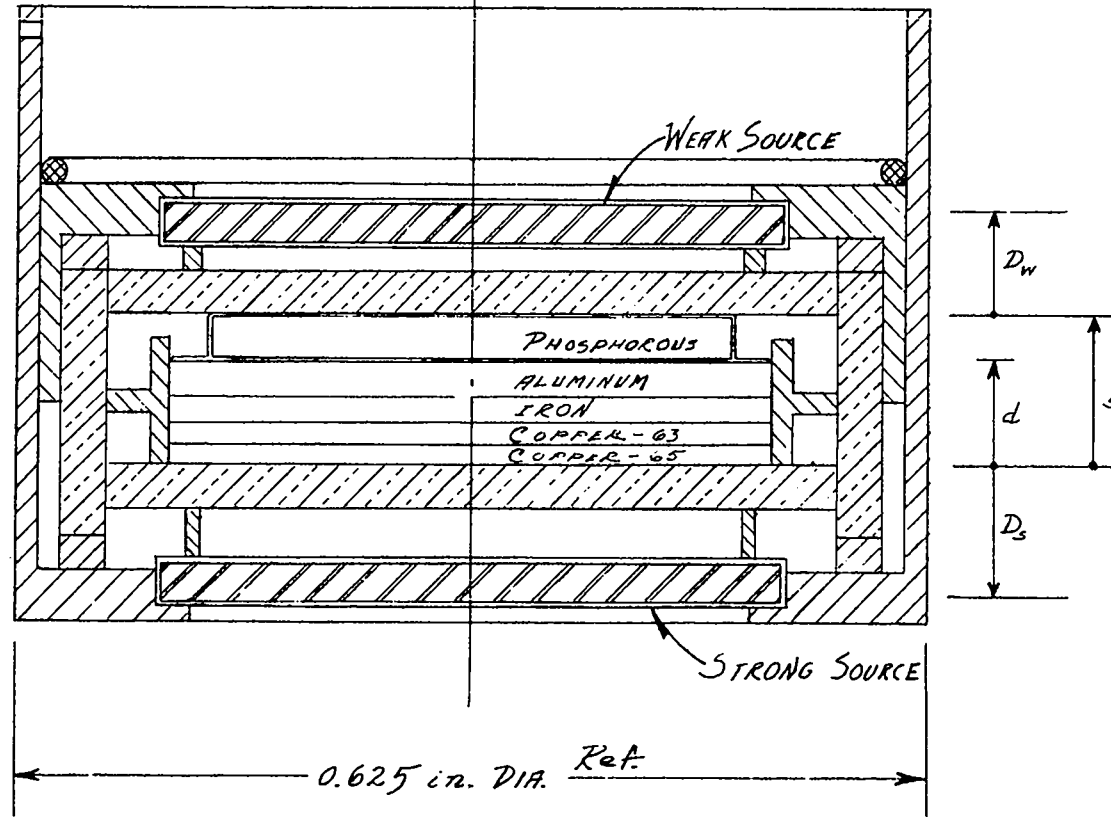
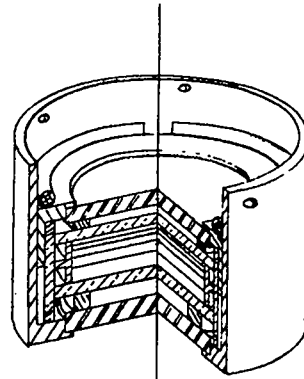


Fig. 2-3: Source-detector assembly showing detector disks, in a typical case, surrounded with cadmium and sandwiched between fission source disks. Anisotropic thermal flux gives rise to unequal source strengths distinguishing strong and weak source disks below and above the detector disks.

produce any direct spectral perturbation as there are no moderating materials present; but the inelastic scattering, by removing neutrons from the region of high-energy detector sensitivity, will affect spectral indices which compare the high and low energy detectors.

Recently, a more comprehensive but still qualitative estimate was obtained through a simple DSN transport computation involving a 1.3 cm diameter iron sphere with a fission spectrum source near the center. Using the sixteen-group cross sections of Ref. 61Ha, a maximum perturbation of the spectrum results at the surface of the sphere as follows:

Table 2-1: Fission Spectrum Perturbation By a
1.3 cm Diameter Sphere of Iron

<u>Energy No.</u>	<u>Group Range</u>	<u>Pure Fiss. Spectrum</u>	<u>Spectrum At Sphere Surface</u>
1	3-∞	0.204	0.192
2	1.4-3	0.344	0.334
3	0.9-1.4	0.168	0.174
4	0.4-0.9	0.180	0.188
5	0.1-0.4	0.090	0.097
6	0.017-0.1	0.014	0.0147
7-16	0.00-0.017	0.000	0.000

With this arrangement, equivalent to the actual source-detector assembly in total number of atoms present, we

see that some 3% of the spectrum is shifted to below 1.4 Mev. This small disturbance will not affect the comparison of spectra, but some absolute spectral indices of Chapter 5 will require corrections of this order.

Three nearly identical pairs of source disks were used, U235, U233, and Pu239, and may themselves be counted to obtain relative source strengths; total source strength of a source pair in the 4" diameter cavity with Hydro at ~ 1.5 KW is about 3×10^9 neut/sec, and the upper to lower source strength ratio ~ 0.6. The table below lists source specifications:

Table 2-2: Source Disk Specifications

<u>Source</u>	<u>Source Diameter</u>	<u>Source Thickness</u>	<u>Wt.</u>	<u>Can</u>	<u>Impurities</u>
U235	0.455"	0.030"	1.45gm	0.001"A1	5% U238 1% U234
U233	0.454"	0.034"	1.44gm	0.010"Ni	----
Pu239	0.455"	0.035"	1.35gm	0.010"Ni	5% Pu240

The fission source density in these disks decreases rapidly with depth, and an estimate of the density variation is necessary to accurately calculate the flux profile in the region of the detectors as well as to ascertain the average source to detector distance for background determinations. For isotropic incidence of thermal neutrons the density as function of depth t is

$$\rho_i(t) = [\exp(-t/\lambda) + t/\lambda E_i(-t/\lambda)],$$

where $E_i(-X) = - \int_x^\infty \exp(-\alpha)/\alpha \, d\alpha$; and $\lambda =$ mean free path for thermal fission. The final determination of the mean source depth, $0.010'' \pm 0.002$ for all three fission sources, took into consideration: (1) anisotropy of incident thermal neutrons, (2) dilution by nonthermal fissioning isotopes, (3) flux hardening (simple 10% reduction of cross section), and (4) distribution of the source in the specific source-detector geometry. Fortunately, all but the geometry factor affect the result by $0.001''$ or less.

2.4 Flux Profiles and Detector Backgrounds

The formation of spectral indices later on will require a knowledge of the flux profile between the two source disks, and also an estimate of the return background for each detector. Both problems involve a calculation of the average source to detector distance for a coaxial disk geometry, or equivalently, the effective flux incident on a detector disk coaxial with a disk source. This general problem for a thin detector is carried out in Appendix 2.

For the arrangement we are considering, the effective flux versus separation distance (in units of detector radii) given in Fig. A2-2, Appendix 2, is applicable with

only a small correction for edge enhancement of the source due to neutrons incident on the edge of the source disks. Except for the phosphorous and fission detectors, source and detector radii are all equal: $a = r_s = 0.225" = 0.57\text{cm}$; so the abscissa of Fig. A2-2 is read at $Z/0.57$ and the corresponding ordinate divided by $1/(0.57)^2$ to obtain the flux. The effective flux vs. separation distance, obtained in this way, is shown by the solid line in Fig. 2-4 and forms the basis for generating the flux variation in the region between the sources.

The flux from the strong source is represented in Fig. 2-4 such that the abscissa Z is the distance ($D_s + d$) shown in Fig. 2-3. The curve of flux from the weak source is an appropriate segment of the strong-source curve, properly oriented, with ordinate reduced by the ratio of source strengths. In the particular case illustrated by Fig. 2-4, which applies to U235 sources, the location of the weak-source curve corresponds to the following dimensions:

D =	Source	- Source	- Source	+ Source	+ Cadmium
	thk.	Casing	Depth	Spacer	Disk
$D_s =$	0.036	- 0.003	- 0.010	+ 0.035	+ 0.031
					= 0.089"
$D_w =$	0.036	- 0.003	-0.010	+ 0.018	+ 0.031
					= 0.072"

Source Strength Ratio = 0.57

Detector Height, $s = 0.112"$.

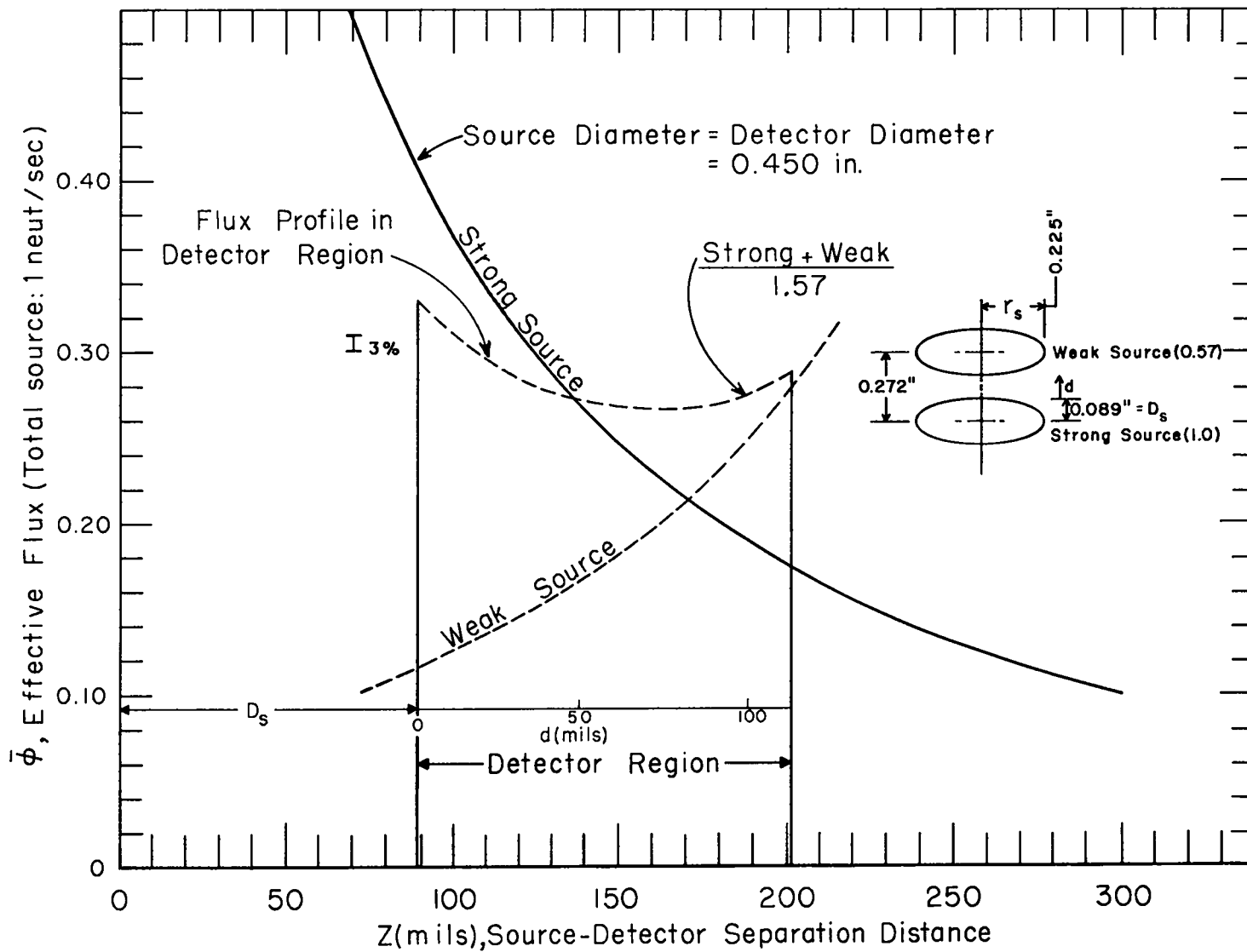


Fig. 2-4: Effective flux distribution for detector disks between twin coaxial U235 source disks of unequal source strengths. Solid line shows the flux vs. separation distance for a single source and detector disk.

The final composite flux profile between U235 disks, a sum of the individual curves adjusted so that total source strength = 1 neut/sec, shows a maximum flux variation of ~ 20% over the region where the detectors are located.

Effective flux profiles for important source and detector arrangements appear in Fig. 2-5, and were generated as outlined above from the single curve of Fig. 2-4 using applicable assembly dimensions. The flux profile obtained experimentally from the activation of iron disks is seen to agree well with computation. The position sensitivity for the primary detector disks, shown in a typical arrangement in the figure, varies from essentially zero to as high as 0.4%/mil for the Cu63 detector.

The phosphorous and fission detector disks with smaller radii (0.190") are exposed to effective fluxes some 8% higher than appear in Fig. 2-5, though the flux profiles are essentially the same. When the phosphorous detector is irradiated with the other high-energy detectors of larger radii, the full 8% bias to higher flux represents a significant increase in the geometry correction and associated uncertainty.

The precision spectral comparisons of the next chapter will require a careful application of these flux profiles to the detector arrangements, even to the point of correcting for the perturbation of effective position due to beta absorption.

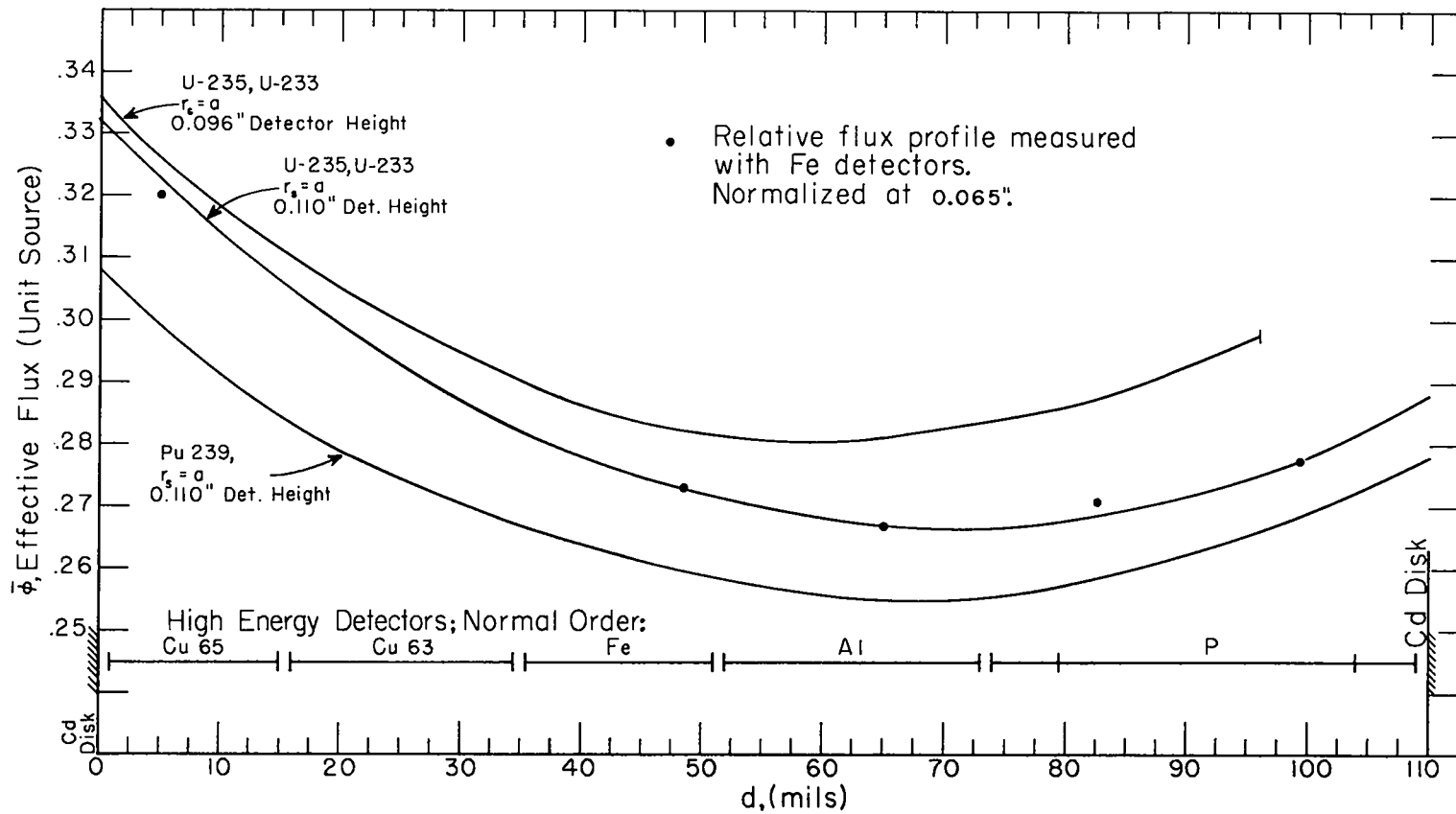


Fig. 2-5: Flux profiles over the detector region for the three fission sources and two detector set heights. A typical detector set assembly is indicated. The abscissa is measured from the inner surface of the cadmium disk nearest the strong source—see Fig. 2-3.

We now can estimate detector backgrounds due to fission neutron return by applying Eq. 2-1:

$$\text{Background} \sim [\varphi_{\text{return}}] 4\pi\bar{Z}^2 \frac{\bar{\sigma}_{\text{return}}}{\bar{\sigma}_{\text{fiss.spec.}}}$$

The factor $4\pi\bar{Z}^2$ is simply the reciprocal of the effective flux; and, referring to Fig. 2-5, let us choose 3.5 as a representative value. Multiplying by the total return flux value of 0.0042 from Table A3-3 of Appendix 3, we have

$$\text{Background} \sim 0.015 \frac{\bar{\sigma}_{\text{return}}}{\bar{\sigma}_{\text{fiss.spec.}}}$$

Average fission cross sections are listed in Table 5-5, and the average return cross sections, U235 excepted, may be estimated from the return spectrum in Table A3-3, column 3, and the cross section curves of Fig. 1-2. From the results, in Table 2-1 below, one sees that the small $\bar{\sigma}_{\text{return}}$ for detectors with thresholds leads to negligible return backgrounds.

Table 2-3: Fission-Neutron Return Background For 10 cm Cavity In a D₂O Reflector

Detectors	σ_{return}	$\frac{\bar{\sigma}_{\text{return}}}{\bar{\sigma}_{\text{fiss.spec.}}}$	Background ($\bar{\varphi} = 0.30$)
P31 (n, p)	0.002b	0.07b	0.06%
U238(n, f)	0.018	0.06	0.05%
Np237(n, f)	0.21	0.15	0.15%
U235(n, f)	9	7.0	10%

For the low energy U235 fission detector the background is not negligible and a more careful estimate of $\bar{\sigma}_{\text{return}}$ is necessary. Reference (61Ha) gives, for U235 and infinite dilution, sixteen-group cross sections which correspond to Table A3-3. The resulting average cross section of $10b$ in the return spectrum yields an 11% return background for an infinitely thin U235 fission detector. For the 0.003" thick detector disk used in these measurements self-shielding of resonance neutrons reduces the return background to 10%, the value in Table 2-1. As the background is based on computation alone with no direct experimental confirmation, we attach to it an uncertainty of one-quarter.

In Chapter 5 this careful estimate of the return contribution will yield, for the first time we believe, the U235 fission detector response in the U235 fission spectrum, under conditions of known background and spectral purity. Combined with the U238 fission response, the long sought spectral index $\bar{\sigma}(U235(n, f)) / \bar{\sigma}(U238(n, f))$ in the fission spectrum will be specified experimentally with a realistic appraisal of the uncertainties involved.

CHAPTER 3

FISSION SPECTRA COMPARISON MEASUREMENTS

3.1 Experimental Procedure and Processing of Counting Data

Having described the activation detectors along with their experimental application in Chapter 1, and the method for producing pure fission neutrons in Chapter 2, the procedure followed for the comparison measurements may be conveniently outlined. For the primary irradiations the small source-detector assembly in Fig. 2-2 was mounted at the center of a four inch diameter glass-walled cavity in the heavy-water thermal column. The eight detectors which form the basis of the spectral comparison are divided into a high-energy set: P, Al, Fe, Cu63, Cu65; and a fission set with a phosphorous monitor: P, Np237, U238, U235. Each set sandwiched between the fission-source disks and surrounded with cadmium (see Fig. 2-3) was irradiated separately, and subsequently, individual detector disks counted in one of the two identical counting systems described in Appendix 1. Computer processing of the automatically recorded counting data followed the method

detailed in section 1.7: fitting by least-squares the necessary number of decaying exponentials, or, in the case of the fission detectors, a decaying power law.

In line with the importance attached to maintaining strict procedures, mentioned in Chapter 1, we might list some details of method which contribute to the precision of the final results. Detector disks, after background counting, were assembled in the same orientation with respect to the strong source disk, and all other parts of the assembly likewise identically placed and oriented. Inserted between detector interfaces of dissimilar materials, 0.001" thick plastic disks eliminated inter-detector contamination. This effect due to recoiling nuclei, has been observed for detectors in contact which differ greatly in specific activity. Final thickness of the assembly was routinely checked and varied by less than 0.005" from the sum of the component parts.

Standard irradiations, of nearly rectangular profile and 20 min duration were measured from $1/e$ of full power. With such a starting time, variations in the approach to the final power level can be shown to produce minimal variations in saturation effects. A positive pile period of 38 ± 2 sec for the start of the irradiation was maintained from 0.01 to $\sim 2/3$ of full power. Detector recovery about 5 min after shutdown made it possible to begin

counting at near 10 min after the end of the irradiation.

To reduce errors and simplify the task of counting, a schedule was developed which minimized foil changing by counting each detector in extended blocks of time. This proved particularly useful when making two irradiations in a single eight hour day. A map of this counting schedule appears in Fig. 3-1 and shows, for both counting systems, when each detector was counted, the counting interval, and the slot and shield used. Twin time scales for each counter are zeroed at the respective reactor shutdown times. The two fission sources themselves were counted at the indicated times with 1/8" lead shields to establish the relative source strengths.

The general treatment of counting data with digital computers in order to extract the counter response (i.e. the detector disk counting rate at some specified time) was described in section 1.7. Some specifics for this application are noteworthy. Statistical errors of total counts, Cu63(n,2n) excepted, were nearly always negligible; and all final data resulted in an acceptable χ^2 -test carried out by the computer as part of its routine of least-squares fitting. Counts during individual intervals which departed by more than three standard deviations were attributed to malfunction of the electronic system or readout and automatically discarded. Such events were rare occurring less than one time in fifty.

SCHEDULE FOR DAILY DOUBLE

I: FIRST IRR.- P, Al, Fe, Cu 63, Cu 65;
 II: SECOND IRR.- P, Np 237, U 238, U 235;

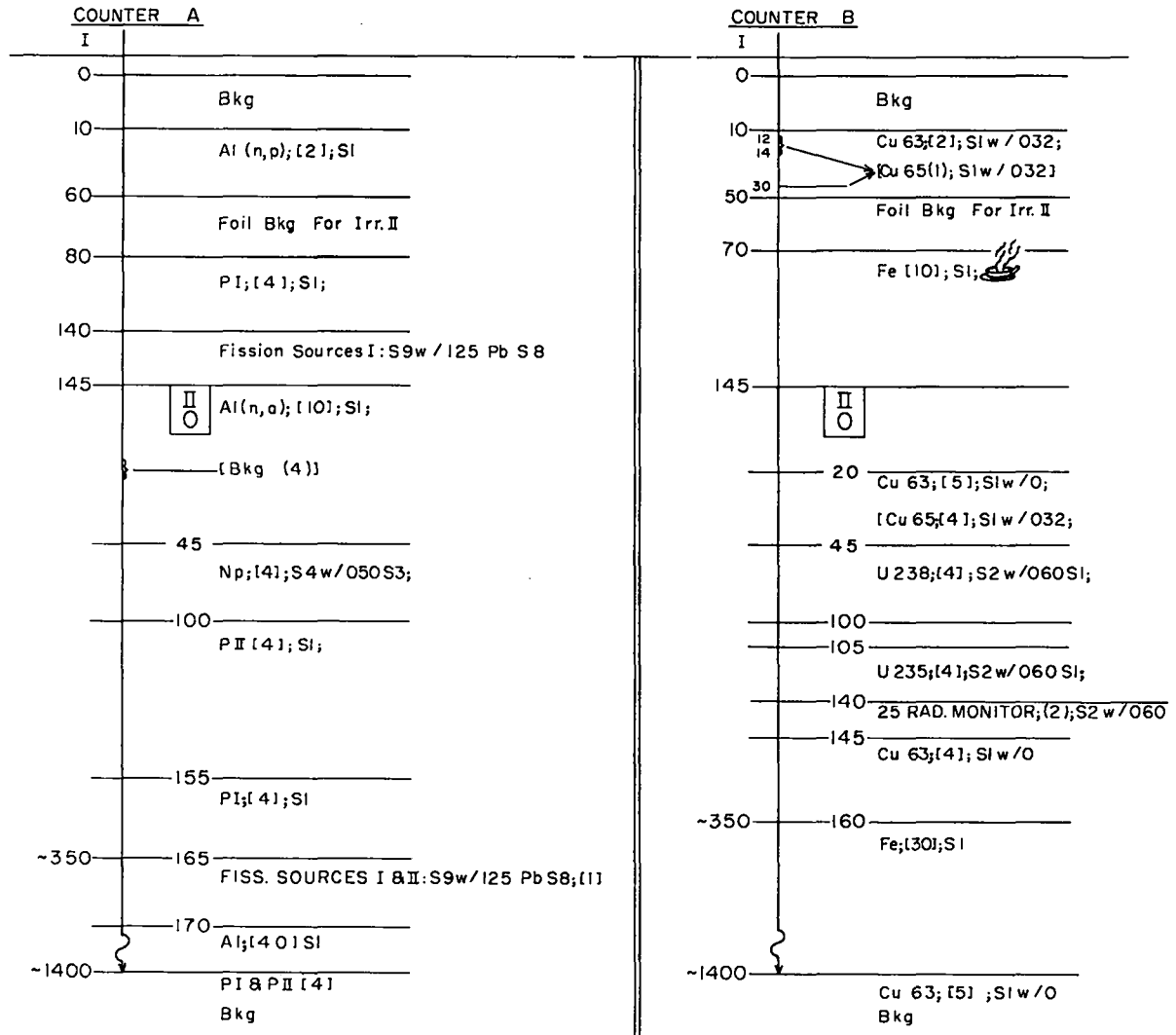


Fig. 3-1: Detector counting schedule for two daily irradiations using two identical counting systems. Twin time scales for each counter express the time after each shutdown in minutes. Detector disks to be counted, counting interval, slot, and shield are given for each block of time. Example: U235; (4); S2w/060Sl calls for counting the U235 detector disk for 4 minutes in slot 2 with a 0.060" aluminum shield in slot 1.

Typical counter responses for a total fission neutron source strength of 3×10^9 neutrons/sec are shown in Table 3-1.

Table 3-1: Typical Counter Responses For 20 Min. Irradiation at $\sim 3 \times 10^9$ neutrons/cm²sec

<u>Detector</u>	<u>Half-Life</u>	<u>Counter response (c/m)</u>
P(n,p)	157 min	7.7×10^4 (ICR)
Al(n,p)	9.5	2.0×10^5 "
Fe(n,p)	154	4.6×10^3 "
Al(n, α)	900	6×10^2 "
Cu63 (n,2n)	9.7	2.4×10^3 "
U235(n,f)	---	4.3×10^4 (120 m)
U238(n,f)	---	1.5×10^4 (60 m)
Np237(n,f)	---	3.0×10^4 (60 m)

It is interesting to note that computer processed data did not often result in significant improvement of a counter response hand calculated from a few counts during the counting period. (An exception is the extraction of the Cu63(n,2n) activity, which is quite time consuming when done by hand.) To some extent, when generous counting rates are available, computer processing only serves to identify poor counting data by disclosing unacceptable deviations.

Data were obtained from 24 fundamental arrangements

distinguished by: two sets of nearly identical detector disks divided into high-energy and fission groups as described above; two detector assembly orders designated normal and interchange; and three different fission sources—U235, U233, Pu239. The two assembly orders gave a composite check of the geometry calculation and of spectral invariance in the detector region by interchanging pairs of detector disks—high energy set, phosphorous and aluminum interchanged—fission set, phosphorous and neptunium interchanged.

3.2 Relative Flux Correction and Response Ratios

Before we can form detector response ratios a correction for relative flux at the detectors must be applied to the counter responses. The flux profile between the coaxial, twin source-disk geometry employed was developed in section 2.4 and Appendix 2; typical profiles over the detector region appeared in Fig. 2-5. Because of the precision attempted in these comparison measurements the final relative flux values assigned to each detector incorporate a beta absorption effect. This was touched upon at the end of section 1.7, and we may apply the transmission factors of Table 1-3 directly to weighting the flux variation over the thickness of each detector disk. The orientation convention for counting, which now becomes

necessary, was chosen as follows: the detector surface facing the strong source faces the counter window.

Figure 3-2 shows all the primary detector arrangements and corresponding effective flux profiles. The ordinate is the flux value for a total source strength of one neutron per second and a detector diameter of 0.450 inches; for the smaller diameter phosphorous and fission detectors, the ordinate must be multiplied by 1.075. The detector arrangements laid out in the figure show the normal and interchange order for each set; and relative flux values for each detector are specified with respect to phosphorous, which is common to both the high-energy and fission detector sets. Notice that the P:Fe interchange has its largest effect on the flux at the aluminum detector. Flux values are not given for two detectors: Copper 65, an auxiliary capture detector used in interpreting the $\text{Cu}63(n,2n)$ activity, is affected only slightly by the flux profile since most of its activation is due to epithermal reactor neutrons; U235 likewise has a large epithermal reactor background which makes it impossible to get a satisfactory fission spectrum response in this arrangement. Detailed measurements under different circumstances will be described in Chapter 5 where the U235 fission spectrum response is of more interest in determining the fission spectrum shape itself.

We may note that comparison measurements are not

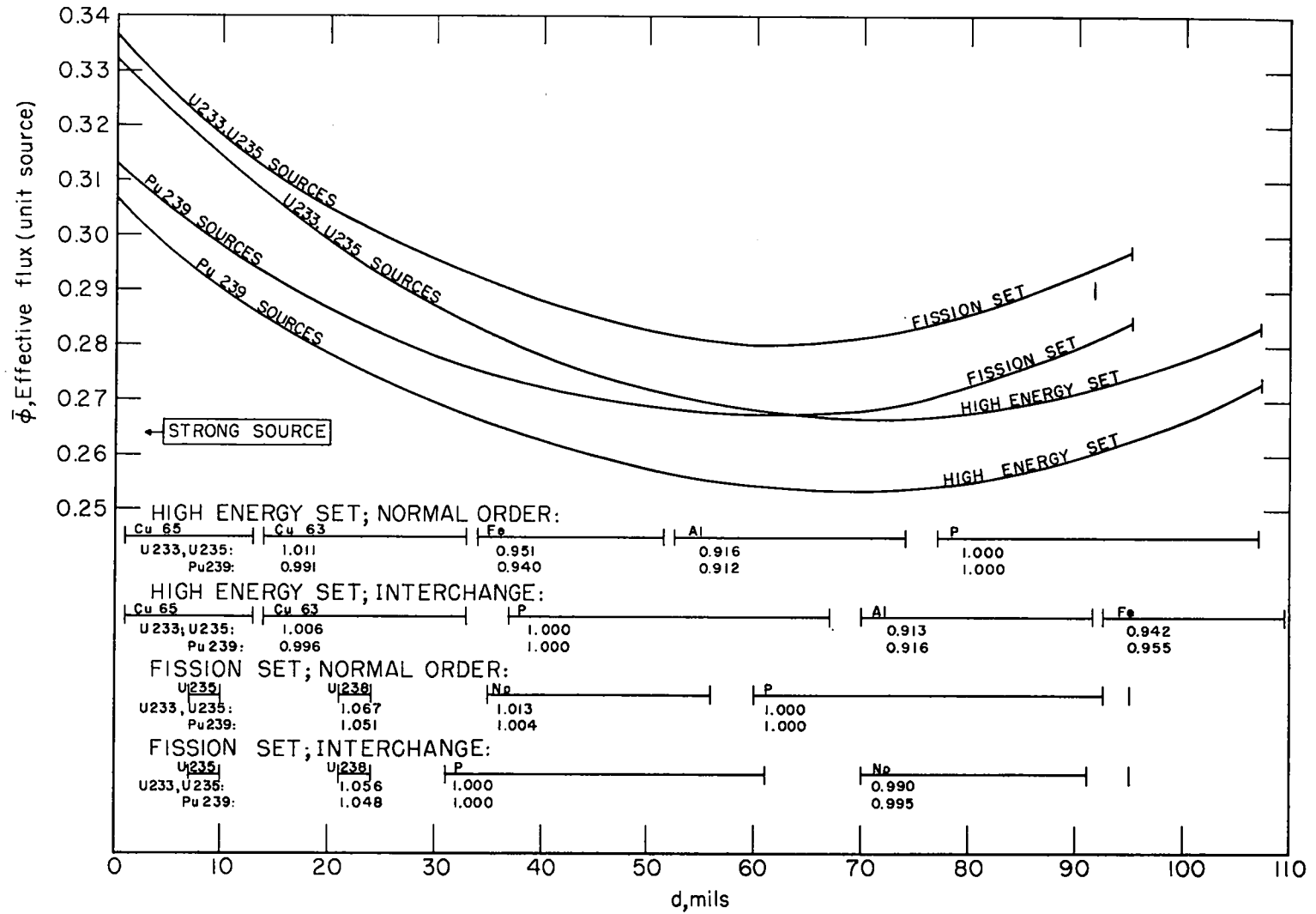


Fig. 3-2: Primary detector arrangements and corresponding flux profiles. The ordinate is directly applicable for Al, Fe, and Cu detectors; for the rest it must be multiplied by 1.075. Relative fluxes normalized to phosphorous are listed below each detector label. The abscissa distance "d" is defined in Fig. 2-3.

affected by the magnitude of the geometry factors, but only by variations associated with uncertainty of detector positions or changes of fission sources. Detector positions relative to each other and to the source disks are estimated to be within 0.002". From the figure, the effects of source change and positioning accuracy are seen to be small, associating a percent or less uncertainty with the geometry correction.

Response ratios may now be formed after applying relevant geometry factors to each counter response. Each response ratio formed may be distinguished by (1) detectors involved, (2) fission source used, (3) order of assembly—normal or interchange, and (4) detector disk set employed (set 1 or 2). The final array of results is presented in Tables 3-2 and 3-3 with all detector ratios formed lower to higher energy sensitivity. The response ratios of columns 3, 4, 7, and 8 are the result of 34 irradiations which provided for repetition of over one third of the data.

All response ratio values following a given fission source in the tables are directly comparable; that is, all intersets calibration and geometry corrections have been applied. Values entered in parenthesis are considered less reliable because of unsatisfactory decays, or the use of "old" source disks of uncertain dimensions.

Table 3-2: Experimental Results—Fission Detectors

Detectors	Fission Source	NORMAL ORDER ⁽¹⁾			Interchange Ratio ⁽⁵⁾	INTERCHANGE ORDER ⁽²⁾		
		Response Ratio ⁽³⁾		Spectral Indices ⁽⁴⁾		Response Ratio		Ratio of Spectral Indices ⁽⁴⁾
		Set 1	Set 2	X/U235		Set 1	Set 2	X/U235
$\frac{\text{Np}(n, f)}{\text{U238}(n, f)}$	Pu239	2.003	2.006 (1.988)	<u>0.970</u>	0.995	1.994	1.994	<u>0.970</u>
	U235	2.067 2.064	(2.12)	<u>1.000</u>	0.994	2.066	2.044	<u>1.000</u>
	U233	2.029	2.034	<u>0.986</u>	1.008	2.062	2.050	<u>1.000</u>
$\frac{\text{Np}(n, f)}{\text{P}(n, p)}$	Pu239	0.550	0.555 (0.546)	<u>0.944</u>	0.986	0.543	0.545	<u>0.949</u>
	U235	0.578 0.592	(0.595)	<u>1.000</u>	0.978	0.573	0.570	<u>1.000</u>
	U233	0.552	0.558 0.561	<u>0.954</u>	1.004	0.564	0.557	<u>0.979</u>

(1) P, Np, U238, U235.

(2) Np, P, U238, U235.

(3) Response ratios are presented for both detector sets with set 2 corrected to set 1 according to intercalibration factors in Table 1-2.

(4) Ratio of response ratio in each fission spectrum to that in the U235 fission spectrum.

(5) Ratio of response ratio for interchange order to that for normal order.

Table 3-3: Experimental Results—High Energy Detectors

Detectors	Fission Source	NORMAL ORDER ⁽¹⁾			Interchange Ratio ⁽⁵⁾	INTERCHANGE ORDER ⁽²⁾		
		Response Ratio ⁽³⁾		Ratio of Spectral Indices ⁽⁴⁾ X/U235		Response Ratio		Ratio of Spectral Indices ⁽⁴⁾ X/U235
		Set 1	Set 2			Set 1	Set 2	
$\frac{P(n,p)}{Al(n,p)}$:	Pu239	0.327	0.328 0.329	<u>0.934</u>	1.011	0.332 0.333	0.333 0.331	<u>0.937</u>
	U235	0.354 (0.346)	0.352	<u>1.000</u>	1.008	0.353 0.356	0.353	<u>1.000</u>
	U233	0.346	0.339 0.340	<u>0.968</u>	1.005	0.338 0.343	0.344	<u>0.966</u>
$\frac{P(n,p)}{Fe56(n,p)}$:	Pu239	16.53	16.33 16.27	<u>0.891</u>	1.019	16.65	16.67 16.75	<u>0.904</u>
	U235	18.38 (18.56)	18.36	<u>1.000</u>	1.004	18.43 18.54	18.42	<u>1.000</u>
	U233	17.57	17.61 17.42	<u>0.953</u>	1.010	17.66 17.74	17.74	<u>0.959</u>
$\frac{P(n,p)}{Al(n,\alpha)}$:	Pu239	103.4	103.6 102.6	<u>0.865</u>	1.005	103.0 104.0	103.8 104.3	<u>0.871</u>
	U235	119.5 (118.4)	119.2	<u>1.000</u>	0.998	119.1 119.5	118.3	<u>1.000</u>
	U233	112.9	113.3 112.3	<u>0.945</u>	1.003	113.2 113.1	113.3	<u>0.950</u>
$\frac{P(n,p)}{Cu63(n,2n)}$:	Pu239	26.7	26.7 27.6	<u>0.757</u>	0.993	26.6	26.7 26.8	<u>0.770</u>
	U235	36.4 (36.4)	34.8	<u>1.000</u>	0.979	34.8 35.1	34.3	<u>1.000</u>
	U233	33.1	32.9 32.0	<u>0.924</u>	0.994	31.8 33.0	33.1	<u>0.955</u>

(1) P, Al, Fe, Cu63, Cu65.

(2) Fe, Al, P, Cu63, Cu65.

(3) Response ratios are presented for both detector sets with set 2 corrected to set 1 according to intercalibration factors in Table 1-2.

(4) Ratio of response ratio in each fission spectrum to that in the U235 fission spectrum.

(5) Ratio of response ratio for interchange order to that for normal order.

3.3 Reliability and Final Experimental Values

The large group of experimental numbers (110 individual response ratios) in Tables 3-2 and 3 are now ready for disposal through suitable averaging. It will be worthwhile to make some consistency checks first in order to ascertain the degree of confidence to be placed in this assemblage of experimental values obtained over a period of eight months and subject to a geometry correction based on computation alone.

We begin by looking at pairs of response ratios which were obtained under identical experimental conditions: same fission source, detector set, and detector assembly order. The average spread of such numbers is less than one percent. Next, noting from Table 1-2 that detector sets 1 and 2 are nearly identical, we can examine the deviations of pairs of response ratios which differ only in the detector set employed. The average spread of 30 such pairs (Cu63(n,2n) excluded) is also less than one percent, with only five exceeding 1.5%. For Cu63(n,2n) the average spread of about 3% is assumed to be associated with uncertainties due to competing activities.

Finally, a comparison of values under assembly interchange will assess uncertainties in the geometry correction (or spectral variation with position if such exists). For each fission source, an appropriate index is the ratio of the average of the response ratios for the interchange

order to that for the normal order. These interchange ratios, shown in column six of the tables, deviate from unity an average of 0.9% with a maximum deviation of 2%. The deviations are comfortably small except for the manner in which the ratios fall above and below unity consistent with a slight hardening of the spectrum at the ends of the detector assembly or a small error in the calculated flux profiles. This conclusion may be seen by following the movement of the detectors on interchange in Fig. 3-2 and noting the departure direction for various response ratios in the tables.

There are sufficient uncertainties in the relative flux calculation, e.g. source strength ratios and exact specifications of nickel coated source disks, to account for the one percent or so bias appearing in the interchange. In any case, since the effect is small, it is of concern only for determining absolute spectral indices; for spectral comparison it should be negligible.

We now proceed to reduce the array of data by averaging together values having the same assembly order, and from these form ratios of response ratios between fission sources. These double ratios, taken with respect to the U235 source are now ratios of spectral indices (see section 1.3), and appear underlined in Tables 3-2 and 3. The less reliable values in parenthesis have been lightly weighted in the averaging; some weighting against other

values with noticeably large deviations from comparable numbers was also felt to be justified.

The effect of interchange may again be examined. The average deviation of normal and interchanged values, excluding Cu63, is 0.8% but now includes the propagated error of eight activation measurements rather than four as with response ratios. The nearly consistent increase in the ratio of spectral indices as one goes from normal to interchange order cannot be correlated with geometry or spectral biases. Again, the magnitudes are very small.

The final reduction of experimental results appears in Table 3-4. For each indicated detector ratio a single "best" response ratio is tabulated for each of the three fission spectra investigated, and now includes a small reactor background correction from Table 3-5. Ratios of spectral indices taken with respect to U235 appear underlined and are the fundamental data for the interpretation of spectral differences. The uncertainties assigned to the response ratios are primarily from consideration of the spread of comparable values in Tables 3-2 and 3 and the consistency criteria discussed above. All of the random errors inherent in source-detector assembly, irradiation procedure (activities nearly saturated are directly compared here to unsaturated activities which accurately integrate the irradiation profile), and counting are indicated

Table 3-4: Final Response Ratios and Ratios of Spectral Indices

DETECTORS	FISSION SPECTRA		
	<u>Pu239</u>	<u>U235</u>	<u>U233</u>
$\frac{Np(n, f)}{U238(n, f)}$:	2.00 ₀ ±0.013	2.06 ₀ ±0.013	2.04 ₇ ±0.013
X/U235:	<u>0.971±0.006</u>	<u>0.994±0.006</u>	
$\frac{Np(n, f)}{P(n, p)}$:	0.543±0.004	0.571±0.005	0.554±0.004
X/U235:	<u>0.951±0.009</u>	<u>0.970±0.009</u>	
$\frac{P(n, p)}{Al(n, p)}$:	0.330±0.0025	0.353±0.0025	0.342±0.0025
X/U235:	<u>0.934±0.007</u>	<u>0.966±0.007</u>	
$\frac{P(n, p)}{Fe56(n, p)}$:	16.5 ₅ ±0.16	18.42±0.12	17.6 ₃ ±0.15
X/U235:	<u>0.899±0.009</u>	<u>0.957±0.009</u>	
$\frac{P(n, p)}{Al(n, \alpha)}$:	103.4±0.7	119.2±0.7	113.0±0.8
X/U235:	<u>0.868±0.009</u>	<u>0.948±0.009</u>	
$\frac{P(n, p)}{Cu63(n, 2n)}$:	26.8±0.6	35.2±0.7	32.8±0.6
X/U235:	<u>0.762±0.016</u>	<u>0.931±0.014</u>	

Table 3-5: Source-Reactor Background Measurements

Conditions	Np(n, f)	U238(n, f)	P(n, p)	Al(n, p)	Fe(n, p)	Al(n, α)	Cu63(n, 2n)
Pu239 Source, 4" Cavity:	2.0%	2.8%	0.8%	0.7%	1.2%	0.6%	0.0%
U235 Source, 4" Cavity:	1.8	2.7	1.0	---	---	---	---
U233 Source, 4" Cavity:	2.7	2.6	1.4	---	---	---	---
W Disk, 4" Cavity:	3.0	2.0	0.25	---	0.8	---	---
U235 Source, 7" Cavity:	4.6	7.5	2.8	2.8	5.5	3.5	---
Final Background Estimate:	1.8 \pm 0.8%	1.8 \pm 0.8%	0.7 \pm 0.5%	0.5 \pm 0.5%	0.5 \pm 0.5%	0.5 \pm 0.5%	0.5 \pm 0.5%

63

by the spread of the data in Tables 3-2 and 3.

Systematic uncertainties due to competing activities or involved in the geometry correction are more difficult to assess. From preliminary work, competing activities are believed to contribute a negligible uncertainty to all detectors except $\text{Cu63}(n,2n)$ where they may be controlling. The relative detector fluxes given in Fig. 3-2 are judged to be no worse than ± 0.006 for comparison measurements, i.e. ratios of spectral indices.

The numbers in Table 3-4 are directly indicative of fission neutron spectrum differences. Remembering that all detector ratios are formed lower to higher energy response, it is qualitatively clear that the fission of Pu-239 yields a more energetic distribution of neutrons than U-235, that there is a divergence with increasing energy, and that the U-233 distribution falls in between and somewhat closer to U-235. An immediate quantitative result from the $\text{Cu63}(n,2n)$ detector is interesting: above about 12 mev the Pu239 fission spectrum yields nearly 40% more neutrons than U235. Detailed interpretations of the results will appear in the next chapter.

3.4 Background Measurements

Two sources of background may be distinguished: non-thermalized neutrons from the source reactor Hydro; and

neutrons from the fission disks which return to the detectors after undergoing one or more collisions in any surrounding material, i.e. the cadmium enclosure, glass wall of cavity, or heavy water. The latter background, which has been computed, is not directly assessable experimentally, but the first one is.

If the cadmium and fission source disks be interchanged without disturbing the rest of the source-detector assembly, see Fig. 2-3, the detectors will see neutrons from Hydro through the same intervening materials. Under these conditions direct counting of fission disks indicates a source strength reduction of about 130 so that a 1 to 2% residual detector activation due to fission neutrons may be expected. Replacing the fission disks with equivalent tungsten disks (tungsten has similar inelastic scattering behavior - ^{61}Th) is an alternative which samples the reactor background alone but with reduced absorption.

A small number of irradiations were carried out with the fission sources inside the cadmium enclosure and with the source disks replaced by tungsten. The results, shown in Table 3-5 suggest a true source-reactor background with some fission-source activation superimposed. The uncertainty in the numbers varies greatly and the best are probably no better than $\pm 20\%$. Neptunium with its high natural background is particularly difficult, perhaps accounting for the too-high tungsten disk background.

Geometry corrections have not been included in these results. The 7" diameter cavity shows a significant increase in the background, presumably due to more poorly-thermalized neutrons reaching the source disks—see Fig. 2-2. The estimates of applicable reactor backgrounds for each detector, listed in the last column of the table, have been used to correct the final response ratios of Table 3-4.

The results seem to justify the assumption of equivalent reactor backgrounds for all fission sources. For high-energy detectors it is difficult to see any way in which the reactor background, which never exceeds 3%, could perceptibly perturb the response ratios when the source disks are changed.

In the last chapter it was shown through machine calculations that high-energy detectors are negligibly affected by fission neutrons which are scattered back from the D_2O —see Table 2-3. Experimental confirmation of this result, though indirect, can be obtained by examining a short series of measurements using a 7.25" cavity, carried out before the 4" diameter cavity was found to be more satisfactory. Response ratios for the larger cavity, listed in Table 3-6, show essentially no departure from the primary data with the 4" cavity in view of the estimated uncertainties, large because of significant but poorly

Table 3-6: Response Ratios For 7" Diameter Cavity

<u>Detector Ratios</u>	<u>Fission Source</u>	<u>Response Ratios</u>	<u>Departure From Primary Data (4" Cavity)</u>
$\frac{Np(n, f)}{U238(n, f)}$:	Pu239	2.06±4%	+ 3%
	U235	2.14±3%	+ 4%
$\frac{Np(n, f)}{P(n, p)}$:	Pu239	0.558±4%	+ 1%
	U235	0.586±3%	+ 1%
$\frac{P(n, p)}{Al(n, p)}$:	Pu239	0.356±5%	0%
	U235	0.375±4%	- 1%
$\frac{P(n, p)}{Fe56(n, p)}$:	Pu239	17.3±6%	- 3%
	U235	19.3±5%	- 2%
$\frac{P(n, p)}{Al(n, \alpha)}$:	Pu239	110±4%	- 1%
	U235	129±4%	+ 1%
$\frac{P(n, p)}{Cu63(n, 2n)}$:	Pu239	28.3±4%	- 2%
	U235	38±7%	+ 1%

known reactor background. A harder spectrum with the larger cavity would result if neutron return were appreciable. There is no such indication.

One final check of the purity of the fission spectra consisted of a single Pu239 irradiation in which the entire source-detector assembly was enclosed in a brass can nearly doubling the amount of scattering material in the source-detector assembly. The results in the table below,

Table 3-7: Response Ratios with Brass Scatterer

Detector Ratios:	<u>P/Al(n,p)</u>	<u>P/Fe</u>	<u>P/Al(n,α)</u>	<u>P/Cu(n,2n)</u>
Response Ratios:	0.357	18.1	112	28
Departure From Primary Data:	0%	+ 2%	+ 1%	- 2%

show no discernible perturbation due to the additional material for the high energy detectors.

3.5 Comparison With Fast, Metal, Critical-Assemblies

The neutron spectrum above about 2 Mev, at the center of unreflected metal critical assemblies of U235, U233, and Pu239 are very nearly fission spectra (60Gr). These spherical assemblies—Godiva (U235), Jezebel-23 (U233), and Jezebel-49 (Pu239)—are described in references (56Pe) and (60Ja). Since the average neutron energy in these assemblies is about 1.5 Mev, comparing response ratios

with the corresponding ratios for thermal-neutron-induced fission spectra might indicate a spectral shift due to incident neutron energy.

Detector response ratios at the center of these unreflected assemblies have been measured, though not with the precision of the fission spectra work. In balance however there are no problems of geometry or background in such assemblies. Restricting consideration to the high-energy detectors which have energy sensitivities greater than 2 Mev, Table 3-8 shows the ratios of spectral indices between the fast critical assemblies and the corresponding thermal-neutron-induced fission neutron spectra. With a single exception all the results fall below unity indicating a slightly harder fission neutron spectrum in the metal assemblies. In the next chapter this comparison will be related quantitatively to shifts in fission spectrum average energy.

We may inquire as to how seriously we should take this apparent spectral hardening. At the moment the uncertainties attached to each value are of the order of one half the departure of each number from unity. More important is the question of whether or not assembly spectra above 2 Mev are virgin fission neutrons to a precision of a few percent. It seems clear that, though the high energy portion of the assembly spectra may be affected by absorption, inelastic scattering, and energy-sensitive neutron

See Attached
Errata Sheet

Table 3-8: Ratio of Spectral Indices Between Thermal-Neutron-Induced Fission Spectra and Corresponding Fast, Critical Assembly Spectra

<u>Detectors</u>	<u>Godiva</u> <u>U235</u>	<u>Jez-23</u> <u>U233</u>	<u>Jez-49</u> <u>Pu239</u>
$\frac{P(n, p)}{Al(n, p)}$	0.980	0.957	0.927
$\frac{P(n, p)}{Fe56(n, p)}$	0.985	0.972	0.915
$\frac{P(n, p)}{Al(n, \alpha)}$	0.958	0.920	0.902
$\frac{P(n, p)}{Cu63(n, 2n)}$	1.040	0.943	0.875
$\frac{Al(n, p)}{Al(n, \alpha)}$	0.978	0.961	0.973

leakage, the influence, if any, should be a softening of the spectrum. The observed hardening of the assembly spectra, then, may be safely taken as the lower limit of a fission spectrum shift, presumably associated with the increased energy of the incident neutrons producing fission.

CHAPTER 4

INTERPRETATION OF COMPARISON MEASUREMENTS

4.1 The Maxwellian Density Function

We have seen that the fission-neutron flux spectra of U235, U233, and Pu239 differ significantly; yet, they appear sufficiently similar to warrant trying a one parameter description of the changes. A single-parameter spectral function facilitates simple but comprehensive treatment of experimental results, and, conveniently, the parameter may always be taken as the average energy of the distribution.

From the best available measurements, plotted in Fig. I-1 of the Introduction, it is clear that the simple one parameter Maxwellian density function,

$$N(E) = \frac{2}{\pi^{1/2} T^{3/2}} E^{1/2} \exp(-E/T); \quad \bar{E} = \frac{3T}{2}, \quad 4-1$$

adequately fits the existing fission-neutron flux data. The spectral parameter T is an average nuclear temperature of the fission fragments, defined essentially by the

expression itself. In terms of the Maxwellian function, then, we will associate the measured ratios of spectral indices with differences in average energy of the three fission spectra under investigation; at the same time the adequacy of the function to describe the changes will be judged. Later on, this treatment will conveniently parallel the theoretical approach of J. Terrell (59Te).

It is notable that the Maxwellian density function which describes the fission spectrum through more than four orders of magnitude has to date no direct theoretical justification. It may be remarked that such a spectral distribution would be expected if the following two assumptions were fulfilled: (1) only a few neutrons with no degeneracy share in the energy of the excited nucleus prior to fission, and (2) all of these neutrons escape at the moment of scission. For the latter it can be mentioned that there is no direct evidence that fission neutrons are emitted from moving fragments as is usually assumed; the correlation between fragment direction and neutron emission observed by Fraser and others (52Fr, 61Bo2) does not preclude assumption 2.

4.2 Computed Spectral Indices and Variation with Average Energy

Assuming the Maxwellian description, each spectral

index may be computed from the expression,

$$S_{AB}(\bar{E}) = \frac{\bar{\sigma}_A(\bar{E})}{\bar{\sigma}_B(\bar{E})} = \frac{\int_0^{\infty} \sigma_A(E) E^{1/2} e^{-E/T} dE}{\int_0^{\infty} \sigma_B(E) E^{1/2} e^{-E/T} dE} \quad 4-2$$

(see Eq. 1-4), and is considered a function of the average energy of the spectrum through the relationship $\bar{E} = 3T/2$.

Using the excitation functions of Fig. 1-1 and a best value $\bar{E} = 1.935$ Mev for the average fission neutron energy of U235, suggested by Terrell (59Te), average detector cross sections $\bar{\sigma}_f$ have been computed and are listed in Table 4-1 below:

Table 4-1: Computed Average U235 Fission Spectrum Cross Sections

Detector	Np237(n, f)	U238(n, f)	P(n, p)	Al(n, p)
$\bar{\sigma}_f$ (mb):	1370	300	37.0	3.98
Detector	Fe56(n, p)	Al(n, α)	Cu63(n, 2n)	
$\bar{\sigma}_f$ (mb):	0.950	0.625	0.128	

For spectral comparison the variation of each spectral index with \bar{E} is required. The dependence of $\bar{\sigma}_f$ on average energy has been computed in the vicinity of $\bar{E} = 2$ Mev, and in Fig. 4-1 the variation is shown normalized to its value at $\bar{E} = 1.935$ Mev from Table 4-1. Since the variation is closely logarithmic over this small energy region, it is meaningful to specify a sensitivity factor, presented in

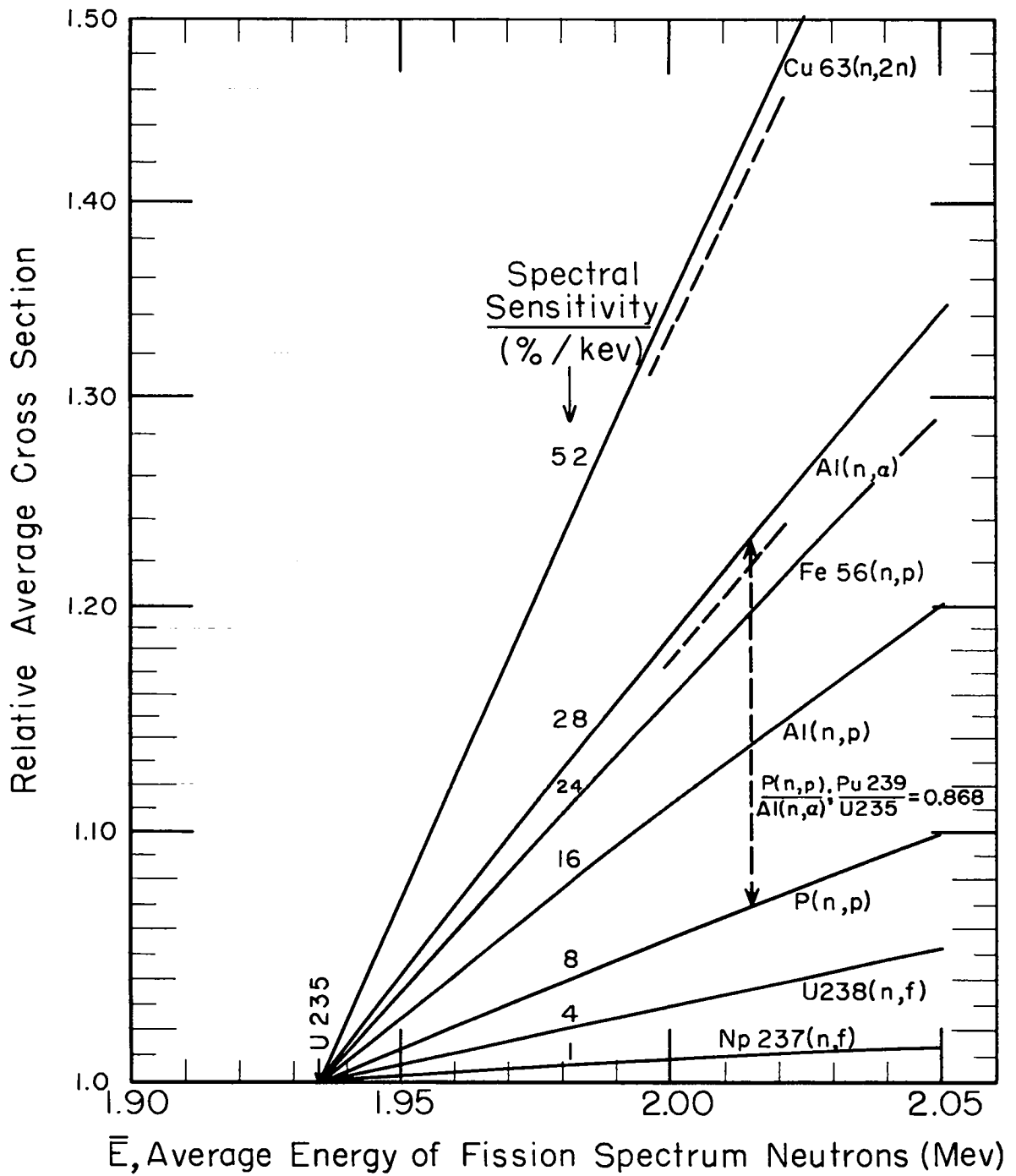


Fig. 4-1: Variation of average fission spectrum cross sections with average fission spectrum energy on the basis of the Maxwellian density function. The spectral sensitivity factor is the percent change in cross section for one kev change in average energy.

the figure as percent change in cross section for a 1 kev change in average fission spectrum energy. The spectral sensitivity for a cross section ratio or spectral index A/B is given by the ratio $(1+\epsilon_A)/(1+\epsilon_B)$, where ϵ_A is the spectral sensitivity for detector A as given in the figure converted to decimal form. A ratio of spectral indices (taken with respect to the U235 fission spectrum) is given by an ordinate ratio between the detectors involved, and the corresponding abscissa is the average energy of the spectrum being compared with U235. For example, in Table 3-4 the ratio of the P(n,p)/Al(n, α) spectral index between Pu239 and U235 is listed as 0.868; on the plot this ordinate ratio between P(n,p) and Al(n, α) curves occurs at $\bar{E} = 2.015\text{Mev}$. These two detectors therefore predict that the average fission spectrum energy of Pu239 is 2.015Mev, or more precisely that the average fission spectrum energy of Pu239 is 4.1% higher than U235. The logarithmic ordinate makes it easy to locate a ratio of spectral indices with a ruler or calipers. This is useful when, as here, 21 independent indices will be involved.

The detectors are seen to be exceedingly sensitive to the single spectral parameter. An indication of how uncertainties in excitation function reduce this single-parameter detector sensitivity is suggested by the dotted lines in Fig. 4-1 which correspond to the following changes: (1) reduction of energy scale for the Cu63(n,2n) excitation

function (Fig. 1-1) by 0.4Mev; and (2) 40% reduction of the $A_1(n,\alpha)$ cross section above 8.2Mev, its mean response energy. The effect upon a spectral comparison of these rather gross changes is seen to be quite small.

4.3 Graphical Display of Fission Spectrum Average Energy Shift

To display the spectral changes predicted by the experimental data graphically we take $Np_{237}(n,f)$ as a preferred detector; it has the lowest mean response energy—1.8 Mev—and least spectral sensitivity. Maintaining the convention of forming all detector ratios lower to higher energy sensitivity, a set of ratios of spectral indices based upon Np may be formed directly from Table 3-4 by combining pairs of values. New uncertainties will be more like the average uncertainty of a pair rather than the rms propagation as with independent numbers. Table 4-2 presents the resulting spectral comparison on this new basis.

The variation of each spectral index $Np(n,f)/B$ with average energy \bar{E} may be obtained from Fig. 4-1 by taking ordinate ratios for each detector with respect to the Np curve. The resultant curves, displayed in Fig. 4-2, represent the variation of each $Np(n,f)/B$ spectral index around the average energy 2Mev as governed by the Maxwellian density function (Eq. 4-1); they form a group of functions

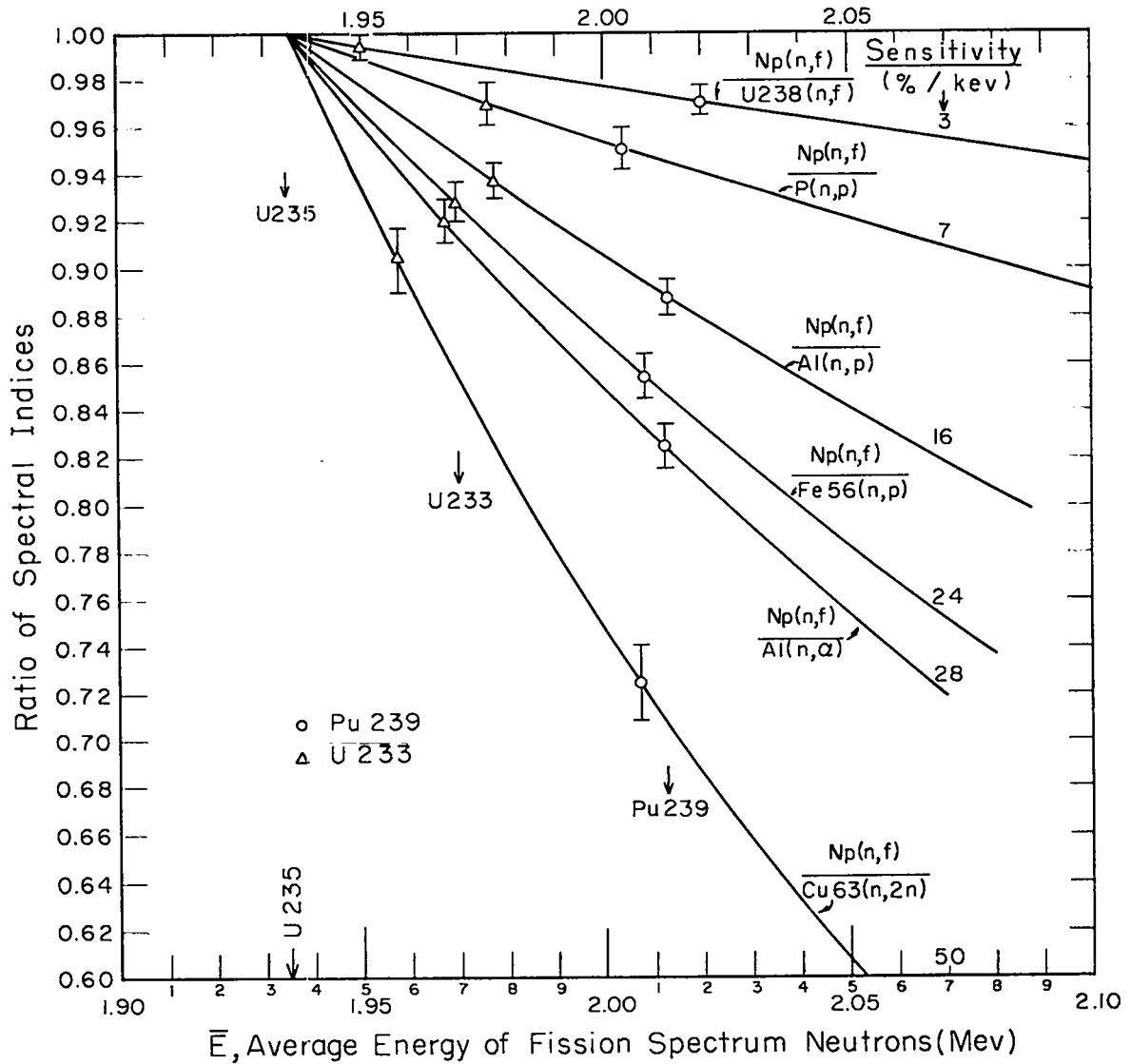


Fig. 4-2: Display of fission spectrum comparison showing computed variation of spectral indices vs average fission spectrum energy. Experimental ratios of spectral indices are plotted on corresponding curves. Abscissa values below each are the predicted average energies for U233 or Pu239 based on 1.935MeV for U235.

upon which experimental ratios of spectral indices of Table 4-2 may be plotted.

Table 4-2: Ratio of $N_p(n, f)/B$ Spectral Indices

Detectors	$\frac{\text{Pu239}}{\text{U235}}$	$\frac{\text{U233}}{\text{U235}}$
$\frac{N_p(n, f)}{\text{U238}(n, f)}$:	0.971 ± 0.006	0.994 ± 0.006
$\frac{N_p(n, f)}{P(n, p)}$:	0.951 ± 0.009	0.970 ± 0.009
$\frac{N_p(n, f)}{\text{Al}(n, p)}$:	0.888 ± 0.008	0.937 ± 0.008
$\frac{N_p(n, f)}{\text{Fe}(n, p)}$:	0.855 ± 0.009	0.928 ± 0.009
$\frac{N_p(n, f)}{\text{Al}(n, \alpha)}$:	0.825 ± 0.009	0.920 ± 0.009
$\frac{N_p(n, f)}{\text{Cu63}(n, 2n)}$:	0.725 ± 0.016	0.903 ± 0.014

Abscissa values below each point represent the average fission spectrum energy predicted by the index involved, and a vertical array of points for a given spectrum confirms the adequacy of the spectral function and the correctness of the excitation functions.

Examining first the Pu239:U235 data in the figure we see that all measured indices are consistent with an average energy of 2.013Mev; within experimental error (i.e. intersection of error flag with curve, translated to

the energy abscissa) they fall in a vertical array. Note the large variation in precision with which the various indices predict the average energy; insofar as the chosen spectral function is correct, high precision is associated with a wide separation in average response energy. Since, however, the Maxwellian function is considered only an approximation, there must be increased emphasis on detectors that sample more of the spectrum when investigating changes in average energy.

Examination of the U233:U235 results in the figure reveals relatively poor agreement between the six indices, and we find no single \bar{E} that includes all of them. Looking forward to theoretical considerations, the value 1.970 Mev is chosen as the best average energy for U233 fission neutrons. Two indices predict significantly lower average energies: the first, Np/U238, has the poorest spectral sensitivity, and the other, Np/Cu63, involves less than 1/2% of the spectrum. A pattern in the U233 results suggests that the spectral function is not quite right: the four highest detectors monotonically predict lower average energies. We conclude that, relative to U235, the fission spectrum of U233 has fewer neutrons as one goes to higher energies than the spectral function with $T_{U233} = (1.964/1.935) T_{U235}$ predicts.

The uncertainties in Fig. 4-2 indicate a sensitivity of 1/2% or less to changes in average energy. This remains

less than 1% after considering the effect of excitation function errors on the computed curves as discussed in section 4.2. Final assignment of uncertainties will await consideration of all detector combinations, to be taken up in the next section.

4.4 Average Energy Shift Based On All Independent Detector Combinations

To put all detectors on an equal basis it is necessary to consider the 21 independent spectral indices that may be formed from the seven detectors used. Using Table 3-4 the corresponding ratios of spectral indices have been formed, and appear in Table 4-3. The convention for forming ratios, lower to higher energy sensitivity, is maintained; and relevant values with uncertainties in percent appear at the intersection of horizontal and vertical lines from the detector labels. The mean response energy and response range are shown underneath each detector label.

In Table 4-4 the entries in the matrix array are predicted average fission neutron energy shifts in Mev from $\bar{E}(U235) = 1.935$ Mev. These were obtained from Figure 4-1 in the manner described in section 4.2; the uncertainties, shown for Pu239 but applicable to U233 as well, were obtained directly from the uncertainties in Table 4-3

Table 4-3: Ratios of All Independent Spectral Indices Comparing Pu239 and U233 Fission Spectra to U235

Detectors (a)		U233						
Np(n, f) $\frac{1.8}{-1.0}^{+2.3}$		0.994	0.970	0.937	0.928	0.920	0.903	
	U238(n, f) $\frac{2.7}{-1.1}^{+2.9}$		0.976	0.943	0.934	0.926	0.908	
0.971 $\pm 0.6\%$								
0.951 ± 0.9	P(n, p) $\frac{3.7}{-1.5}^{+2.3}$	0.980 $\pm 0.8\%$		0.967	0.957	0.949	0.931	
0.888 ± 0.9		0.915 ± 0.7	0.933 $\pm 0.9\%$	Al(n, p) $\frac{5.7}{-1.7}^{+2.3}$		0.990	0.981	0.963
0.855 ± 1.0		0.881 ± 0.9	0.899 ± 1.0	0.964 $\pm 0.9\%$	Fe56(n, p) $\frac{7.3}{-1.9}^{+3.2}$		0.991	0.973
0.825 ± 1.1		0.850 ± 0.9	0.867 ± 1.1	0.929 ± 0.9	0.963 $\pm 0.9\%$	Al(n, α) $\frac{8.2}{-1.5}^{+2.8}$		0.982
0.725 ± 2.2		0.747 ± 2.0	0.762 ± 2.1	0.817 ± 2.0	0.847 ± 1.9	0.879 $\pm 1.8\%$	Cu63(n, 2n) $\frac{13.6}{-1.4}^{+2.7}$	
		Pu239						

(a) Mean detector response energy and response range included under each detector label.

Table 4-4: Fission Spectrum Average Energy Shift (mev) Predicted By Each Independent Detector Combination

Detectors (a)		U233					
0.073b	Np(n, f) 0.075(c) $\frac{1.8}{+2.3}$ $\frac{-1.0}{-1.0}$	0.015	0.036	0.037	0.034	0.032	0.023
	0.067 ± 0.020	U238(n, f) 0.071 $\frac{2.7}{+2.9}$ $\frac{-1.1}{-1.1}$	0.063	0.050	0.048	0.035	0.023
0.074	0.069 ± 0.013	0.051	P(n, p) 0.070 $\frac{3.7}{+2.3}$ $\frac{-1.5}{-1.5}$	0.042	0.030	0.028	0.019
0.075	0.078 ± 0.005	0.077	0.094	Al(n, p) 0.074 $\frac{5.7}{+2.5}$ $\frac{-1.7}{-1.7}$	0.015	0.019	0.013
0.075	0.074 ± 0.003	0.071	0.074	0.059	Fe56(n, p) 0.074 $\frac{7.3}{+3.2}$ $\frac{-1.9}{-1.9}$	0.025	0.012
0.071	0.078 ± 0.003	0.076	0.082	0.077	0.116	Al(n, α) 0.078 $\frac{8.2}{+2.8}$ $\frac{-1.5}{-1.5}$	0.010
	0.071	0.071	0.074	0.069	0.073	0.068	Cu63(n, 2n) 0.071 $\frac{13.6}{+2.1}$ $\frac{-1.4}{-1.4}$

- (a) Mean detector response energy and response range included under each detector label
 (b) Average of values along indicated diagonal.
 (c) Average of the six values involving the detector adjacently labeled.

transformed to average energy through the spectral sensitivity factors. For example, the ratio of spectral indices $U238(n,f)/Al(n,\alpha)$ between Pu239 and U235 is $0.850 \pm 0.9\%$, and the average energy shift predicted from Fig. 4-1 is 0.076 ± 0.004 Mev.

Values along a principal diagonal represent detector combinations with adjacent energy response, the combinations least sensitive to the spectral parameter. With some overlap, further-removed parallel diagonals represent detector combinations whose energy responses are more separated and consequently more sensitive to both the spectral parameter and the adequacy of the spectral function. Averages of values along the six diagonals for each spectrum are listed along the margins of the table.

Ratios of spectral indices involving the same detector compare one energy region to each of the others. Corresponding energy shifts appear in the row and column which intersect at the detector label. A monotonic change of values along such a path is evidence of a failure of the spectral function. For each detector, the average of the six values involving that detector appears in the triangles on either side of the detector label.

Looking first at Pu239, no monotonic pattern appears in going to higher energy detectors, i.e. down a column, and right to left across a row. Diagonal averages, along the left margin, are **very** close with no apparent pattern.

The single-detector averages, which have been weighted against the divergent values involving the insensitive adjacent detectors, show a maximum departure of ~ 0.007 Mev, well within the uncertainties involved. The consistency of these single-detector averages indicates that the detector excitation functions involved are correct. Ignoring the most insensitive indices along the principal diagonal the maximum spread of predicted energy shifts is 0.013 Mev or about 0.7% of the 2 Mev average fission spectrum energy.

Turning to the U233 results it is apparent that the general consistency is not as good. The diagonal averages are acceptable (maximum spread ~ 0.010 Mev), but the predicted energy shifts involving a single detector become lower as one moves to higher energy regions. For Cu63(n,2n) and Al(n, α) the pattern is quite clear, confirming and emphasizing the graphical indication in Figure 4-2. The single-detector averages (in the triangles) also decrease uniformly as one goes to higher energies. These inconsistencies are reflected, of course, in the nearly 0.04 Mev spread in the results, three times larger than with Pu239. In view of the excellent consistency of the Pu239 results, which tends to confirm the excitation functions, it seems reasonable to conclude that the Maxwellian description

$$\varphi(E) \sim E^{1/2} e^{-E/T}$$

is not quite adequate for describing the difference between U235 and U233 fission neutron spectra. The two fission spectrum tails at higher energies tend to become more nearly parallel than the slow divergence described by

$$\frac{\exp(-E/T_{U233})}{\exp(-E/T_{U235})} = \exp(+E \frac{T_{U233} - T_{U235}}{T_{U235} T_{U235}}) \approx \exp(+0.006E);$$

$$T = \frac{3\bar{E}}{2}.$$

For Pu239 the divergence with energy, $\exp(0.019E)$, is apparently maintained.

4.5 Final Specification of Spectral Shifts and Comparison with Other Measurements

The final numbers for the fission spectrum comparison arise out of averages from Table 4-4 which were weighted in favor of intermediate-energy detectors:

$$\frac{\bar{E}(\text{Pu239})}{\bar{E}(\text{U235})} = 1.039 \pm 0.003; \quad \frac{\bar{E}(\text{U233})}{\bar{E}(\text{U235})} = 1.016 \pm 0.003.$$

These ratios also apply to T the spectral parameter.

Assuming $\bar{E}(\text{U235}) = 1.935$ Mev:

$$\Delta\bar{E}(\text{Pu239}) = 0.075 \pm 0.006 \text{ Mev}$$

$$\Delta\bar{E}(\text{U233}) = 0.030 \pm 0.008 \text{ Mev.}$$

Uncertainties are judged from the spread of values in

Table 4-4 as discussed in the last section. The uncertainty attached to the U233 comparison does not include the apparent failure of the simple spectral function but is taken to be the uncertainty in the true change in average energy, as the results for higher energy detector that sample few neutrons are averaged with reduced weighting.

The Pu239 comparison is in excellent agreement with the value $\Delta E(\text{Pu239:U235}) = 0.074$ Mev from preliminary work reported in 1956 (56Gr). Two other direct comparison measurements appear in the literature. The first activation measurements by Kovalev et al. are very briefly reported (57Ko). Using Np, U238, and Th232 fission detectors along with P(n,p), Al(n,p), and $\text{Pr}^{141}(\text{n},2\text{n})$ high energy detectors, one finds, with his results and Figure 4-1, 0.07 ± 0.01 and 0.05 ± 0.01 Mev as the average energy shifts of Pu239 and U233 spectra relative to U235. The energy sensitivity of $\text{Pr}^{141}(\text{n},2\text{n})$ is assumed equivalent to $\text{Cu63}(\text{n},2\text{n})$.

T. W. Bonner using a $\text{Li}^6\text{I}(\text{Eu})$ scintillation detector surrounded by polyethylene spheres of various diameters (5-30 cm) measured the neutron energy shift in U235, U233, Pu239, and Cf252 fission (61Bo1). The method is not very sensitive to spectral changes above three or four Mev, and detector response for all spheres show appreciable sensitivity down to thermal energies. The sensitivity of response to average energy change varies from 3 to 8%/keV

depending upon the diameter of the spheres being compared. Spectral shifts of 0.074 ± 0.006 and 0.035 ± 0.006 Mev are quoted for Pu239 and U233 fission neutrons relative to U235. The uncertainties given, however, encompass only about one third of the experimental results.

The three measurements agree very well for Pu239:U235; but, by comparison, the U233:U235 results are poor. Better agreement between Bonner and the present work is obtained by considering lower energy detectors, say Al(n,p) and below. Then, from Table 4-4, the average spectral shift appears to be 0.034 ± 0.01 for U233:U235. Again it seems that the high-energy tails of the U233:U235 fission spectra do not continue to diverge as do the Pu239:U235 spectra.

Though the average energy changes observed for the Pu239 and U233 fission spectra appear relatively small, according to the Maxwellian spectral function, they represent significantly greater numbers of neutrons at higher energies. Flux spectrum changes in going from U235 to Pu239 are shown in Table 4-5, for six energy groups which correspond roughly to the various detector response regions (see section 5.4). Clearly there exists a considerable perturbation in the spectral shape.

Table 4-5: Six-Group Display of Spectral Comparison

Energy Groups No.	Range	U235 Fission	Pu239/U235
		$N(E) \sim E^{1/2} \exp(-E/1.29)$	$N(E) \sim E^{1/2} \exp(-E/1.34)$
1	0.0-0.60	0.1819	0.955
2	0.60-1.4	0.2797	0.971
3	1.4-3.0	0.3392	1.001
4	3.0-6.0	0.1737	1.066
5	6.0-11.0	0.0248	1.163
6	11.0-∞	0.00069	1.351

4.6 Fission Spectrum Changes In the Fast, Critical Assemblies

The resulting neutron-flux spectrum may be expected to depend upon the energy of the neutron that initiates fission, as well as the nature of the nuclide that undergoes the reaction. Measurements that suggest such an effect, comparisons of spectra at the center of metal, critical assemblies with corresponding thermal-neutron-induced spectra, were discussed and critically evaluated in section 3.5. Ratios of spectral indices were presented in Table 3-8. With the aid of Fig. 4-1 spectral shifts predicted by each of the five detector combinations may be ascertained as in previous sections. Table 4-6 lists

the percent change in average energy as one goes from the thermal-neutron-induced fission spectrum to the corresponding critical assembly fission spectrum component. With but one exception all the detectors show the central spectra of the critical assemblies in the energy region greater than 2 Mev to be more energetic than the corresponding thermal-neutron spectra. A notable trend is the larger spectral shift as one moves to more energetic fission spectra.

Table 4-6: Average Energy Ratio Between the Spectra of Fast Critical Assemblies and Corresponding Thermal-Fission Spectra

Detectors	<u>Godiva</u> U235	<u>Jez-23</u> U233	<u>Jez-49</u> Pu239
$\frac{P(n, p)}{Al(n, p)}$:	1.013	1.029	1.053
$\frac{P(n, p)}{Fe56(n, p)}$:	1.005	1.010	1.033
$\frac{P(n, p)}{Al(n, \alpha)}$:	1.012	1.025	1.031
$\frac{P(n, p)}{Cu63(n, 2n)}$:	0.994	1.008	1.018
$\frac{Al(n, p)}{Al(n, \alpha)}$:	1.011	1.020	1.014
Weighted Av:	1.009	1.020	1.025

As mentioned in section 3.5, the influence on assembly spectrum of leakage, scattering, and absorption by the

fissile material is expected, if anything, to degrade the spectrum. For this reason the final values of Table 4-6 are proposed as lower limits for the corresponding spectral shift due to incident neutron energy. Experimental uncertainties were estimated crudely in section 3.5 and translate here to one half the departure of each spectra from the one to which it is compared.

4.7 Theoretical Considerations and Experimental Correlation

The following discussion of fission energetics, for the most part, follows in outline the detailed treatment by Terrell (59Te, 57Te), and leads to a relation between average fission neutron energy and $\bar{\nu}$ the average numbers of neutrons emitted per fission. Prompt neutrons from fission are customarily assumed to be evaporated from highly excited fission fragments moving at their maximum velocity (10^{-20} to 10^{-14} sec after fission). In general, the average energy in the laboratory system of an emitted neutron \bar{E} is simply

$$\bar{E} = \bar{E}_f + \bar{E}_{cm}, \quad 4-3$$

the sum of the average fragment kinetic energy per nucleon and the average center-of-mass energy \bar{E}_{cm} of the neutron. A number of measurements have established that $\bar{E}_f = 0.78$

Mev remains nearly constant over a wide range of Z and A for fissioning nuclides, implying that fragment kinetic energy is primarily due to Coulomb repulsion.

To determine the center-of-mass energy distribution $\varphi(\bar{E}_{cm})$ of neutrons emitted by the fragment, Weisskopf's statistical model of the nucleus is employed (37We). The Maxwellian "evaporation" spectrum which arises,

$$\varphi(\bar{E}_{cm}) = \text{Const} \times \bar{E}_{cm} e^{-\bar{E}_{cm}/T}, \quad 4-4$$

involves a nuclear temperature given by an equation of state,

$$E_e = a T^2, \quad 4-5$$

where E_e is the excitation energy of the nucleus and the constant "a" the nuclear level density. The latter is an approximation based on considerations of the excited nucleus as a degenerate Fermi gas. The average energy of an evaporation spectrum is just

$$\bar{E}_{cm} = 2T;$$

so we may write equation 4-3 as

$$\bar{E} = 0.78 + 2\bar{T}, \quad 4-6$$

where \bar{T} is the average fragment temperature. This temperature is not the same as that appearing in Eq. 4-1, though

as both are linearly related to the average neutron energy in the laboratory system, it is valid to use them interchangeably to describe fractional changes in average energy.

The distribution of fragment temperatures may be estimated indirectly through Eq. 4-5 if the distribution of fragment excitation be ascertained. The latter has been deduced from the number distribution of prompt neutrons per fission ($\nu - \bar{\nu}$) an experimentally accessible quantity (57Te). Each neutron emitted is assumed to reduce the excitation energy by $E_0 \approx 6.7$ Mev, consisting of its binding energy (~ 5 Mev) plus an average evaporation energy of $2T$. The observed Gaussian distribution of prompt neutron numbers transforms then into a Gaussian distribution of the initial fragment excitation energies with average energy $(\bar{\nu} + 1)E_0/2$ and rms deviation $E_0/2$. Using the equation of state to transform residual excitation energies after neutron emission into temperature, Terrell derives an expression for average fragment temperature as a function of $\bar{\nu}$:

$$\bar{T} = \text{const} \times E_0 (\bar{\nu} + 1)^{1/2}. \quad 4-7$$

On this basis the average fission neutron energy is given by Eqs. 4-6 and 4-7 as

$$\bar{E} = 0.78 + 0.62 (\bar{\nu} + 1)^{1/2}, \quad 4-8$$

where the constant has been chosen to make $\bar{E} = 1.935$ Mev for the U235 fission spectrum value of $\bar{\nu} = 2.41$.

This slowly varying relation between average fission neutron energy and average number of prompt neutrons per fission is shown in Figure 4-3 along with experimental determinations from section 4.5. Using $\bar{\nu}$ values from Diven (62Di), the agreement appears reasonably good. The square root dependence on $(\bar{\nu} + 1)$ is reasonably well established if one accepts three experimentally verified quantities: average fission neutron energy for U235, average number of neutrons per fission for U235, and average fragment kinetic energy independent of Z and A. For comparison, a linear relation with $(\bar{\nu} + 1)$, under these assumptions, is shown by the dotted line in Figure 4-3. The established variation as the square root in turn verifies the T^2 dependence in the equation of state (Eq. 4-5). Available results from the spontaneous fission of Cf252 are seen to be in considerable disagreement.

According to the data of Wahl (54Wa) and others the average fragment kinetic energy is little affected by incident neutron energy, indicating that such energy must appear as fragment excitation. In terms of the simplified theory employed here an increase in incident neutron energy will produce an increase in $\bar{\nu}$:

$$\frac{d\nu}{dE_n} \approx 1/E_0 \approx 0.15, \quad 4-9$$

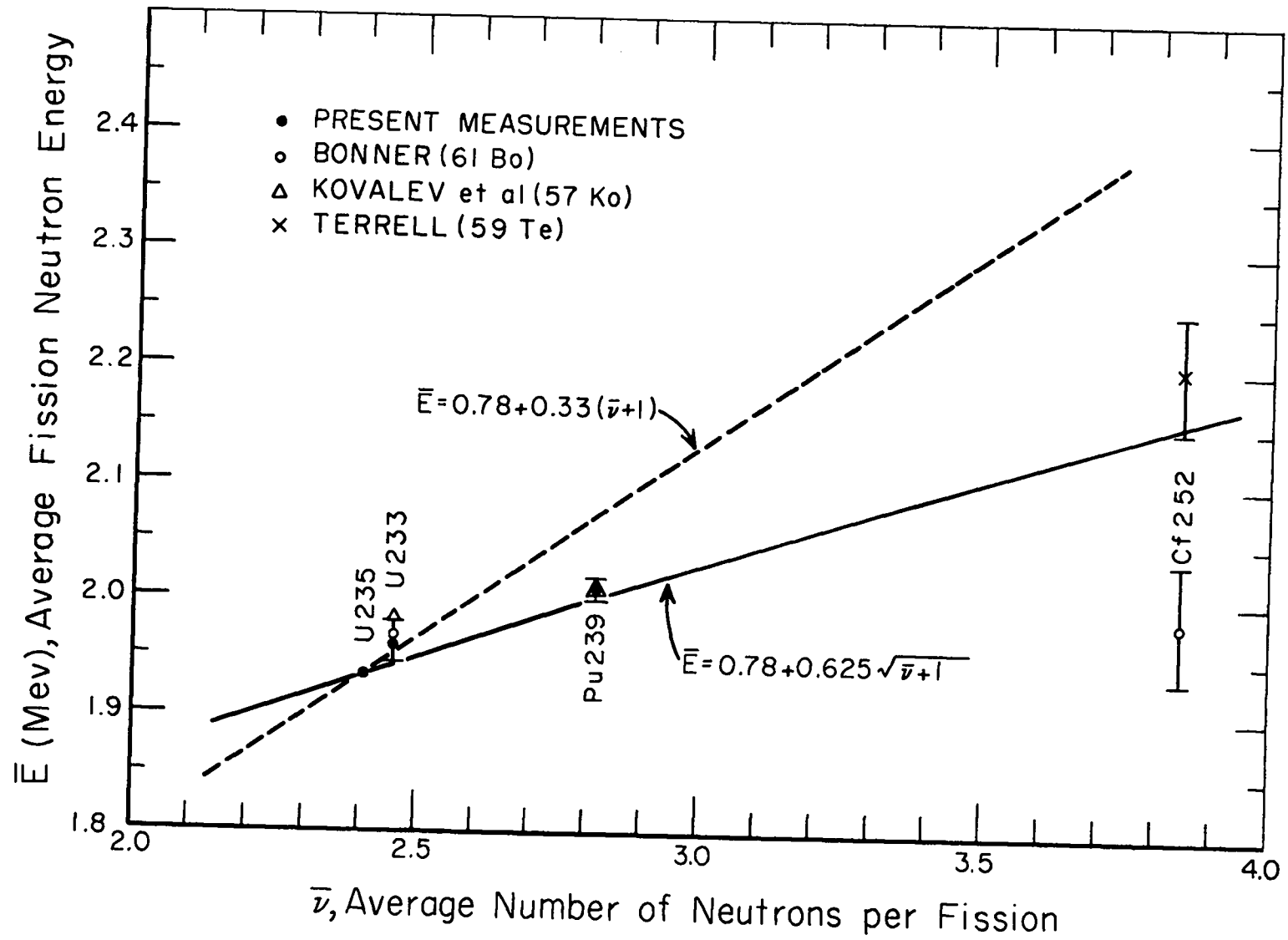


Fig. 4-3: Average fission neutron energy as a function of $\bar{\nu}$. Solid line is the theoretical prediction according to Terrell (59Te).

where E_n is the incident neutron energy and E_o the average excitation change per emitted neutron. Together with Eq. 4-8 the result

$$\frac{d\bar{E}}{dE_n} \approx 0.047/(\bar{\nu} + 1)^{1/2} \quad 4-10$$

is obtained for the fission spectrum shift due to incident neutron energy. The average energy of neutrons producing fission in the fast, critical assemblies discussed in sections 3.5 and 4.7 is around 1.5 Mev, implying by Eq. 4-10 about a 4% increase in average energy of the resulting fission neutrons. This exceeds the observed shifts shown in Table 4-4. Whether or not the observed lower limits of 2-3% for the spectral shifts could be reduced this much by energy-dependent leakage and interaction with the fissile materials of the assemblies cannot be resolved at this time.

CHAPTER 5

SUPPLEMENTARY STUDIES—DETECTOR CALIBRATION AND SHAPE OF U235 FISSION SPECTRUM

The detailed spectral comparisons presented in the last two chapters will be extended here to a study of the fission spectrum shape itself, though with a considerable loss in precision. Monoenergetic irradiations at the Los Alamos Van de Graaff provide a basis for specifying spectral indices, at the same time confirming—and improving—existing knowledge of detector excitation functions. Special measurements described make it possible to extract the fission spectrum response for the U235(n, f) detector. With a complete set of calibrated detector responses established, the adequacy of familiar spectral functions to describe the fission spectrum will be investigated. A secondary goal of this dissertation will also be fulfilled, the comprehensive explication of the activation detector set as an instrument for measuring distributed neutron spectra.

5.1 Van de Graaff Calibration

Fourteen irradiations at the large Los Alamos Van de Graaff are the basis of the calibration and verification of detector excitation vs. energy. The fundamental excitation functions, shown in Fig. 1-1, have been "sampled" by simultaneous irradiation of all detectors at thirteen separate neutron energies.

A schematic diagram of the arrangement appears in Fig. 5-1 showing the detectors positioned close to the target where energy spreads are large enough to average out the fine structure of the excitation functions. The fission counter shown in the schematic proved helpful as a relative flux monitor. The same set of foils used for the fission spectrum measurements were irradiated for twenty minutes, and subsequently counted and analyzed in the usual manner. Relative activation of the two phosphorous foils at the ends of the foil pack agreed with calculated flux gradients to better than 3%.

Response ratios, formed with respect to $U238(n, f)$, were first multiplied by the cross section of $U238(n, f)$ chosen as the reference cross section. The result for neutron energy E , according to section 1.3, is proportional to the cross section of detector A ,

$$\frac{A_E}{[U238(n, f)]_E} \times \sigma_{U238}(E) \sim \sigma_A(E).$$

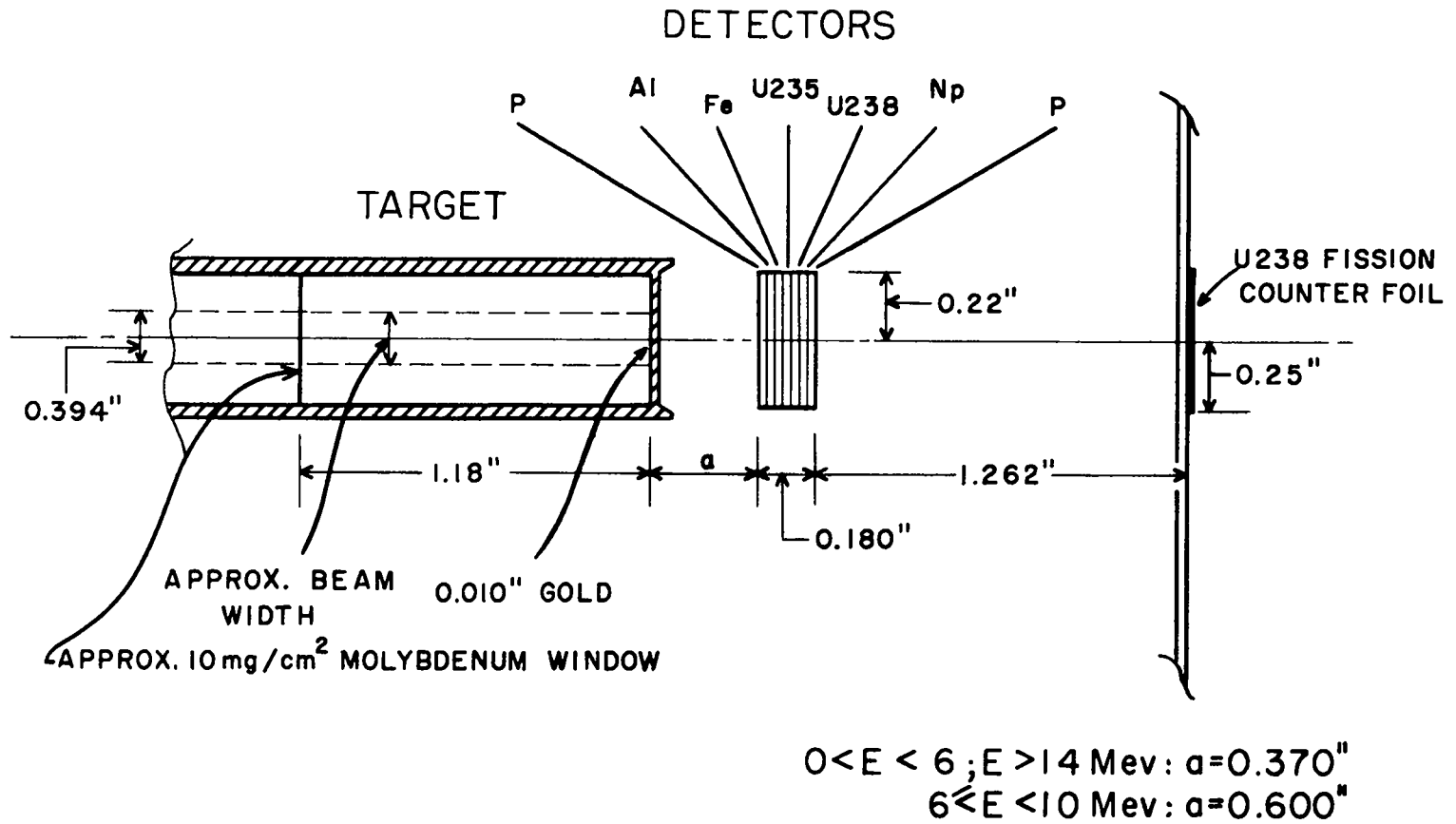


Fig. 5-1: Van de Graaff arrangement for detector calibration by simultaneous irradiation of detector disks close to the target.

The relative cross section sets thus obtained were normalized to a cross section value giving the best fit to Fig. 1-1. Table 5-1 lists the results, giving for each irradiation the center-of-target and zero degree neutron energy, estimated energy spread at the detectors, cross section normalized to the value underlined, and estimated experimental error which assesses conditions of irradiation and counting relative to the same factors in the fission spectrum measurements.

The last line of the table presents derived calibration ratios which directly convert $N_p(n,f)/B$ response ratios to spectral indices. Ratios of pairs of values in the $N_p(n,f)/B$ set are calibration ratios for other detector combinations. The uncertainties assigned are applicable to spectral analysis only, i.e. they do not include errors in the underlined normalization cross sections. Such estimates require highly subjective judgments on a great variety of published material and have no relevance for spectral determinations based on calibration with neutrons of known energy distribution, e.g., monoenergetic or fission spectrum. If a different normalization is convenient computed spectral indices need only be adjusted accordingly. Factors considered in assigning uncertainties to the calibration ratios were: (1) experimental errors assigned to the individual cross section determinations; (2) reliability, consistency, and scope of excitation function

Table 5-1: Cross Section Determinations and Calibration Ratios

Neutron Energy (Mev)	U235(n, f)		Np237(n, f)		U238(n, f)		P(n, p)		Al(n, p)		Fe(n, p)		Al(n, α)		Cu63(n, 2n)	
	$\sigma_v^{(1)}$ (mb)	$\Delta\sigma(\%)$ (2)	σ_v (mb)	$\Delta\sigma(\%)$	$\sigma_{28}^{(3)}$ (mb)	Response ⁽⁴⁾ Relative to Chamber	σ_v (mb)	$\Delta\sigma(\%)$	σ_v (mb)	$\Delta\sigma(\%)$	σ_v (mb)	$\Delta\sigma(\%)$	σ_v (mb)	$\Delta\sigma(\%)$	σ_v (mb)	$\Delta\sigma(\%)$
* 2.22 ^{+0.15} _{-0.20}	1416	± 8.5%	1843	±7.0%	565±3%	0.94	--	--	--	--	--	--	--	--	--	--
2.50 ^{+0.16} _{-0.40}	<u>1420</u>	± 4.5	1807	±4.5	565±3	<u>1.00</u>	52	±4.5%	0.023	±15%	0.0	--	--	--	--	--
* 3.15 ^{+0.15} _{-0.20}	1323	± 4.5	<u>1710</u>	±4.5	545±3	0.85	134	±4.0	--	--	--	--	--	--	--	--
* 3.40 ^{+0.16} _{-0.20}	1274	± 4.5	1691	±4.5	550±3	1.11	111	±4.0	--	--	--	--	--	--	--	--
4.04 ^{+0.12} _{-0.52}	1208	± 4.0	1471	±4.0	563±3	0.97	<u>115</u>	±4.0	6.7	±4.0	0.0	--	0.0	--	--	--
5.00 ^{+0.10} _{-0.58}	1175	± 4.0	1545	±5.0	568±2	--	174	±4.0	25	±3.5	0.83	±6.0%	0.0	--	--	--
6.00 ^{+0.53} _{-0.76}	1111	± 6.5	1566	±5.5	610±4	0.98	139	±5.5	46	±5.5	11.5	±5.5	1.5	±7%	--	--
7.00 ^{+0.45} _{-0.75}	1582	± 7.0	1958	±7.0	880±5	--	139	±6.5	<u>59</u>	±7.0	<u>25</u>	±6.0	14.6	±8	--	--
* 8.10 ^{+0.23} _{-0.35}	1839	± 7.5	2240	±6.5	1015±4	1.09	152	±6.5	80	±6.5	41	±6.5	<u>42</u>	±6.5	--	--
* 8.25 ^{+0.22} _{-0.35}	1830	± 9.0	2302	±7.0	1020±4	0.95	158	±7.0	80	±7.0	38	±7.5	34.4	±7.0	--	--
10.0 ^{+0.26} _{-0.76}	2332	± 7.0	2670	±6.0	1150±5 ⁽⁵⁾	1.02	171	±6.5	93	±6.5	63	±6.0	81	±6.5	--	--
* ⁽⁶⁾ 14.1±0.1	1881	± 8.5	2139	±6.0	1165±3	--	102	±5.0	82	±5.0	111	±4.5	130	4.5	<u>500</u>	±4.5%
17.2 ^{+0.65} _{-1.05}	2202	±12.0	2167	11.0	1380±4	1.06	60	±8.5	55	±8.5	76	±8.0	90	±8.0	794	±10.0
.....																
⁽⁷⁾ Calibration Ratio (G_B/G_{Np}):																
	0.698±4%		1.00		2.11±4%		59.8±9%		1545±7%		127±8%		28.2±9%		637±11%	

(1) σ_v = Observed average cross section over indicated energy spread relative to U238 and normalized to FIG. 1-1 at value underlined.

(2) Estimated experimental errors including U238 relative cross section uncertainty.

(3) U238 fission is the reference reaction and its cross section is taken from 58A1 and 59Sm. Uncertainties listed apply to relative cross section only.

(4) Comparison of U238 detector response with U238 fission counter flux monitor, normalized to unity at 2.50 Mev.

(5) Cross Section includes 150 mb for D(n, p n) reaction (56Cr2).

(6) This neutron energy was obtained at the Los Alamos Cockcroft-Walton under experimental conditions similar to those at the Van de Graaff.

(7) Spectral index Np/B is given by (calibration ratio) x (response ratio). Error includes an estimate of uncertainties in excitation functions.

* Reduced reliability: different detector disks, target-detector arrangement, or flux monitor.

measurements in the literature; and (3) agreement of latest Van de Graaff work with existing measurements including the obscurity introduced by energy spreads and extent of tailoring needed to fit our results.

Except for the problem of energy-sensitive efficiency factors, the calibration depends only upon knowing the energy distribution of neutrons incident on the detectors. Two factors, ionization loss in the target gas and angular spread of detectors, lead to an asymmetric energy distribution about the zero degree neutron energy at the center of the target. These distributions at the detector which encompass about 1 Mev of energy do not directly affect the investigation of much broader neutron spectra such as from fission. They do, however, make it difficult to verify or choose among the measurements of others in determining a best excitation function. A qualitatively correct incident neutron distribution for 6 Mev d-d neutrons appears in Fig. 5-2. The mean neutron energy is seen to be some 350 kev below the nominal 6 Mev produced at the center of the target. Table 5-1 lists the nominal center-of-target, forward-direction energy, and maximum energy spreads. The fitting of data does take into account, qualitatively, the effect of these energy distributions.

For the fission detectors the consistency of the results is excellent. Mean departures from Fig. 1-1 of 2.0 and 1.2% for U235 and Np, respectively, lend considerable

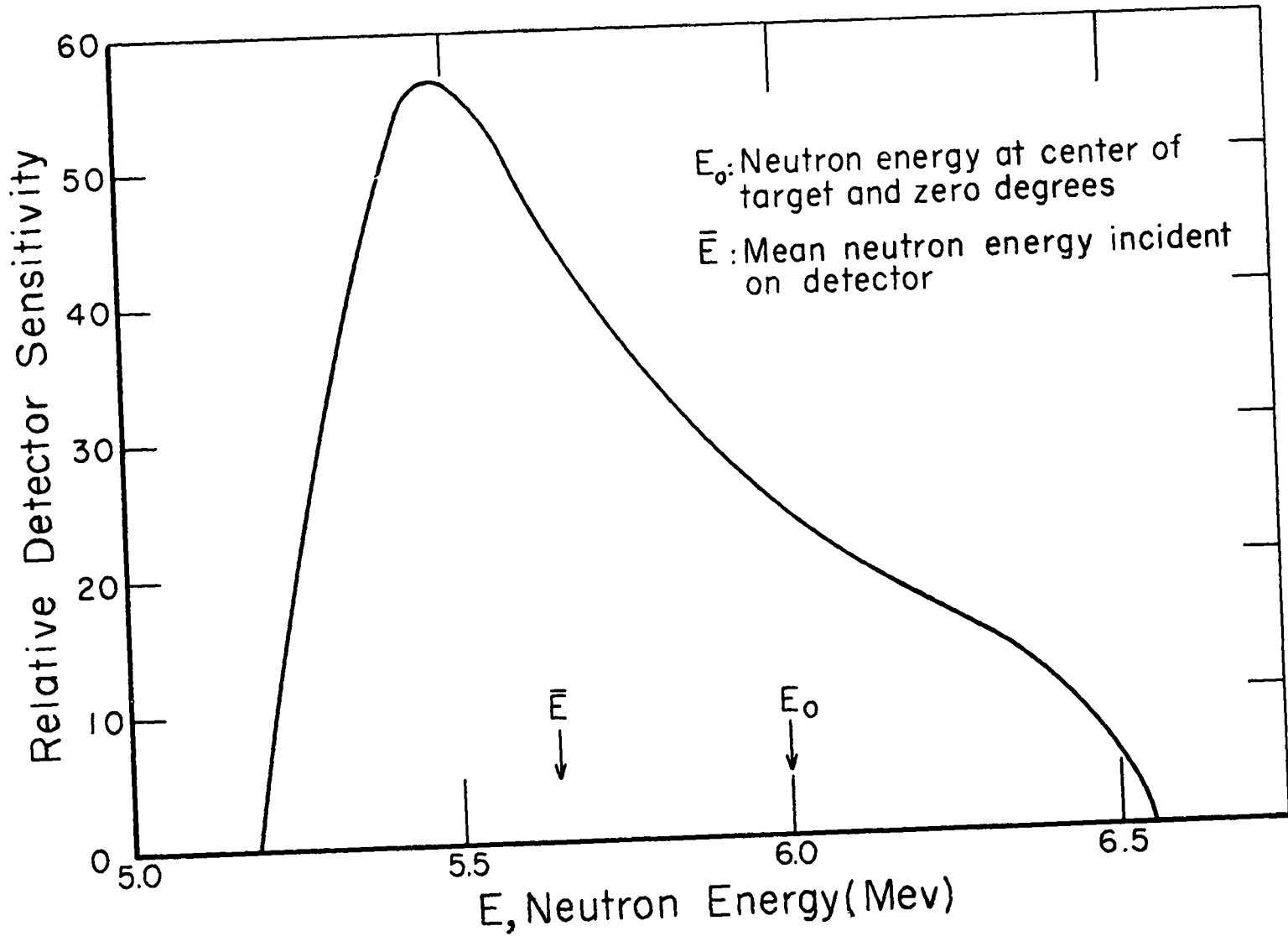


Fig. 5-2: Energy distribution incident on detectors for nominal 6 Mev, d-d neutrons.

confidence to the calibration ratios obtained. The fission cross sections of Fig. 1-1 are based entirely on the reference given and have not been tailored to these calibrations. Unfortunately, the present measurements do not go low enough in energy to encompass more than half the the response region, except for Np, where the cross sections below 2 Mev have been carefully measured.

The rest of the detectors yield mean departures of the order of 5% from Fig. 1-1, and some tailoring of the excitation functions — generally not very well known — to these measurements was considered desirable. For the P(n,p) detector in particular, where structure is severe and gross discrepancies appear in the literature, these results were emphasized.

A special problem, alluded to in Chapter 1, is associated with the complex decay of the fission detectors. It is well known that the fission mode and consequently the fission product distribution varies with energy of the incident neutrons; and though the counting system randomly samples a large number of decay chains, it is necessary to investigate the constancy of the detector efficiency factor with neutron energy. The U238 fission fragment ionization chamber which monitored the relative flux on most irradiations made this possible. A value of "response relative to chamber" listed in Table 5-1 is based on the ratio of U238(n,f) reference detector response to

that of the U238 fission chamber monitor. In this case the result is independent of the U238(n,f) cross section. Up to 10 Mev the U238 efficiency factor is apparently constant; the departures at 3.15, 3.4, and 8.1 Mev are assumed to be experimental—they were taken together months earlier using a U235 fission counter with a 1" diameter deposit. At 17 Mev some warping of the efficiency factor is indicated, though difficulties with the fission counter during the 17 Mev run increase the uncertainty of the resulting 6% shift observed.

In energy regions where detector sensitivities overlap, the calibration procedure followed here incorporates the energy variation of the efficiency factor into the excitation function without disturbing applications to analysis of distributed neutron spectra. In such cases, the U238 monitor is not required. When detector response regions are widely separated as in the extreme case of Np(n,f) and Cu63(n,2n) the flux monitor must be relied upon to relate responses between regions.

5.2 U235(n,f) Detector Response in the U235 Fission Spectrum

The response of a U235 fission detector to its own fission neutron spectrum is a difficult measurement; significant background activation by resonance and intermediate

energy components are always present and exceedingly difficult to determine. With the cavity fission spectrum developed for these measurements we depend upon a computation of the number and spectrum of the small fraction of low energy neutrons which return to the detectors from the surrounding D_2O . The resulting return background for a $U235(n,f)$ detector is discussed in section 2.4, and Table 2-3 lists an estimate of 10%. With a background of this order and the relative calibrations of the last section, it would seem possible to ascertain the fundamental fission-spectrum spectral index, $U235(n,f)/U238(n,f)$, to perhaps five percent.

Unfortunately with the primary Hydro cavity-fission-spectrum arrangement the measurable source-reactor background for the $U235(n,f)$ detector varied from 40 to 60% depending upon the fission source and the exact source-cadmium interchange arrangement (see Fig. 2-3 and section 3.2). This is too large to correct for satisfactorily, and an alternative arrangement was employed for separate measurements which included all of the fission detectors. Changes in the standard arrangement described in section 2.3 were as follows: (1) increase of the D_2O between cavity and reactor by 3-1/4", (2) use of cadmium cylinders of identical thickness for fission and background irradiations, and (3) placement of a 0.027" spacer ring between

the U235 detector disk and the cadmium shield (or fission source in the case of background assembly order). With this system four irradiations of the U235, U238, and Np fission detectors were necessary: two with U235 and Pu239 sources exposed, and two with sources enclosed in the cadmium shield. The additional D₂O reduced the U235 reactor background to 19%, and the spacer resulted in a more consistent background determination. A reduced source strength ratio compared to that in the standard cavity position changed the flux profile enough to warrant a redetermination of the relative geometry factors.

Response ratios and the corrections applied appear in Table 5-2. The Np/U238 response ratios for the U235 and Pu239 spectra are in excellent agreement; the expected 2% shift due to spectral differences (see Fig. 4-2) brings them to within 1% of each other. Also, they agree very well with the equivalent values obtained in the standard arrangement as recorded in Table 3-4. Uncertainty assignments for the response ratios, higher than for equivalent measurements described in Chapter 3, reflect the fact that the measurements were not repeated, and the non-compensating errors applicable to the spectral index determination to follow.

The agreement of the U235/U238 ratios for the Pu239 and U235 fission sources is most welcome. (The expected

Table 5-2: Fission Detector Response Ratios in Improved Arrangement

Fission Source:	<u>Np(n, f) / U238(n, f)</u>		<u>U235(n, f) / U238(n, f)</u>	
	<u>Pu 239</u>	<u>U235</u>	<u>Pu239</u>	<u>U235</u>
Uncorrected Counter Response Ratios:	1.96 ₅	1.99 ₅	1.89 ₅	1.92 ₃
Reactor Bkg. Correction:	±0.8%	+0.6%	-19.5%	-18.5%
U238 Contribution to U235 Response:	---	---	-2.0%	-1.5%
Relative Geometry Correction:	+3	+3.5	-4	-5
Cavity Return Bkg. Correction:	~-0.1%	~-0.1%	-9.0%	-8.0%
Inelastic Scattering In Source-Detector Assembly:	-1.0%	-1.0%	-2.0%	-2.0%
Response Ratio:	2.02±0.04	2.05±0.04	1.34±0.055	1.37±0.055

spectral shift in this index is about 3.5% yielding agreement to nearly 1%.) A difficulty in extracting the U235 response is the self-shielding by the U235 source disk of resonance neutrons in the reactor background. This may not be precisely accounted for in the interchange method used to obtain the reactor background. Likewise source disk self-shielding will affect the cavity return background by an estimated one percent for the U235-source. The agreement then between Pu and U235 fission source is evidence that these resonance effects are small and correctly taken into account.

The source-detector inelastic scattering corrections were estimated from computed spectral perturbations as given in Table 2-1. Average detector cross sections in a spectrum perturbed by a 1.3cm dia. iron sphere surrounding a fission spectrum source differ from values in a pure fission spectrum as follows:

Detector:	U235	Np237	U238
Percent Change:	0%	-1.5%	-4%

As the spectral perturbation computed is an overestimate of the actual situation, a reduced value is applied in Table 5-2.

Fundamental spectral indices for fission detectors in the fission spectrum may now be specified on the basis of Table 5-2 and the calibration ratios of Table 5-1. The

results in Table 5-3 below are accompanied by two uncertainties: the first, applicable to spectral analysis based on neutronic calibration, does not include errors in absolute cross section, i.e. position of excitation functions in Fig. 1-1; the second, represents an attempt to assess all errors associated with the values taken as true average cross section ratios. The review article by Allen and Henkel (58A1) and the Np measurements of Schmidt (59Sc) were the primary basis for estimating absolute uncertainties.

Table 5-3: Fission Detector Spectral Indices for the U235 Fission Neutron Spectrum

<u>Detectors</u>	<u>Spectral Index</u>	<u>Relative Cross Section Uncertainty</u>	<u>Absolute Cross Section Uncertainty</u>
$\frac{U235(n, f)}{U238(n, f)}$	4.14	± 0.23	± 0.35
$\frac{Np237(n, f)}{U238(n, f)}$	4.33	± 0.22	± 0.45
$\frac{U235(n, f)}{Np237(n, f)}$	0.956	± 0.057	± 0.10

5.3 Spectral Indices and Comparison With Maxwellian Fission Spectrum Function

Possessing satisfactory fission detector results, we may go on to convert a complete set of response ratios for U235 fission spectrum neutrons, Tables 3-4 and 5-2, to spectral indices using the calibration ratios of Table 5-1. Results of the conversion along with associated uncertainties appear in Table 5-4. It must be emphasized that the spectral indices as specified depend upon the normalizing cross sections underlined in Table 5-1, whereas spectral information to be derived from them does not.

Larger errors are seen to accompany the response ratios in Table 5-4 now that the geometry correction enters directly, including the effect of differences in detector diameters—see section 2.4. Also a two percent correction has been applied to response ratios involving high-energy detectors to account for inelastic scattering in the source-detector assembly (see section 2.3, Table 2-1, and the last section). The uncertainty of this correction is about equivalent to the magnitude of the correction. The final estimate of spectral index precision in Table 5-4, an rms combination of response and calibration ratio uncertainties, does not assess the absolute error in the normalizing cross sections of Table 5-1 or equivalently the relative positioning of the excitation functions of Fig. 1-1; the error intervals assigned are not an estimate of how close these

Table 5-4: Observed Spectral Indices For The U235 Fission Neutron Spectrum

<u>Detector</u>	<u>Response Ratio</u>	<u>Calibration Ratio</u>	<u>Spectral Index</u> ⁽¹⁾
U235(n, f)/U238(n, f)	1.37 ± 0.055	3.02 ± 0.11	4.14 ± 0.23
Np(n, f)/U238(n, f)	2.05 ± 0.04	2.11 ± 0.10	4.33 ± 0.22
Np(n, f)/P(n, p)	0.560 ± 0.015	59.8 ± 5.7	33.5 ± 3.4
Np(n, f)/Al(n, p)	0.198 ± 0.007	1545 ± 120	306 ± 25
Np(n, f)/Fe(n, p)	10.31 ± 0.30	127 ± 10	1309 ± 110
Np(n, f)/Al(n, α)	66.5 ± 1.5	28.2 ± 2.6	1875 ± 180
Np(n, f)/Cu63(n, 2n)	19.6 ± 0.7	637 ± 70	12485 ± 1400

(1) Errors specified do not include uncertainties associated with normalizing cross sections of Table 5-1.

values come to the true average cross section ratio. The position of the excitation functions in Fig. 1-1, accepted for both experimental and computed spectral indices, do not influence spectral determinations.

The cross sections of Fig. 1-1 do however represent our best estimate of absolute values based on existing experimental information, and we would suggest that absolute uncertainties are less than a factor of two larger.

The spectral indices of Table 5-4 with their carefully considered uncertainties complete the specification of the eight activation detectors as spectral analyzers. Coupled with the cavity method for producing pure fission spectrum neutrons—described in Chapter 2—detectors in most any form, and associated counting systems, may be conveniently calibrated. Unknown spectra may then be related to the fission spectrum with a precision superior to what may be expected from techniques of absolute measurement. Even monoenergetic calibration, unless sufficiently extensive and precise to improve the excitation functions, will not yield better spectral determinations in view of the accuracy with which the fission spectrum is known.

Average fission spectrum cross sections for individual detectors may be specified from Table 5-4 on the basis of the 313mb value for the $U^{238}(n,f)$ average fission spectrum cross section measured by Leachman (57Le). Results appear in Table 5-5 where again listed uncertainties are

Table 5-5: Experimental Average Detector Cross Sections for the Fission Spectrum of U235

<u>Detector</u>	<u>Cross Section (mb)</u>	<u>Relative Uncertainty (%)</u> (1)
U235(n, f)	1296	$\pm 4\frac{1}{2}\%$
Np(n, f)	1355	± 4
U238(n, f)	<u>313</u> ⁽²⁾	± 3
P(n, p)	40. ₄	± 9
Al(n, p)	4.4 ₃	± 7
Fe56(n, p)	1.03 ₅	$\pm 7\frac{1}{2}$
Al(n, α)	0.72 ₃	± 9
Cu63(n, 2n)	0.108 ₅	± 10

(1) Assigned errors, applicable to spectral analysis, do not include absolute uncertainties associated with normalizing values of Table 5-1.

(2) Normalizing cross section from "double-chamber" measurement by Leachman (57Le).

relative, applicable to spectral index formation and analysis based on calibration with neutrons of known energy distribution.

To compare these detector results with two commonly used functional descriptions of the fission spectrum we employ again the matrix-like array of section 4.4. Spectral indices computed from both the Maxwellian and Watt functions,

$$\text{Maxwellian: } N(E) = (0.770) E^{1/2} \exp(-E/1.29),$$

$$\text{Watt: } N(E) = (0.453) \exp(-E/0.965) \sinh \sqrt{2.29E},$$

are compared to the observed indices derived from Table 5-5. The parameter in the Maxwellian function is from a least-squares fit to differential data of Fig. I-1 of the Introduction. The results along with applicable uncertainties appear in Table 5-6, Watt function comparison to the left and below the label diagonal and Maxwellian to the right. The convention for forming indices, lower energy sensitivity detector in the numerator, is maintained. Ratios of spectral indices appear at the intersection of the row and column matching relevant labels. The triangles on either side of a detector label show the computed average detector cross section for each spectral function using the corresponding cross section of Fig. 1-1; ratios of these are the computed spectral indices.

Assuming that the excitation functions are correct

Table 5-6: Observed U235 Fission Spectrum Compared With Maxwellian and Watt Spectral Functions

(1) Detectors σ_f (mb), computed with $N(E) \sim E^{1/2} \exp(-E/1.29)$

	U235(n, f) 1337	0.98 ± 0.07	0.93 ± 0.05	0.89 ± 0.10	0.87 ± 0.07	0.90 ± 0.08	0.84 ± 0.08	1.15 ± 0.13	
	0.99 ± 0.07	Np(n, f) 1391 1.8 ^{+2.3} _{-1.0}	0.95 ± 0.04	0.91 ± 0.09	0.89 ± 0.08	0.91 ± 0.08	0.86 ± 0.08	1.17 ± 0.13	
	0.96 ± 0.05	0.96 ± 0.04	U238(n, f) 309 2.7 ^{+2.9} _{-1.1}	0.96 ± 0.09	0.94 ± 0.07	0.96 ± 0.08	0.90 ± 0.09	1.24 ± 0.13	
	0.92 ± 0.10	0.93 ± 0.09	0.97 ± 0.09	P(n, p) 38.5 3.7 ^{+2.3} _{-1.5}	0.98 ± 0.11	1.01 ± 0.12	0.94 ± 0.12	1.30 ± 0.18	
	0.89 ± 0.07	0.89 ± 0.08	0.923 ± 0.07	0.96 ± 0.11	Al(n, p) 4.04 5.7 ^{+2.6} _{-1.7}	1.03 ± 0.10	0.96 ± 0.11	1.32 ± 0.16	
	0.86 ± 0.08	0.86 ± 0.07	0.89 ± 0.07	0.926 ± 0.11	0.968 ± 0.09	Fe56(n, p) 0.914 7.3 ^{+3.2} _{-1.9}	0.94 ± 0.11	1.29 ± 0.16	
	0.78 ± 0.07	0.78 ± 0.07	0.81 ± 0.08	0.84 ± 0.11	0.88 ± 0.10	0.91 ± 0.11	Al(n, α) 0.661 8.2 ^{+2.8} _{-1.5}	1.38 ± 0.19	
	0.77 ± 0.08	0.77 ± 0.08	0.80 ± 0.08	0.83 ± 0.11	0.87 ± 0.11	0.90 ± 0.11	0.99 ± 0.13	Cu63(n, 2n) 0.086 13.6 ^{+2.7} _{-1.4}	

σ_f (mb) computed with $N(E) \sim \exp(-E/0.965) \sinh(2.29E)^{1/2}$

Spectral Indices Compared: Experimental/Computed (Watt)

Spectral Indices Compared: Experimental/Computed (Maxwellian)

(1) Mean detector response energy and response range included under each detector label—see section 1.5.

(2) Spectral indices are formed with the detector of lower energy sensitivity in the numerator.

within the quoted uncertainties, we may consider each detector pair as testing the ability of the spectral function to describe the relative flux in two more or less distinct energy regions defined by the respective detector response ranges. With few exceptions the departure of the observed spectral indices from those computed are within two error intervals for both spectral functions; yet, a consistent pattern of deviations is apparent.

The largest discrepancies exist in the $\text{Cu63}(n,2n)$ indices and indicate a spectral depletion relative to the Maxwellian description for very high energies—approximately 20% fewer neutrons above 11 Mev. The variation of the departures suggest probable distortions from the Maxwellian in other parts of the spectrum. The Watt spectrum on the other hand falls below the observed spectrum in the energy region of Cu63 response, and a distinct failure (departures from unity > 1.5 error intervals) of the Watt function extends down thru the $\text{Al}(n,\alpha)$ response. The nearly zero departure of the $\text{Al}(n,\alpha)/\text{Cu63}(n,2n)$ spectral index confirms the existence of a more energetic observed spectrum above 8 Mev at least.

Both spectral functions are essentially empirical, the Maxwellian clearly so (see however section 4.1), and the Watt in that it employs without justification a Maxwellian distribution for the center-of-mass neutron emission from the moving fragments (see 59Te).

Coincidentally, the Maxwellian description corresponds closely to the comprehensive fission spectrum calculations by Terrell (^{59}Te) which combine a number of center-of-mass evaporation spectra that match experimentally derived temperature distributions of the excited fragments (see section 4.7). The more rapid falling off of the observed spectrum then suggests that the derived temperature distribution of the fragments is too high. Generally, we might attribute such a failure to the limited fission fragment excitation energy available for neutron emission—perhaps a maximum of 20 Mev. The statistical theories of emission which assume that unlimited energy is available lead to the exponential behavior of the spectrum at high energies. On physical grounds, this high-energy tail must turn over at some point and go to zero. That this is apparently so in the energy range 12 to 16 Mev is consistent with an energy cut-off some few Mev beyond.

The rapid decay of the theoretical spectrum in this energy region, a factor of two per 900 kev, illustrates the degree to which the excitation function must be correct in order to support the cut-off conclusion: a 400 kev error in the energy scale describing the $\text{Cu}63(n,2n)$ excitation function would produce the same observed shift of indices. A distortion of 40% or so in the initial rise of the excitation function could likewise cause the shift. The agreement between three independent sets of cross section

measurements, as detailed in Fig. 1-1, is felt to make errors of these magnitudes unlikely.

The fact that the Watt spectral function falls off even more rapidly than the observed spectrum is due to the use of a single distribution for emission from the fragments so that to fit the bulk of the spectrum too low a prediction results for the extremes. Further discussion will be restricted to the Maxwellian description, as it is supported by detailed computations.

A second conclusion from the comparison in Table 5-6 is apparent. Almost all of the values, except Cu63, fall below unity implying a slightly more energetic spectrum than predicted by the Maxwellian function. The conclusion is supported not so much by the magnitude of departures which are marginal compared to the uncertainties, but by the consistency displayed. This uniformity also tends to confirm the detector excitation functions and suggests smaller uncertainties than estimated.

We will pursue this indicated spectral distortion briefly by grouping the detectors as follows: (1) the fission detectors, designation F-set, energy range 0 to 5 Mev; and (2) the remaining high-energy detectors excluding Cu63(n,2n), designation H-set, energy range 3 to 11 Mev. All spectral indices not involving Cu63(n,2n) fall into one of three groups—F:F(3), F:H(12), H:H(6)—where the number

of indices in each group are indicated. Each group occupies a separate region of the matrix display. On this basis it is seen that negative departures greater than one error interval predominate in the F:H group implying more neutrons above 3 Mev than predicted by the spectral function. The F:F and H:H groups present mixed arrays with generally smaller departures. In the table below are listed in percent the average absolute departures $|\bar{\Delta}|$ for each group, the average directed departure $\bar{\Delta}$, and the average estimated experimental uncertainty ϵ :

Table 5-7: Average Absolute and Directed Experimental Departures From Maxwellian Fission Spectrum Function

	$ \bar{\Delta} $	$\bar{\Delta}$	ϵ
F:F(3)	5%	-5%	5%
F:H(12)	11	-11	9
H:H(6)	4	-2	6½

An enhancement of the spectrum above 3 Mev is indicated, but not conclusively.

5.4 Adjustment of Maxwellian Spectrum

Though the average departures are not much larger than the estimated uncertainties, the consistent indication of a spectral shift towards higher energy makes it worthwhile to assess quantitatively what spectral changes will yield a

better fit to these activation detector results. A fit by adjusting the parameter T in the Maxwellian spectral function $E^{1/2} \exp(-E/T)$ is not adequate as can be seen by plotting some values from Table 5-6 on Fig. 4-2. Rather than attempting a comprehensive adjustment of the spectral form with additional analytic functions, six energy groups will be set up that are appropriate to the individual detector response regions as shown in Fig. 1-2 of Chapter 1. Specification of this group structure is presented in Table 5-8. The average group cross sections and the fractional group responses for each detector are computed from the spectral function for U235 and the cross section curves of Fig. 1-1. The last line lists average detector cross sections computed with the nominal Maxwellian function.

By informed trial and error the Maxwellian fission spectrum flux in each energy interval may be altered to obtain smaller departures between computed average cross sections and the observed cross sections of Table 5-5. Just a few tries were required to get a smooth fit in which no strong oscillation of adjacent group fluxes or detector uncertainties was allowed. It is then possible to propagate the uncertainties of Table 5-5 and estimate a group flux uncertainty. The adjusted fission spectrum in terms of the six energy groups appears in Table 5-9 along with its departure from the standard Maxwellian. Photoplate data

Table 5-8: Six-Group Specification For Fission Spectrum Adjustment

Energy Groups			Fiss. Spec. Group Flux ⁽²⁾	U235(n, f)		Np(n, f)		U238(n, f)		P(n, p)		Al(n, p)		Fe(n, p)		Al(n, α)		Cu63(n, 2n)	
No.	Range	E_i ⁽¹⁾		σ_i ⁽³⁾	r_i ⁽⁴⁾	σ_i	r_i	σ_i	r_i	σ_i	r_i	σ_i	r_i	σ_i	r_i	σ_i	r_i	σ_i	r_i
1	0-0.60	0.338	0.1818	1451	0.20	149	0.02	0		0		0		0		0		0	
2	0.60-1.4	1.00	0.2797	1261	0.26	1471	0.30	49	0.05	0		0		0		0		0	
3	1.4-3.0	2.10	0.3393	1381	0.35	1776	0.44	489	0.55	31	0.28	0.05	0.01	0		0		0	
4	3.0-6.0	4.04	0.1737	1224	0.16	1597	0.20	560	0.32	132	0.62	13.1	0.56	0.85	0.15	0		0	
5	6.0-11.0	6.90	0.0248	1552	0.03	1990	0.04	893	0.08	142	0.10	65.7	0.41	29.5	0.77	22.1	0.88	0	
6	11.0-∞	11.8	0.00070	1800		2000		1000		120		87	0.02	101	0.08	110	0.12	183	1.00
$\bar{\sigma}^{(5)}$ (mb)				1337		1369		300		37.0		3.98		0.950		0.625		0.128	

(1) Mean group energy, i.e. $\bar{E} = \sum_{i=1}^6 \bar{E}_i N_i = \int_0^{\infty} E N(E) dE$.

(2) Normalized group flux for $N(E) \sim E^{1/2} \exp(-E/1.29)$, the nominal Maxwellian description for U235 fission spectrum.

(3) Group Cross section in mb weighted according to the Maxwellian fission spectrum function.

(4) Fraction of detector response in each group.

(5) Average cross section computed with group flux of column 4.

Table 5-9: Six-Group Adjusted U235 Fission Neutron Spectrum

<u>Energy Groups</u>	<u>Maxwellian Spectral Function</u>	<u>Adjusted Spectrum</u>	<u>Photoplate Measurements</u> ⁽¹⁾
0-0.6 Mev	0.181 ₅	0.165 ±28%	— (2)
0.6-1.4	0.280	0.263 ±16%	0.275 ± 2%
1.4-3.0	0.339	0.342 ± 7%	0.332 ± 2%
3.0-6.0	0.174	0.200 ±11%	0.185 ± 3%
6.0-11.0	0.0248	0.0294± 7%	0.0246± 5%
11.0-∞	0.00070	0.0006 ₁ ±10%	0.0005 ₁ ±10%
- - - - -	- - - - -	- - - - -	- - - - -
Av. Energy:	1.935 Mev	2.055 Mev	1.958 Mev

(1) Energy range 1.4 to 11 Mev from ⁵⁶Cr1; above 11 Mev from ⁵²Wa. Normalization assumed a Maxwellian flux in 0-0.6 Mev group.

(2) Cloud Chamber data by Bonner (⁵²Bo) normalized to the Maxwellian at 250 kev (see Fig. I-1) yields 0.190 for the flux in the first energy group.

(not functional fits to them) reduced to this group structure by a Maxwellian extrapolation below the 0.3 Mev cutoff are included in the table; suitably propagated uncertainties are those recommended by the experimenters.

Qualitatively we may note that both measurements and the functional description agree, most uncertainties overlap, and the remarkable adequacy of the simple one parameter Maxwellian function to describe the fission spectrum over a wide range of energy and flux is illustrated. Looking in more detail we see a 15% fall off of the spectrum in the highest energy group, the significance of which was discussed above. The larger group fluxes above 3 Mev required by the activation detectors is not borne out by the photoplate measurements though uncertainties obscure the conclusion. Again lack of precision excitation functions puts the activation detectors at a disadvantage with respect to the carefully done photoplate work. A comprehensive completion of the Van de Graaff calibration (section 5.1) covering all energies with suitably wide but adjacent energy spreads could substantially reduce the uncertainties in the adjusted spectrum. The effect of the spectral distortion on average energy is shown in the last line of Table 5-9.

The improvement in detector response brought about by the adjusted spectrum may be seen in Table 5-10 which lists average absolute departures for each set of six indices

involving a single detector (Cu63 excluded).

Table 5-10: Average Absolute Departures of Observed Spectral Indices Involving a Single Detector

<u>Detectors</u>	<u>Maxwellian Spectrum</u>	<u>Adjusted Spectrum</u>
U235(n, f)	11%	2%
Np237(n, f)	9	2
U238(n, f)	6	2
P(n, p)	6	2
Al(n, p)	7	2
Fe56(n, p)	6	5
Al(n, α)	10	4
Cu63(n, 2n)	26	2

Only the Fe56 detector shows no real improvement, and we may note that measurement of the associated excitation function is the least detailed of any. Again it must be emphasized that it is the consistency rather than the magnitude of the detector response departures that suggest a spectral distortion.

APPENDIX 1

VERSATILE, HIGH-STABILITY PROPORTIONAL COUNTER FOR ACTIVATION MEASUREMENTS

A1.1 General Principles and Development

A reliable and flexible counting system is essential for activation measurements. Counting rates vary widely and yet important information often comes from very small differences in counting rates. Some significant factors considered in the development of a suitable counter are discussed below.

Any calibrated counting system to be used reliably day in and day out must operate on a plateau. Geiger counters achieve this at the considerable disadvantage of long dead times, while scintillation counters present some inherent problems making it difficult to maintain constant sensitivity over long periods, not the least of which are fatigue effects at high counting rates. The remaining option, proportional counters, was chosen though care in design and operation is required to obtain good plateaus. The main problem is to equalize pulses to

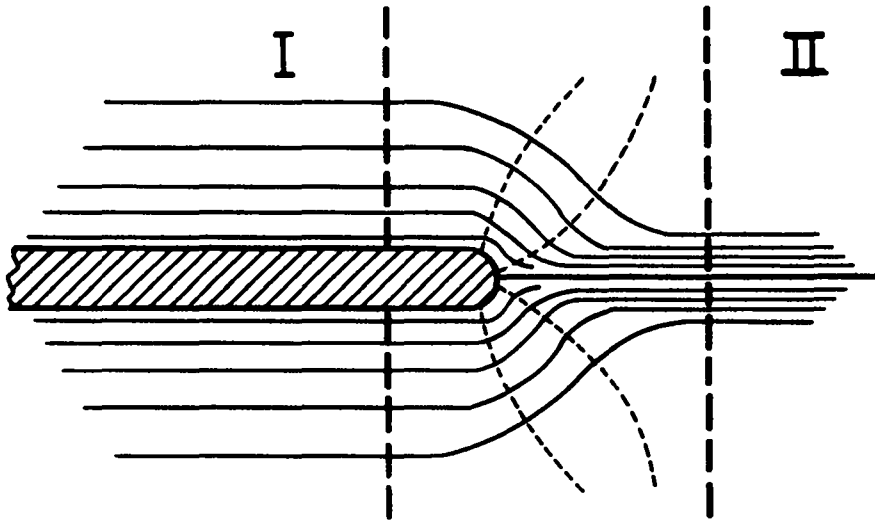
such an extent that the smallest are brought to a reasonable discriminator level while the largest do not paralyze the amplifier or unduly disturb subsequent pulses. In the system developed, pulse variation is about a factor of 70 so that an overloadable amplifier must be used.

Chamber pulses arise from (1) source betas which enter through a window and cross the chamber volume one or more times (back scattering of betas from chamber walls is surprisingly large, 57Mu) at all orientations to the collector wire and (2) betas emitted from the walls due to photoelectric conversion or Compton scattering of source gammas which are not ordinarily restricted by the window.

The specific ionization of a beta-particle is relatively constant down to ~ 0.2 Mev, but rises sharply below ~ 0.1 Mev. Beta ranges in methane are ~ 200 cm for a 0.5 Mev beta and about 15 cm for 0.1 Mev (50Wi). Clearly, very large pulses from the chamber are infrequent and are due to low energy or nearly spent betas emitted or scattered from the walls—especially those with ionization paths ending in the chamber. These pulses may be reduced in number by (1) keeping chamber volume small and (2) having chamber walls thin to betas; both precautions reduce the probability of path endings in the chamber gas.

Small pulses arise from single ionization paths across the chamber of electrons with energy greater than about 0.2Mev. In particular, single paths which traverse only a short distance in the chamber or are directed near radially to the collector wire will contribute greatly reduced pulse heights. Small pulses, therefore, are essentially a geometry problem, and it is relatively easy with a suitable window to eliminate short path lengths by source betas. The more penetrating gammas, on the other hand, are not so easily restricted and "corner paths" may remain significant since Compton scattering will quickly undo any external source collimation. A larger chamber volume enhances the height of the smaller pulses, but is accompanied by an increase in natural counter background as well as the number of large pulses as mentioned above. There must be a compromise.

Another consideration of practical importance in design concerns collector wire mounting. A counting wire of radius a_2 ($\approx 0.002''$) attached coaxially to a cylindrical mounting rod of radius $a_1 \gg a_2$ will give rise to collapsing potential lines qualitative as shown below, indicating that the field of the mounting rod extends into the region of the collector wire.



In regions I and II where the fields are radial the ratio of electric field strengths at equal distances from the axis is given by:

$$\frac{E_1}{E_2} = \frac{\ln b/a_2}{\ln b/a_1},$$

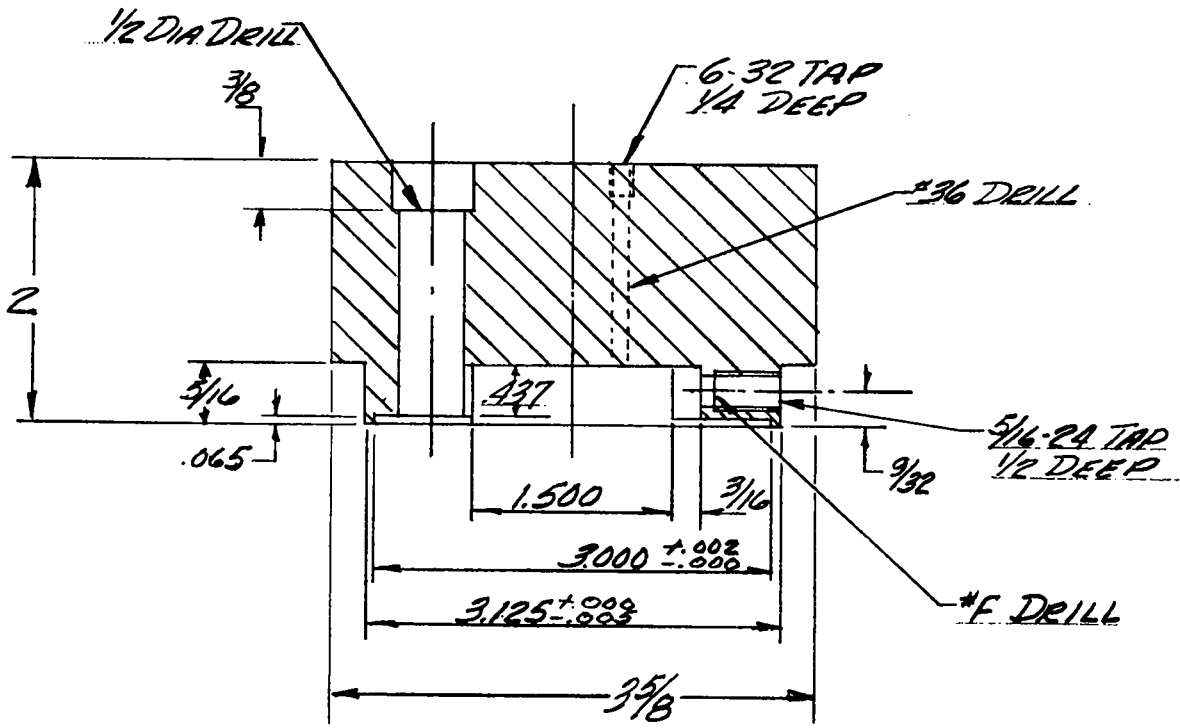
where "b" is the radius of the chamber enclosure. For typical values ($b \sim 1"$, $a_2 \sim 0.001"$, $a_1 \sim 0.030"$), $E_1/E_2 \sim 2$. It is possible therefore to have significant scavenging of ions by nonmultiplying support electrodes resulting in poor pulse equalization. This effect is often not important when sources are far from supports in elongated counting chambers. When a small chamber volume is desirable, adequate protection may be obtained by keeping support rods within simple recesses in the chamber wall.

These factors influencing proportional counter

performance were not systematically examined experimentally. However, a 4" diameter hemispherical chamber in which some design parameters could be varied was operated and the general effect of windows, wire diameter, chamber geometry, and in particular supporting electrodes were investigated.

A1.2 Counter Design and Performance Specification

The final system employs a windowed, methane-flow proportional counter coupled to a Los Alamos Model 260 overloadable amplifier. The chamber design is a flat cylinder (1.5" dia. x 7/16" deep) with a 0.003" gold plated tungsten wire mounted centrally along a diameter. An assembly diagram and drawing of the counter chamber are shown in Figs. A1-1 and A1-2; details of fabrication are on Los Alamos dwg. no. 19Y29541D1, 2. A convenient mounting design makes wire replacement quite simple, and such replacement does not affect counter sensitivity. The counter wire is soldered to parts 4 and 12 in Fig. A1-2, and part 12 is pushed into teflon insulator 11 to tighten (about 1/16" inch protrusion of part 12 should be allowed). Two mil aluminum covers the 1" diameter window. Since counting samples are always of significant thickness the advantages of a windowed counter vs insertion type—protection of chamber from damage and contamination, as well as freedom



SECTION A-A

MAT'L: BRASS

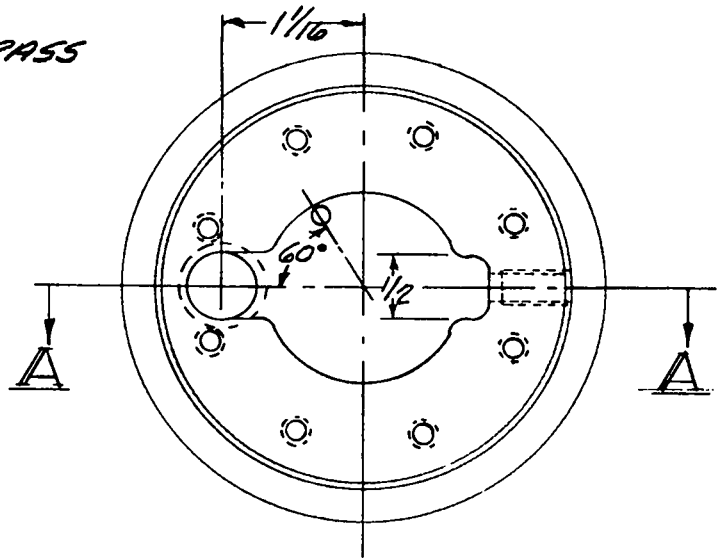


Fig. A1-1: Proportional Counter Chamber.

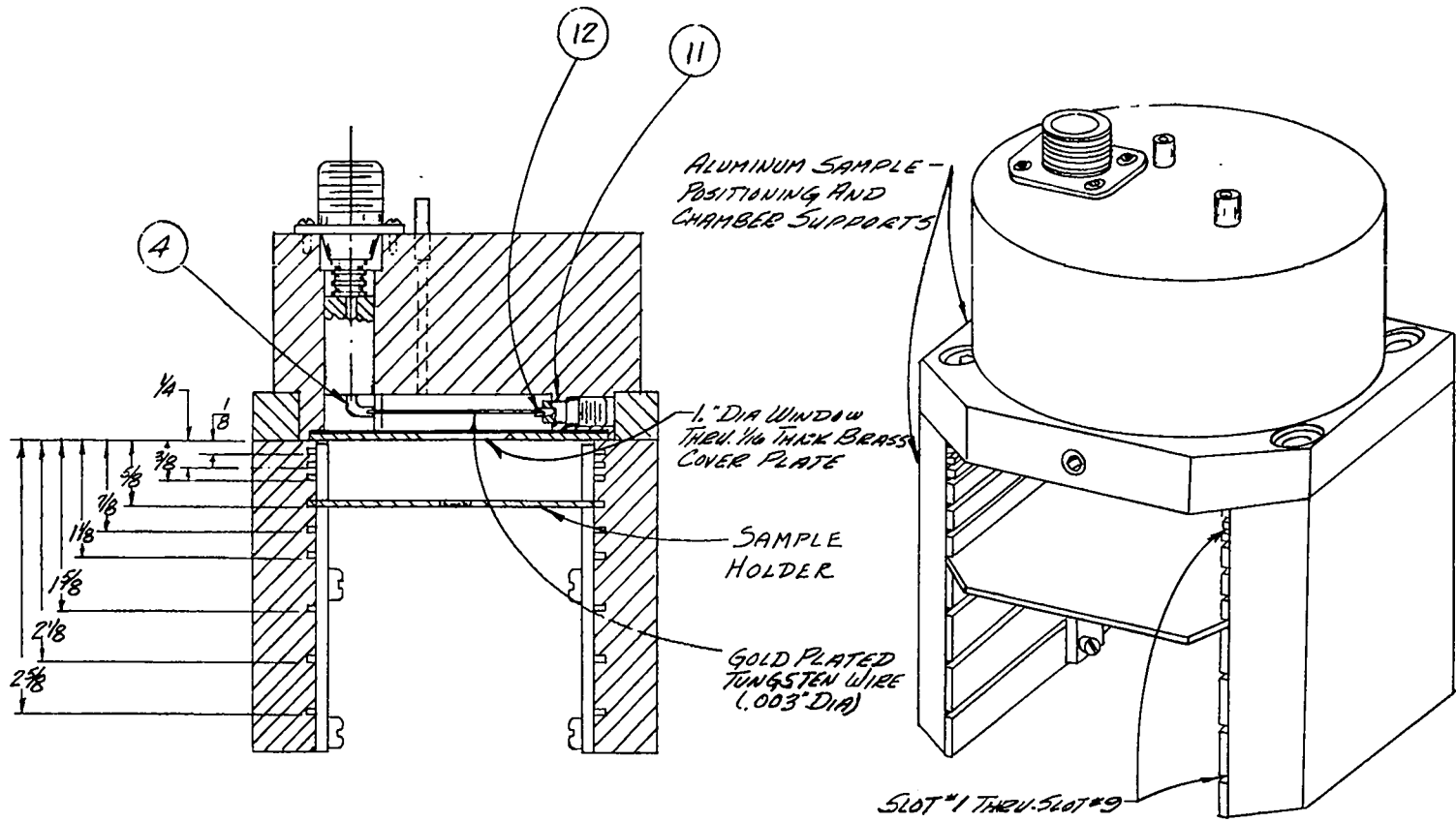


Fig. A1-2: High-Stability Proportional Counter for Activation Detector Measurements.

for sample positioning and shielding—are not compromised.

Brass disk holders 1/16" thick are recessed to hold the counting disks flush with the top surface of the holder and on the center-line of the chamber. Nine slots for the holders provide for sample to window distances of 1/8" to 2-5/8". A shield holder placed in an adjacent slot allows 3/4" diameter aluminum or lead shields to be interposed.

Presently two identical systems (a great advantage in isolating malfunctions) are in operation along with associated automatic readouts and computer processing. Operating specifications and characteristics are listed below:

- A. Chamber: total output capacitance $\sim 70\mu\text{f}$, chamber capacitance $\sim 5\mu\text{f}$, high voltage = 3450 volts, output pulses between 0.007 and 0.5 volts.
- B. Coupling circuit: coupling condenser = $100\mu\text{f}$, HV isolation resistor = 1.3 megohm.
- C. Amplifier: Los Alamos Model 260 (nonoverloading) set for gain of 3000. Resulting pulses are $\sim 3\mu\text{sec}$ wide with a 25 volt maximum undershoot and $25\mu\text{sec}$ maximum recovery time. Overload factor ~ 15 , dead time $\sim 2.5\mu\text{sec}$, discriminator setting 10 volts.
- D. Plateaus: bias plateau $\sim 0.02\%$ /volt in range of

ten to thirty volts for a normal uranium foil (mainly beta activity of Pa234). With a pure gamma source, Cs137, the slope is ~0.06%/volt in the same region. Chamber voltage plateau over range 3400-3500 volts is ~ 0.04%/10 volts. Break-down occurs somewhere beyond 4000 volts.

E. Standards: normal uranium disks 0.750 inch in diameter and unpolished are used as standard sources. Mounted flush in a brass holder in the closest slot (S1) they give counting rates vs. thickness as shown below:

Thickness:	0.008"	0.016"	0.024"	0.040"	Inf.
c/m x 10 ⁵ :	1.21	1.25	1.26	1.27	~ 1.28

F. Beta and Gamma Sensitivity: Chamber efficiency for betas is essentially 100%. The geometry for slot 1 is ~ 40%, and for non-fission detectors described in Table 1-2, Chapter 1, detector efficiencies are between 20 and 35%. Typical low chamber efficiencies for gamma detection are given in the following table:

	<u>Mev/disintegration</u>	<u>Chamber gamma efficiency (%)</u>
Co(n,γ)	~ 0.07	0.05 ± .04
Al(n,p)	~ 1	~ 1.5
Al(n,α)	~ 4.1	~ 5

- G. Foil positioning: Long term reproducibility is likely to be most affected by this factor. For the 0.75" uranium standards lateral position sensitivity is 0.1% per 0.01", but vertical position sensitivity can exceed 2% per 0.01" for the most sensitive slots.
- H. Background: natural counter background is 20c/m inside a 2" lead shield at 7,000 ft. altitude.
- I. Chamber gas: commercial grade methane with flow rate not less than 50cc/min.

APPENDIX 2

COAXIAL DISK GEOMETRY

Many commonplace source-detector geometries can be generated from thin coaxial disks (i.e., thin compared to neutron mean free paths). A general solution for the fundamental problem of the reaction rate in a thin detector disk coaxial with a source disk is straightforward. Integrals are set up below and IBM 704 results presented.

Consider first an axial point source of unit strength a distance "z" from a disk detector of radius "a" as shown in Fig. A2-1. The reaction rate $dR_p(z, r)$ in an annular element of the detector given by

$$\begin{aligned}
 dR_p(z, r) &= \frac{1}{4\pi r^2} (1 - e^{-\frac{t}{\lambda}}) 2\pi r \sin\theta r d\theta; \quad \lambda = \text{mean free path} \\
 &= \frac{1}{2} (1 - e^{-\frac{t}{\lambda}}) \sin\theta d\theta = \frac{-t}{2\lambda} d\cos\theta \qquad \text{A2-1}
 \end{aligned}$$

$\lambda = \text{mean free path}$

is applicable for $t \ll \lambda$, and $a \gg z$.

For detector thickness $t \ll z, a$, this expression can be integrated with $l = t/\cos\theta$. Changing the variable of integration

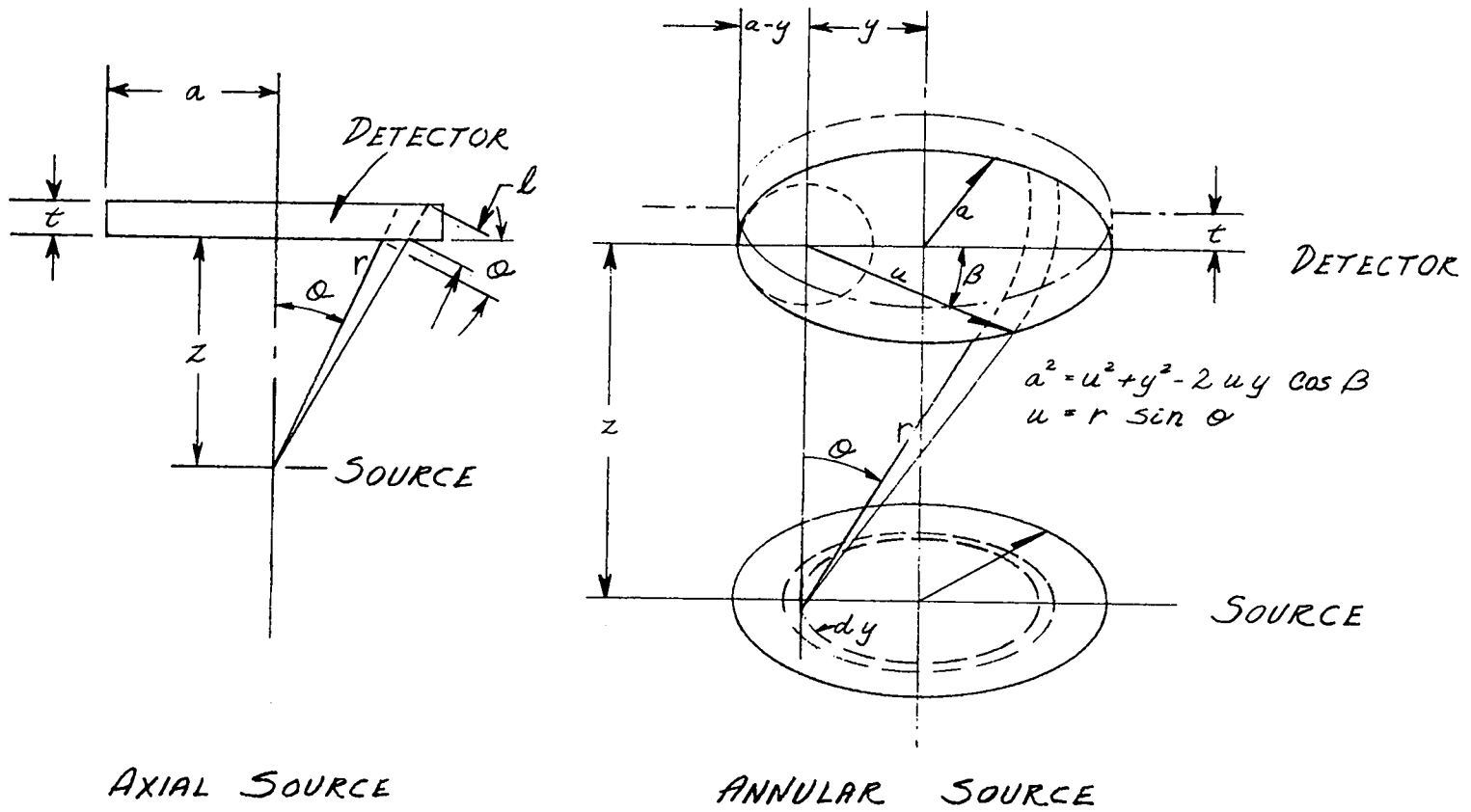


Fig. A2-1: Coaxial Disk Geometry.

to $v = \cos \theta$ the reaction rate is given by

$$R_p(z) = -\frac{1}{2} \int_1^\alpha \frac{t}{\lambda v} dv; \quad \alpha = z/\sqrt{a^2 + z^2}$$

$$= \frac{t}{4\lambda} \ln \left(1 + \frac{a^2}{z^2}\right). \quad \text{A2-2}$$

For $z \gg a$ the inverse square limit $a^2 t / 4z^2 \lambda$ is obtained.

Extending the source to a radius r_s and dividing it into annular elements, the reaction rate due to such source elements in a detector of radius $a \geq r_s$ (see Figure A2-1) may be derived as follows:

for $0 < \theta < \arctan \frac{a-y}{z}$

$$dR_d\left(\frac{z}{a}, \frac{y}{a}\right) = \frac{-1}{2} \left(1 - e^{-\frac{t}{\lambda \cos \theta}}\right) d\cos \theta = \left(\frac{t}{\lambda \cos \theta}\right) \frac{d\cos \theta}{2},$$

and for $\arctan \frac{a-y}{z} < \theta < \arctan \frac{a+y}{z}$

$$dR_d\left(\frac{z}{a}, \frac{y}{a}\right) = \left(\frac{t}{\lambda \cos \theta}\right) \beta \frac{\sin \theta d\theta}{2},$$

where $\beta = \frac{1}{4\pi} \arccos \left[\frac{u}{2y} + \frac{y}{2u} - \frac{a^2}{2uy}\right]$, and $u = z \tan \theta$.

The solution for the first region is given above; the second region is best evaluated by changing to the variable $u = z \tan \theta$:

$$R_d\left(\frac{z}{a}, \frac{y}{a}\right) = \frac{-t}{2\lambda} \int_1^\alpha \frac{d\cos \theta}{\cos \theta} + \frac{t}{2\lambda} \int_{a-y}^{a+y} \beta \frac{u du}{u^2 + z^2}, \quad 0 < y < 2a,$$

where $\alpha = \frac{z}{[z^2 + (a-y)^2]^{1/2}}$.

For the case $a < r_s$, an additional integral for $y > a$ is

necessary:

$$R_d\left(\frac{z}{a}, \frac{y}{a}\right) = \frac{t}{2\lambda} \int_{y-a}^{y+a} \beta \frac{u \, du}{u^2 + z^2}, \quad y > a.$$

A final integration over the source disk of unit strength and radius r_s gives the total reaction rate in the detector disk, a distance z away:

$$R_d\left(\frac{z}{a}, \frac{r_s}{a}\right) = \frac{1}{\pi} \left(\frac{r_s}{a}\right)^2 \int_0^{r_s/a} R_d\left(\frac{z}{a}, x\right) 2\pi x dx. \quad A2-3$$

The geometry is thus described by just two parameters, z/a and r_s/a , the ratios of separation distance and source radius to detector radius.

Numerical solutions of

$$C\left(\frac{z}{a}, \frac{r_s}{a}\right) \equiv \frac{\pi\lambda}{t} \left(\frac{r_s}{a}\right)^2 R_d\left(\frac{z}{a}, \frac{r_s}{a}\right)$$

for three source radii, $r_s/a = 0.8, 1.0, 1.2$, have been obtained with a simple fortran code on the Los Alamos IBM 704 computers. An effective flux at the detector may be defined by

$$R_d\left(\frac{z}{a}, \frac{r_s}{a}\right) \equiv (\bar{\phi}(z)/\lambda) (\pi a^2 t),$$

$$\bar{\phi}(z) = C\left(\frac{z}{a}, \frac{r_s}{a}\right) / \pi^2 r_s^2. \quad A2-4$$

Fig. A2-2 graphs $\bar{\phi}(z)$ for $a = r_s = 1$ cm.

Another useful interpretation of the computer results defines an average source to detector distance \bar{z} for a given separation distance z/a :

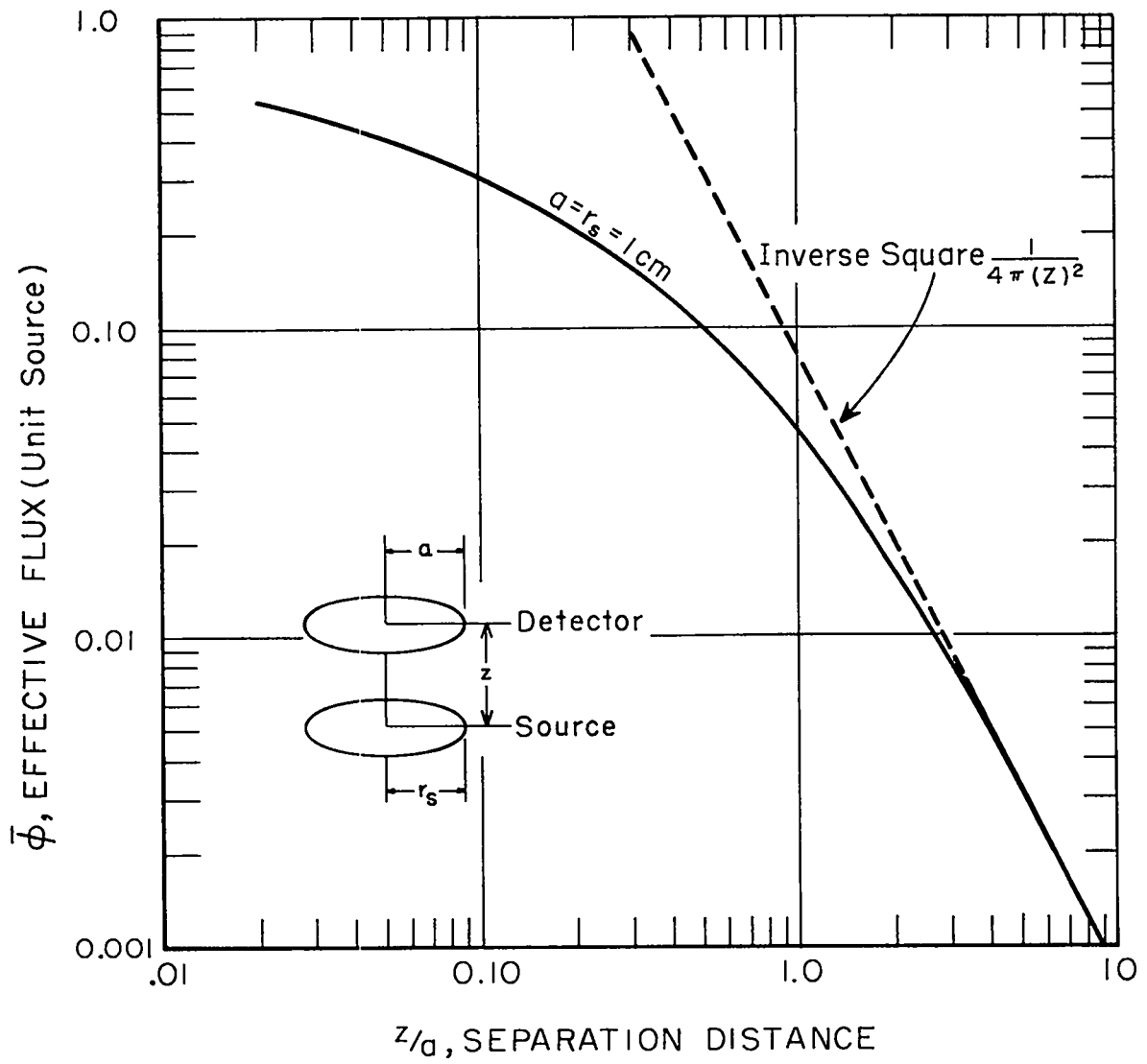


Fig. A2-2: Effective flux for detector disks between coaxial source disks (1 neut/sec), both of 1 cm radius. For separation distances greater than about three radii the behavior becomes inverse square.

$$R_d \left(\frac{z}{a}, \frac{r_s}{a} \right) = \frac{1}{\lambda} \frac{1}{4\pi z^2} \quad \pi a^2 t = \frac{a^2 t}{4\lambda} \frac{1}{z^2},$$

which approaches z as the separation distance increases.

In Fig. A2-3 the ratio z/\bar{z} vs z/a is plotted for three detector radii.

In Chapter 2 these results are used to calculate the effective flux for finite disk detectors in the region between two source disks of finite thickness and non-uniform source density. Another situation still in the process of refinement is the effective flux for disk detectors close to a 3cm long cylindrical gas target at the Los Alamos Van de Graaff.

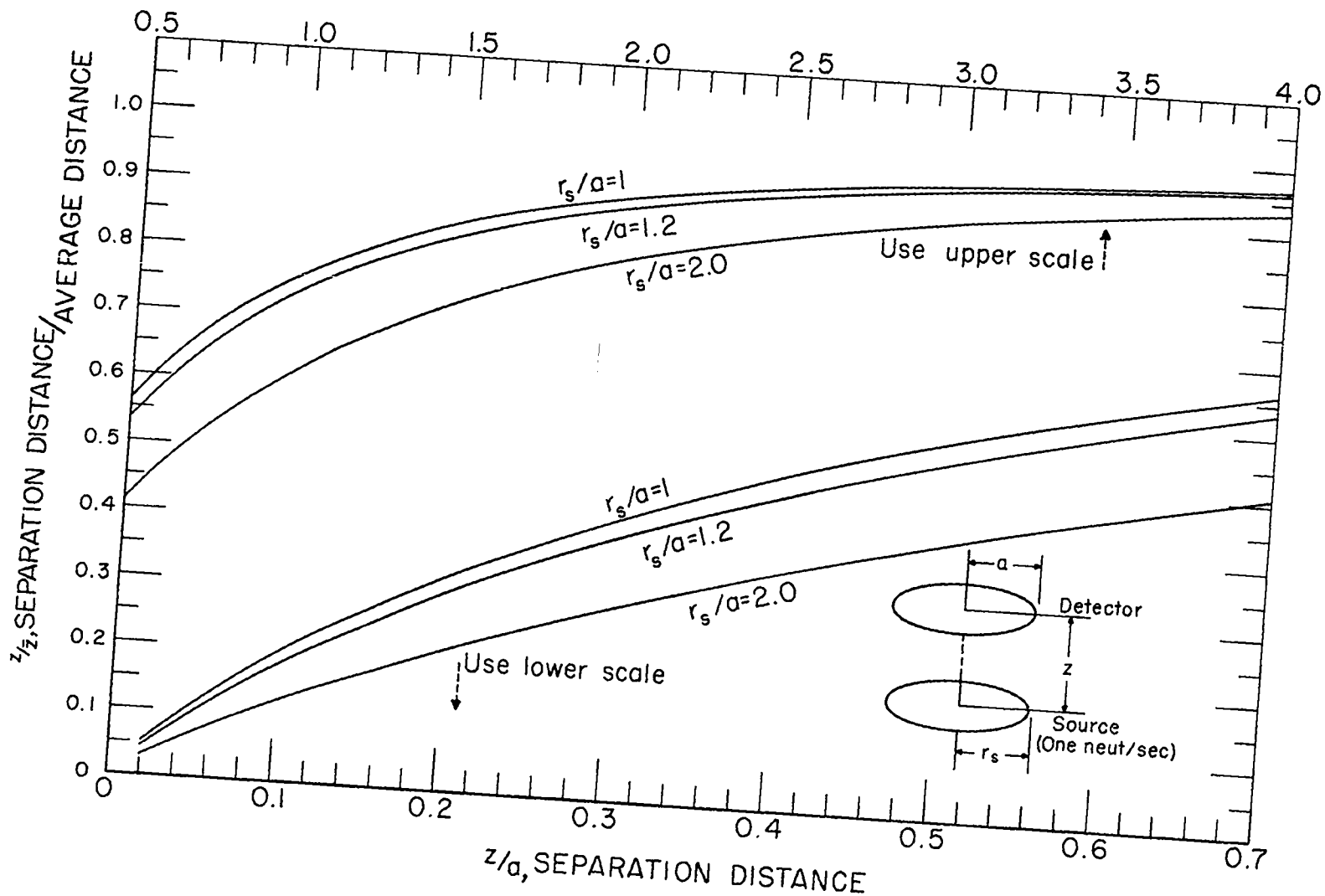


Fig. A2-3: Average distance between coaxial source and detector disks in terms of separation distance. The departure of the curve $r_s = 1.2a$ from $r_s = a$ is applicable, with reverse sign, to $r_s = 0.83a$.

APPENDIX 3

COMPUTATION OF CAVITY RETURN SPECTRA

A3.1 Monte-Carlo Method

Application of this method to the problem of the number and spectrum of neutrons returning to a fission source at the center of a spherical cavity in a large D_2O thermalizing medium is due to Drs. E. D. Cashwell and C. J. Everett. Their monograph "The Monte-Carlo Method" (59Ca) summarizes the general approach to problems of this kind.

Conditions imposed on the calculation were as follows:

- (1) Point source of fission spectrum neutrons located at center of cavity.
- (2) Neutrons followed until (a) energy falls below 0.32 ev or (b) they go beyond a specified radius.
- (3) Neutrons re-entering the cavity recorded into four solid angle divisions (0-0.32, 0.32-1.04, 1.04-1.84, 1.84- 2π steradians) and twenty five energy groups.

(4) Transport correction for anisotropic scattering.

Angular divisions are illustrated in Fig. A3-1. The computation was carried out on the old Los Alamos Maniac computer.

Table A3-1 tabulates total energy-integrated return in each solid angle division for three cavity sizes. Normalized spectra, summed over the first three solid angles, for 10 and 25cm diameter cavities are listed in Table A3-2, based on 10^4 neutrons followed for each arrangement.

A plot of the central flux vs. cavity diameter is shown in Fig. A3-2 along with the total number of cavity traverses per source neutron. The curves are consistent with a central to average flux ratio in the cavity of about 1.6 due to anisotropy of the returning neutrons. An expression $1/(r + k)^2$, r = cavity radius in centimeters, yields $k = 5.6$ cm, an average scattering depth, when fit to the flux plot.

A3.2 DSN Multigroup Transport Method

The DSN Method for approximating the Boltzmann Transport Equation has been used extensively for reactor calculations (58Ca). Simple source problems can also be handled, and give results more quickly than the Monte-Carlo approach. Using the 16 group cross sections developed by G. E. Hansen and W. H. Roach (61Ha) and the S_4 approximation, cavity

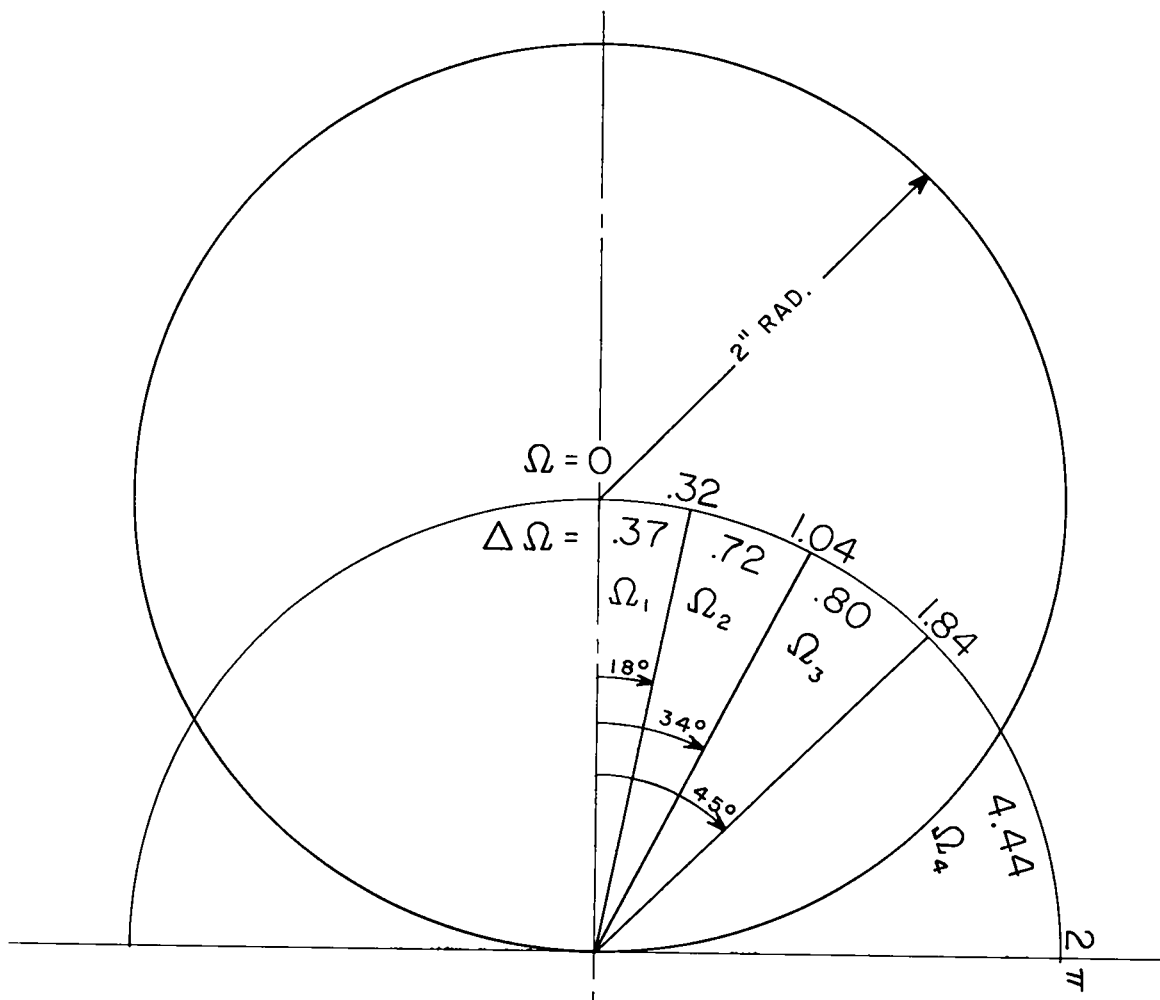


Fig. A3-1: Angular divisions used to describe neutrons returning to the cavity by the Monte-Carlo method.

Table A3-1: Total Neutron Return for Cavity Fission Spectrum
(Monte-Carlo) Solid Angle Divisions (Steradians)

	0 - 0.32	0.32 - 1.04	1.04 - 1.84	1.84 - 2π
<u>3" Dia. Cavity; 12" D₂O Reflector; 7500 Neutrons Followed</u>				
Fraction Returned (Total = 0.27)	0.024	.0533	0.051	.140
Frac. Ret./Ster.	0.074	0.074	0.063	0.032
Central Flux (Unit Source)	0.0051			
<u>4" Dia. Cavity; 12" D₂O Reflector; 22,500 Neutrons Followed</u>				
Fraction Returned (Total = 0.34)	0.029	0.066	0.063	0.175
Frac. Ret./Ster.	0.091	0.092	0.079	0.039
Central Flux (Unit Source)	0.0035			
<u>10" Dia. Cavity; 12" D₂O Reflector; 10,000 Neutrons Followed</u>				
Fraction Returned (Total = 0.66)	0.061	0.131	0.118	0.347
Frac. Ret./Ster.	0.192	0.180	0.148	0.078
Central Flux (Unit Source)	0.0012			
<u>10" Dia. Cavity; 18" D₂O Reflector; 10,000 Neutrons Followed</u>				
Fraction Returned (Total = 0.67)	0.058	0.130	0.123	0.354
Frac. Ret./Ster.	0.181	0.181	0.154	0.080
Central Flux (Unit Source)	0.0011			

Table A3-2: Normalized Flux Spectrum For Neutrons
Returning to Cavity (Monte-Carlo)

Energy	Groups	Flux Spectrum	
		$0 < \Omega < 1.84 \text{ Ster.}$	
No.	Range	10cm dia. cvy. 25cm thk. D ₂ O Refl.	25cm dia. cvy. 17.5cm thk. D ₂ O Refl.
1	4.7 - 10 Mev	0.0005	0.0003
2	2.2 - 4.7 "	0.0146	0.0078
3	1.0 - 2.2 "	0.0242	0.0215
4	0.47- 1.0 "	0.052	0.044
5	0.22- 0.47"	0.1049	0.0852
6	0.10- 0.22"	0.1131	0.100
7	47 - 100 kev	0.1138	0.091
8	22 - 47 "	0.079	0.078
9	10 - 22 "	0.075	0.0666
10	4.7 - 10 "	0.0560	0.055
11	2.2 - 4.7 "	0.062	0.057
12	1.0 - 2.2 "	0.045	0.051
13	0.47- 1.0 "	0.040	0.051
14	0.22- 0.47"	0.044	0.039
15	0.10- 0.22"	0.025	0.039
16	56 - 100 ev	0.0228	0.0260
17	32 - 56 "	0.0186	0.0247
18	18 - 32 "	0.0153	0.0234
19	10 - 18 "	0.0171	0.0256
20	5.6- 10 "	0.0178	0.0221
21	3.2- 5.6 "	0.0158	0.0228
22	1.8- 3.2 "	0.0154	0.0182
23	1.0- 1.8 "	0.0134	0.0153
24	0.56- 1.0 "	0.0156	0.0160
25	0.32- 0.56 "	0.00911	0.0215
Spectrum Above 17 kev:		0.54	0.47
Central Return Flux (Unit Source):		0.0035	0.0012
Av. cross section, U235(n, f):		10.1b	12.5
		U238(n, f): 0.016b	0.011

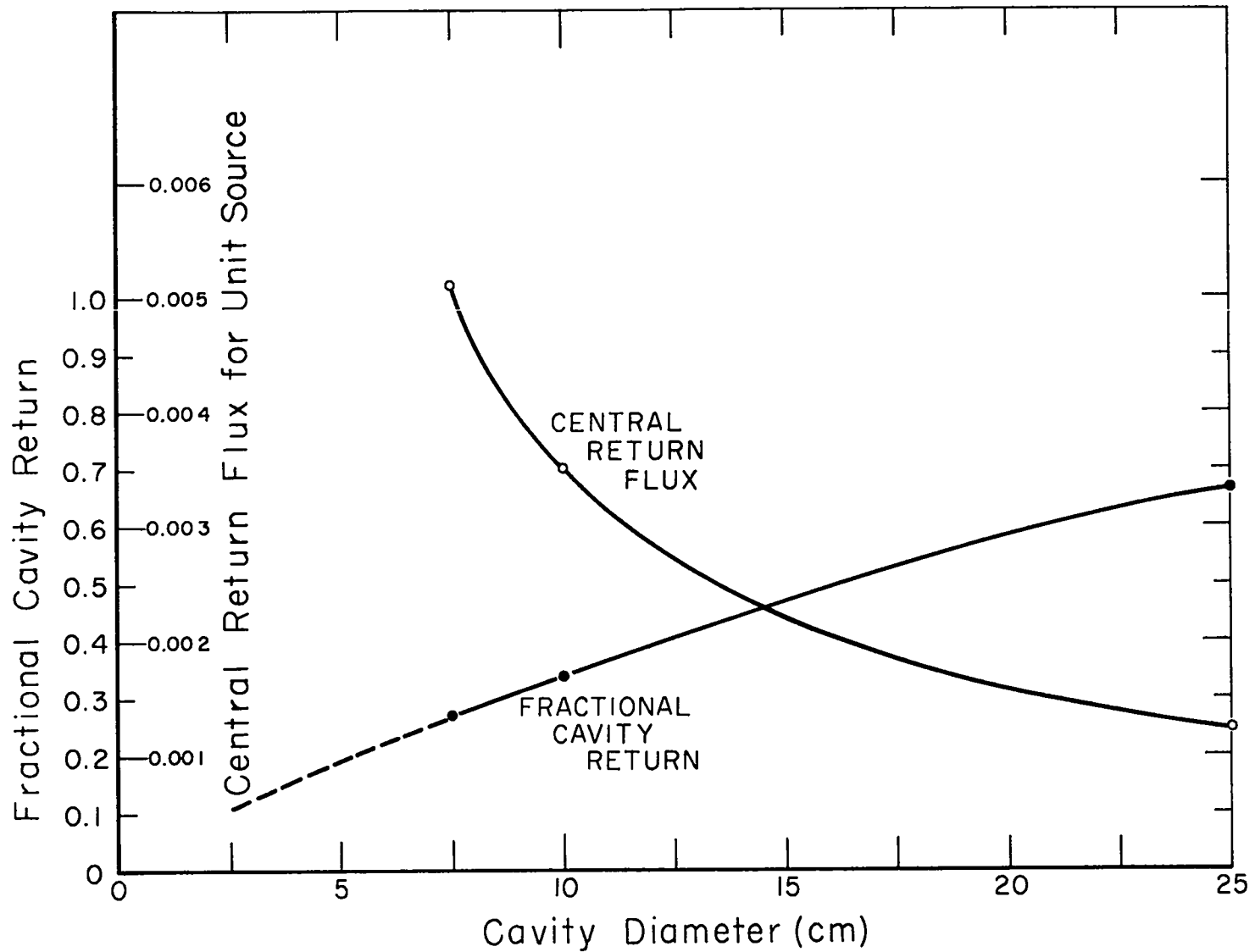


Fig. A3-2: Return flux, by Monte-Carlo method, at center of spherical cavity in heavy water for a unit fission neutron source at the cavity center. The fraction of the neutrons which return to the cavity is also for a unit source at the cavity center.

return spectra and fluxes were obtained for D_2O , H_2O , and graphite reflectors.

Spherical problems with four regions and 82 space points were run on the Los Alamos IBM 7090 computer:

Region	:	1	2	3	4
Outer Boundary	:	0.70cm	0.80cm	2.5-20cm	30-50cm
No. of Space Pts.	:	20	2	30	50

Regions 1, 2, and 3 include the cavity with a fission neutron source placed in region 2; region 4 is the reflector. In Table A3-3 the spectra of neutrons returning to the cavity are tabulated for representative arrangements. Assuming cadmium shielded detectors the spectra are normalized to the total flux above 0.4 ev. Spectral variations are illustrated by the changes in the fraction of neutrons above 17kev, and agree reasonably well with the Monte-Carlo results of Table A3-2.

The total neutron return from the thermalizing medium is conveniently summarized by specifying the return flux at the center of the cavity for a unit fission neutron source (1 neutron/sec) at or near the center. A plot of the total central return flux vs. cavity diameter for various reflectors is shown in Fig. A3-3. Discrepancies of up to 20% are apparent in the total central flux between the two

Table A3-3: Flux Spectrum of Cavity Return Neutrons
(Multigroup Transport Approx.)

Energy	Groups	Cvy.dia:	Flux Spectrum at Cavity Center ^(a)					H ₂ O reflector
			D ₂ O reflector		Graphite reflector (density = 1.7)			
No.	Range		10cm	18cm	10cm	18cm	50cm	10cm
1	3-∞ Mev		0.014	0.012	0.031	0.025	0.016	0.024
2	1.4-3.0mev		0.017	0.012	0.129	0.112	0.087	0.032
3	0.9-1.4mev		0.027	0.024	0.086	0.076	0.049	0.024
4	0.4-0.9mev		0.101	0.082	0.172	0.152	0.115	0.056
5	0.1-0.4mev		0.238	0.21	0.190	0.193	0.164	0.097
6	17-100kev		0.185	0.18	0.138	0.142	0.148	0.121
7	3-17kev		0.118	0.122	0.081	0.092	0.103	0.115
8	0.55-3kev		0.085	0.094	0.056	0.066	0.084	0.112
9	0.1-0.55kev		0.067	0.077	0.041	0.049	0.071	0.107
10	30-100ev		0.040	0.048	0.023	0.0282	0.044	0.073
11	10-30ev		0.032	0.039	0.018	0.021	0.036	0.064
12	3-10ev		0.031	0.039	0.016	0.019	0.034	0.066
13	1-3ev		0.025	0.032	0.012	0.015	0.030	0.058
14	0.4-1ev		0.021	0.028	0.009	0.011	0.021	0.048
15	0.1-0.4ev		(0.024)	(0.031)	(0.011)	(0.013)	(0.03)	(0.145)
16	Thermal		(0.35)	(0.44)	(0.05)	(0.05)	(0.22)	(2.50)
-----			-----					
Spectrum Above 17 kev			0.58	0.52	0.75	0.70	0.58	0.38
(b) Central Return flux (> 0.4ev)			0.0042	0.0024	0.0047	0.0028	0.0009	0.0017
-----			-----					

(a) Flux spectrum above 0.4ev is normalized to unity.

(b) Return flux for a fission source of 1 neutron/sec at center of cavity.

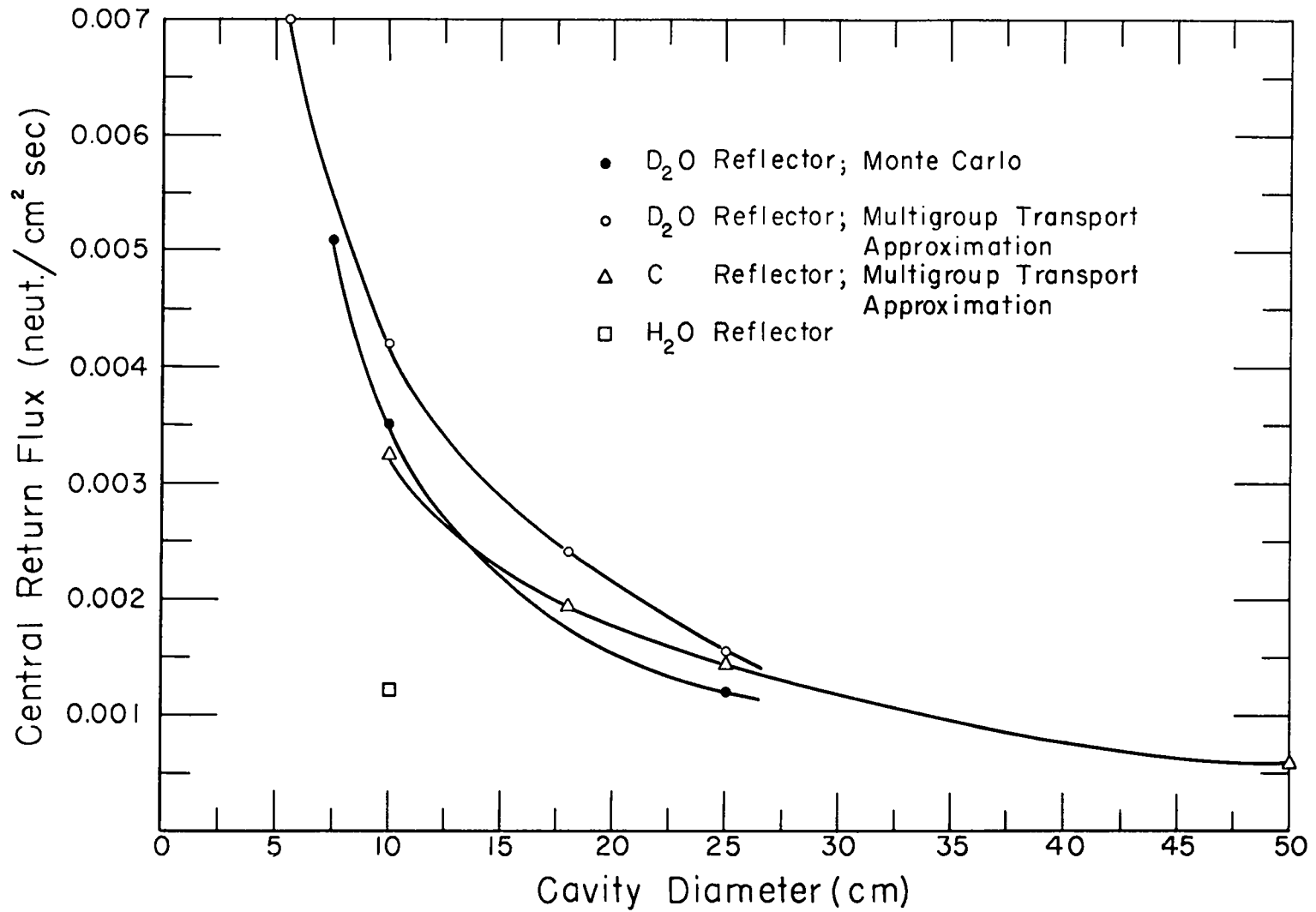


Fig. A3-3: Return flux (> 0.4 ev) at the center of a spherical cavity in various reflectors for a unit fission neutron source at the cavity center.

computational methods and may be attributable the use of different cross sections and center-of-mass anisotropy functions. For the background estimates undertaken in Chapter 2 this discrepancy is not important as the detector response will be overshadowed by other larger uncertainties.

In general, the fission return background at the cavity center is simply

$$\text{Background} \approx [\phi_{\text{return}}] 4\pi \bar{Z}^2 \frac{\bar{\sigma}_{\text{return}}}{\bar{\sigma}_{\text{fiss. spec.}}},$$

where \bar{Z} is the average source to detector distance as discussed in Appendix 2, ϕ_{return} the central return flux as given in Fig. A3-3, and $\bar{\sigma}_{\text{return}}$ the average cross section computed with the spectrum as given in Tables A3-2 or A3-3. For example, with an average source to detector distance equal to about 1/20 of the cavity diameter, the neutron return contribution to a U238 fission detector is $0.004 \times 4\pi(0.50)^2 \times 0.018/0.030 = 0.09\%$ in a 10cm diameter cavity within a D_2O reflector. Other higher energy detectors will receive a smaller contribution from returning neutrons so that rather crude estimates of geometry and average cross sections are adequate.

Noting that the return flux vs. cavity diameter shown in Fig. A3-3 varies approximately as the reciprocal of the cavity diameter, the parameter $\bar{Z}^2/(\text{cavity dia.})$ becomes useful for choosing cavity size and source-detector arrangements.

Both calculations indicate that the return is nearly unaffected by changes of reflector thickness greater than 25cm.

REFERENCES

- 37 We. V. F. Weisskopf, Phys. Rev., 52, 295 (1937); J. M. Blatt and V. F. Weisskopf, "Theoretical Nuclear Physics" (John Wiley and Sons, Inc., 1952).
- 39 Hal. H. Von Halban, Jr., F. Joliot, and L. Kowarski, Nature, 143, 470 (1939).
- 39 Ha2. Ibid. p. 680.
- 40 Tu. L. A. Turner, Rev. Mod. Phys., 12, 11 (1940).
- 48 Ba. G. C. Baldwin and G. S. Klaiber, Phys. Rev., 73, 1156 (1948).
- 50 Fo. J. L. Fowler and J. M. Slye, Jr., Phys. Rev., 77, 787 (1950).
- 50 Wi. D. H. Wilkinson, "Ionization Chambers and Counters," Ch. 2., Cambridge Univ. Press (1950).
- 52 Bo. Bonner, Ferrell, and Rinehart, Phys. Rev., 87, 1032 (1952).
- 52 Br. J. Brolley, Jr., J. Fowler, L. Schlacks, Phys. Rev., 88, 618 (1952).
- 52 Fo. S. G. Forbes, Phys. Rev., 88, 1309 (1952).
- 52 Fr. J. Fraser, Phys. Rev., 88, 536 (1952).
- 52 Ne. N. Nereson, Phys. Rev., 88, 823 (1952).
- 52 Wa. B. E. Watt, Phys. Rev., 87, 1037 (1952).
- 53 Hu. D. J. Hughes, "Pile Neutron Research," Ch. 4., Addison-Wesley, (1953).
- 54 Be. A. I. Berman, and K. L. Brown, Phys. Rev., 96, 83 (1954).
- 54 Wa. J. S. Wahl, Phys. Rev., 95, 126 (1954).

- 55 Gr. G. A. Graves and W. H. Roach, Some Foil Absorption Calculations, LA-1964 (1955); Summary results appear in ANL-5800, section 8, p. 486.
- 56 Cr1. Cranberg, Frye, Nereson, and Rosen, Phys. Rev., 103, 662 (1956).
- 56 Cr2. L. Cranberg, A. H. Armstrong, and R. L. Henkel, Phys. Rev., 104, 1639 (1956).
- 56 Gr. J. A. Grundl and J. R. Neuer, Bull. Am. Phys. Soc. Ser. II, 1, 95 (1956).
- 56 Pe. R. E. Peterson and G. A. Newby, Nuc. Sci. and Eng., 1, 112-125 (1956).
- 57 Ko. Kovalev, Andreev, Nikolaev, Guseinov, J. Exptl. Th. Phys. (U.S.S.R.), 33, 1069 (1957) [Translation: Sov. Phys. JETP, 6, 825 (1958)].
- 57 Le. R. B. Leachman and H. W. Schmitt, J. Nuc. Energy, 1, 1957, Vol 4, pp 38 to 43. Pergamon Press Ltd., London. Recent measurements of $\bar{\nu}$ (62 Di) have been used to extract $\bar{\sigma}_f$ (U238) from the measured quantity $\bar{\nu}\bar{\sigma}_f$.
- 57 Mu. R. H. Muller, Analytic Chemistry, 29, 969 (1957).
- 57 Te. J. Terrell, Phys. Rev., 108, 783 (1957).
- 58 Al. D. W. Allen, R. L. Henkel, "Progress In Nuclear Energy Series 1—Physics and Mathematics Vol. 2," "Fast Neutron Data on the Isotopes of Thorium, Uranium Plutonium" (1958).
- 58 Ca. B. C. Carlson and G. I. Bell, Proc. 2nd Intern. Conf. Peaceful Uses of Atomic Energy, Geneva, 16, 535 (1958); C. E. Lee, LA-2595 (1962).
- 58 Gr. J. A. Grundl, R. L. Henkel, and B. L. Perkins, Phys. Rev., 109, 425 (1958).

- 58 Hu. Hughes and Schwartz, BNL-325 (1958).
- 58 Ko. Kovalev, Stavinskii, *Atomnaya Energiya*, 5, 1588 (1958) [Translation: *Sov. J. Atomic Energy*, 5, 1588 (1958)].
- 58 St. D. Strominger, J. M. Hollander, and G. T. Seaborg, *Table of Isotopes. Revs. Mod. Phys.*, 30, 585 (1958).
- 58 Te. J. Terrell, and D. M. Holm, *Phys. Rev.*, 109, 2031 (1958).
- 58 Tr. J. B. Trice, *Nucleonics*, 16, 7 (1958).
- 59 Ca. E. D. Cashwell, and C. J. Everett, "The Monte Carlo Method," p. 153, Pergamon Press (1959).
- 59 Ha. I. Halpern, *Ann. Rev. of Nuc. Science*, 9, 294 (1959).
- 59 Mu. C. O. Muehlhause, *Am. Nuc. Soc. Trans.*, 2, 123 (1959).
- 59 Sc. H. W. Schmitt and R. B. Murray, *Phys. Rev.*, 116, 1575 (1959); Data renormalized to U238 (n, f) cross section of 59 Sm.
- 59 Sm. Kurt Smith, Private Communication.
- 59 Te. James Terrell, "Fission Neutron Spectra and Nuclear Temperatures," *Phys. Rev.*, 113, 527 (1959).
- 60 Ch. C. G. Chezem, *Nuc. Science and Engineering*, 8, 652 (1960).
- 60 Cu. P. Cuzzocrea, G. Pappalardo and R. Ricamo, *Nuovo Cimento*, 16, 450 (1960).
- 60 Gr. J. Grundl, A. Usner, *Nuc. Sci. and Eng.*, 8, 598 (1960). A number of references to activation detector work are given here.

- 60 Ja. G. A. Jarvis, G. A. Linenberger, J. D. Orndoff, and H. C. Paxton, *Nuc. Sci. and Eng.*, 8, 525 (1960).
- 60 Li. A. Liskien, A. Paulsen, EANDC(E)28, Euratom; Central Bureau for Nuclear Measurements, Geel, Belgium (1961). An excellent display and critical review of measurements through October 1961, for eight threshold detector reactions are included in this document.
- 60 Sc. H. W. Schmitt and J. Halperin, *Phys. Rev.*, 121, 827 (1961).
- 61 Bo1. T. W. Bonner, *Nuc. Phys.*, 23, 116 (1961); R. L. Bramblett, R. I. Ewing and T. W. Bonner, *Nuc. Inst. and Methods*, 9, 1 (1960).
- 61 Bo2. Harry R. Bowman, Stanley C. Thompson, J. C. D. Milton, and Wladyslaw Swiatacki, UCRL-9713, (1961).
- 61 Ch. C. G. Chezem and R. H. Moore, *Photographic Science and Eng.*, 5, No. 6 (1961); R. H. Moore and R. K. Zeigler, Los Alamos Sc. Lab. LA-2367 (1959).
- 61 Ha. G. E. Hansen and W. H. Roach, Six and Sixteen Group Cross Sections for Fast and Intermediate Critical Assemblies, LAMS-2543 (1961); Selected cross sections in *Nucl. Sc. and Eng.*, 8, 621 (1960).
- 61 Mo. J. Moteff and E. R. Beever, "Selected Topics In Radiation Dosimetry," p. 383 (1961); Published by IAEA.
- 62 Bo. M. Borman, S. Cierjacks, R. Langkav and H. Nevert, *Z. Physik*, 166, 477 (1962).
- 62 Di. B. C. Diven, Private Communication (1962).
- 62 Die. O. W. Dietrich and J. Thomas, "Physics of Fast and Intermediate Reactors," Vol. I, p. 377 (1962); Published by IAEA.